Supplementary Information

CSF-1R inhibition alters macrophage polarization and blocks glioma progression

Stephanie M. Pyonteck [1]*, Leila Akkari [1]*, Alberto J. Schuhmacher [1]*, Robert L. Bowman [1], Lisa Sevenich [1], Daniela F. Quail [1], Oakley C. Olson [1], Marsha L. Quick [1], Jason T. Huse [3,4], Virginia Teijeiro [1], Manu Setty [2], Christina S. Leslie [2], Yoko Oei [5], Alicia Pedraza [3], Jianan Zhang [3,4], Cameron W. Brennan [3,4], James C. Sutton [5], Eric C. Holland [1,4], Dylan Daniel [5], and Johanna A. Joyce [1,4 #]

[#] Correspondence should be addressed to: joycej@mskcc.org

Supplementary Figure 1

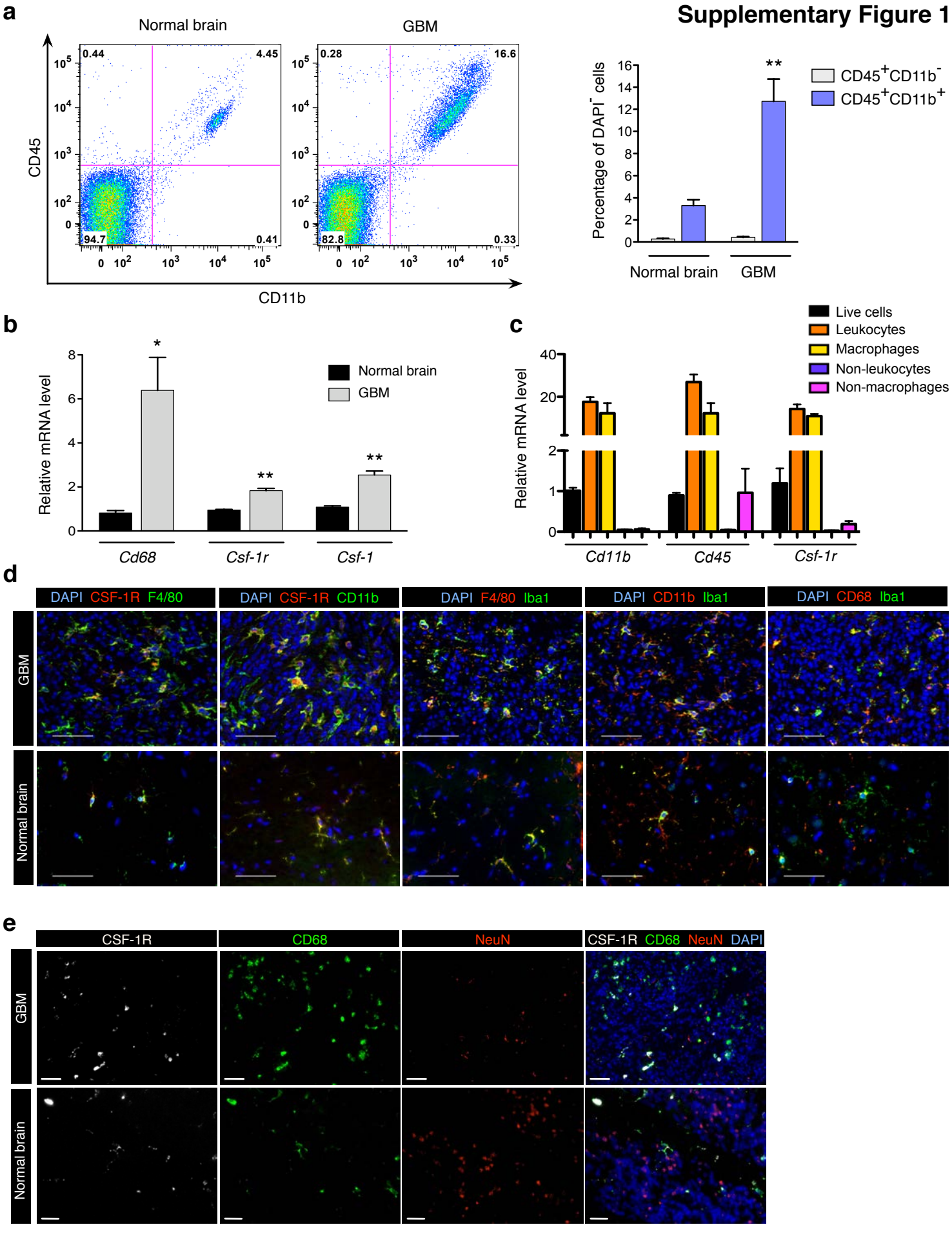

Supplementary Figure 1.

Macrophage numbers are increased in a mouse model of gliomagenesis compared to normal brain and specifically express CSF-1R. (a) Flow cytometric analysis of CD45 and CD11b in cerebrum/ forebrain from uninjected Nestin-Tv-a;*Ink4a/Arf*$^{-/-}$ mice (normal brain) or in grade IV gliomas (GBM) from symptomatic RCAS-PDGF-B-HA/Nestin-Tv-a;*Ink4a/Arf*$^{-/-}$ (PDG) mice (*n*=5 each). There was a significant increase in CD45^{+} leukocytes and CD11b^{+} myeloid cells/ macrophages accounted for the overwhelming majority of infiltrating leukocytes (97% of CD45^{+} cells), with a 3.8-fold increase in CD45^{+}CD11b^{+} cells in GBMs (12.7± 2.0%) compared to normal brain (3.3 ± 0.5%). There was no change in the number of CD45^{+}CD11b^{-} cells in gliomas compared to normal brain. **(b)** Normal brain and GBM tumors (*n*=3 each) were used for RNA isolation, cDNA synthesis, and qPCR. Assays were run in triplicate and expression normalized to *ubiquitin C* (*Ubc*) for each sample. *Cd68, Csf-1r* and *Csf-1* gene expression is depicted relative to normal brain. **(c)** Gliomas from PDG mice (*n*=4) were sorted by FACS into a mixed population of live cells (DAPI^{-}), purified leukocytes (CD45^{+}) or macrophages (CD11b^{+}Gr-1^{-}) prior to analysis of *Csf-1r* mRNA expression in each population. *Cd11b* and *Cd45* were used as cell type-specific control genes for macrophages and leukocytes respectively. Expression is depicted relative to the live cell fraction, and normalized to *Ubc* for each sample. **(d)** Normal brain or GBM tissue sections from symptomatic PDG mice were stained for CSF-1R in combination with the macrophage markers F4/80 and CD11b. F4/80, CD11b, and CD68 were also examined in combination with Iba1 (macrophages/ microglia). DAPI was used for the nuclear counterstain. **(e)** Representative immunofluorescence images of CSF-1R, CD68 (macrophages), NeuN (neurons) and DAPI in PDG GBM (upper panels) and the contralateral non-tumor bearing brain (lower panels), shows that CSF-1R is expressed by CD68^{+} macrophages and not by NeuN^{+} neurons. Scale bar, 50 μm. Graphs show mean + s.e.m. *P* values were obtained using unpaired two-tailed Student's t-test; **P*<0.05, ***P*<0.01.

Supplementary Figure 2

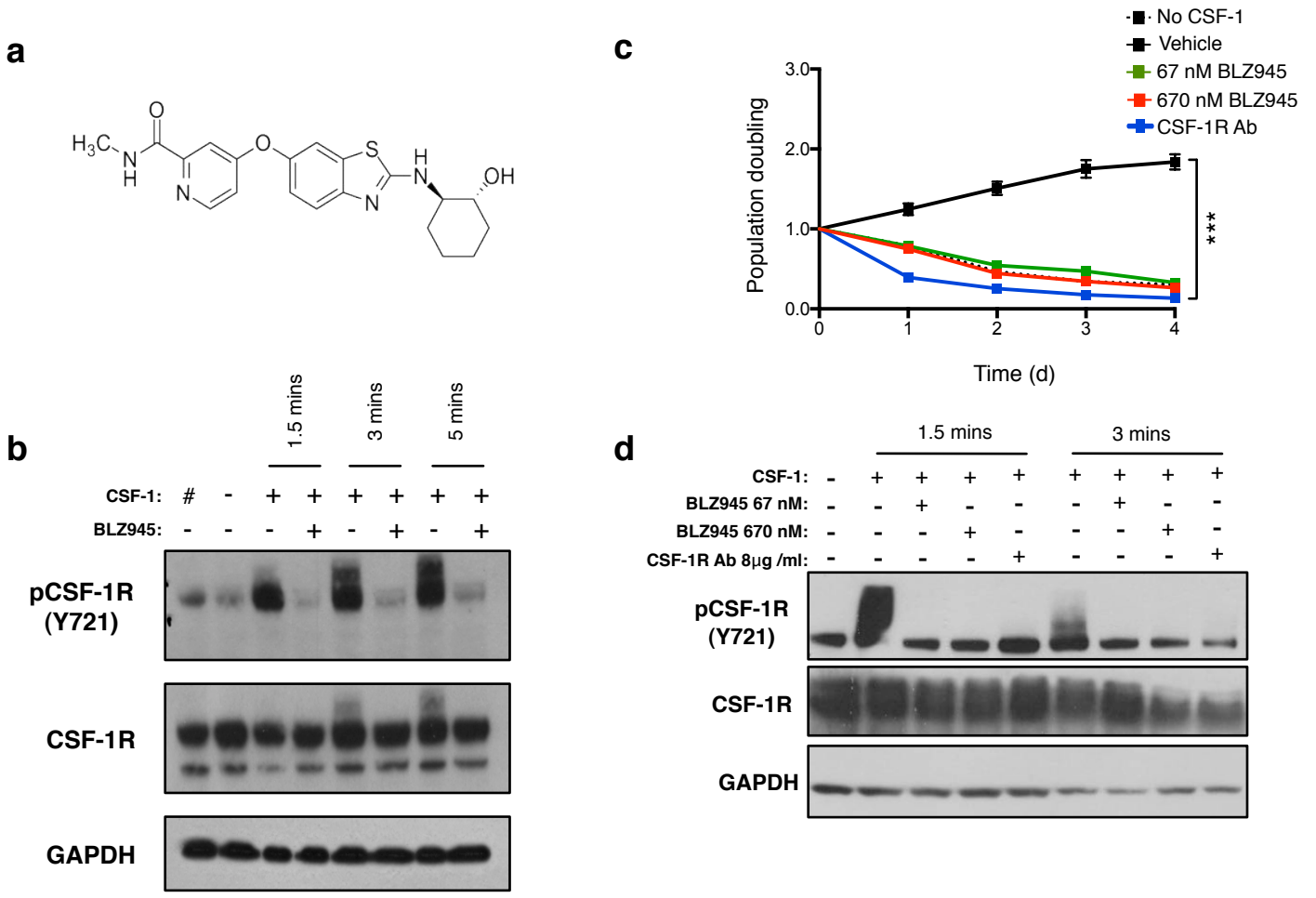

Supplementary Figure 2.
CSF-1R inhibition by BLZ945 or an anti-CSF-1R antibody significantly decreases the viability of macrophages in culture. **(a)** Chemical structure of the CSF-1R inhibitor BLZ945: 4-[2-((1R, 2R)-2-hydroxycyclohexylamino)-benzothiazol-6-yloxy]-pyridine-2-carboxylic acid methylamide. **(b)** Western blot analysis of primary bone marrow-derived macrophages (BMDMs), which were cultured in the absence of CSF-1 for 12 hours prior to stimulation, followed by CSF-1 addition for the time points indicated (1.5, 3 and 5 minutes). This resulted in a progressive increase in CSF-1R phosphorylation that was effectively inhibited by 67 nM BLZ945. In lane 1, marked by #, BMDMs were continuously cultured with CSF-1. The same dose of BLZ945 (67 nM) blocks proliferation of BMDMs (as shown in Fig. 1c). **(c)** A neutralizing antibody against CSF-1R (AFS98, 8 µg/ml) blocked BMDM survival in culture in a similar manner to BLZ945, as determined by MTT assays, *n*=3 replicates. A rat IgG control antibody had no effect on BMDM survival or proliferation (data not shown). **(d)** Western blot analysis of primary BMDMs cultured in the absence of CSF-1 for 12 hours, followed by CSF-1 addition for the time points indicated (1.5 and 3 minutes). CSF-1R phosphorylation was observed following CSF-1 stimulation, and was effectively inhibited by the CSF-1R neutralizing antibody in a comparable manner to 67 nM or 670 nM BLZ945. Graphs show mean ± s.e.m. *P* values were obtained using unpaired two-tailed Student's t-test compared to the vehicle control; ***$P<0.001$.

Supplementary Figure 3

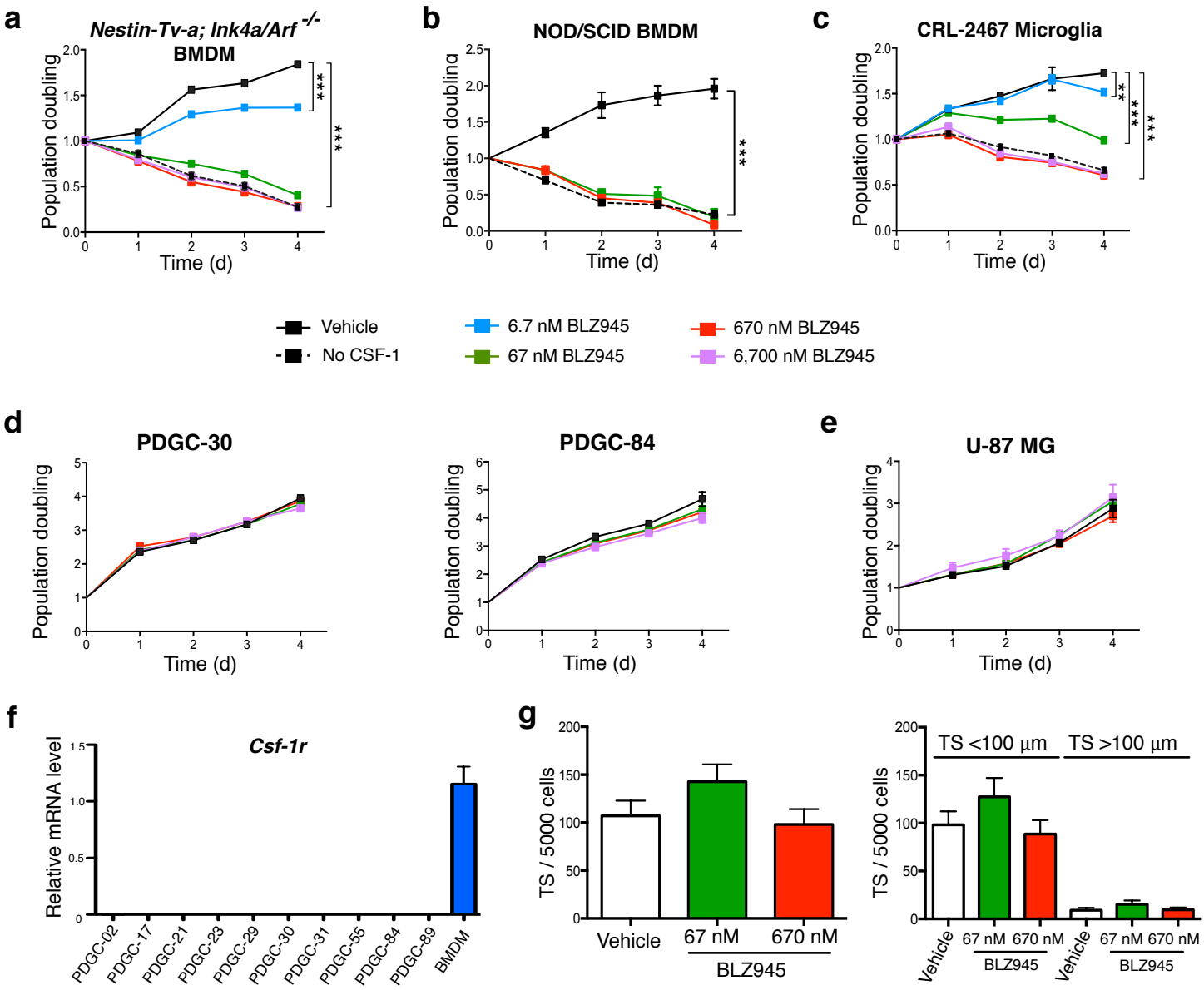

Supplementary Figure 3.
BLZ945 significantly decreases macrophage viability in culture but has no effect on PDG glioma cell line proliferation or tumor sphere formation. (a-b) BLZ945 significantly decreased the survival of BMDMs isolated from Nestin-Tv-a;*Ink4a/Arf*-/- or NOD/SCID immunodeficient mice, as determined by MTT assays. These effects were similar to those of CSF-1 deprivation in culture (dashed line). **(c)** BLZ945 reduced survival of the CRL-2467 microglia cell line. **(d)** The potency of BLZ945 in culture was tested on multiple PDGF-driven glioma cell (PDGC) lines derived from independent mice, including representative cell lines shown here and in Fig. 1d and Supplementary Fig. 7c, using MTT assays. There was no effect of BLZ945, even at concentrations up to 6,700 nM, which is 100x the EC_{50} for CSF-1R inhibition of macrophages in cell-based assays. *n*=3 replicates. **(e)** MTT assays were also used to quantify the dose-dependent effects of BLZ945 on the human glioma cell line, U-87 MG. Concentrations of BLZ945 up to 6,700 nM had no effect on U-87 MG proliferation *in vitro*, *n*= 3 replicates. **(f)** All of the PDGC lines used in this study are negative for *Csf-1r* mRNA expression; shown here relative to BMDMs as a positive control. qPCR assays were run in triplicate and normalized to *Ubc* for each sample. **(g)** BLZ945 did not affect the number or size of secondary tumor spheres (TS) derived from 3 independent mice bearing PDG tumors, which were seeded in duplicate wells for each condition. Graphs show mean ± s.e.m. *P* values were obtained by comparing each concentration of BLZ945 to the vehicle-treated control at the end of the experiment using unpaired two-tailed Student's t-test; ***P*<0.01, ****P*<0.001 in (a-c). For all the comparisons in (d, e) and (g), there were no significant differences.

Supplementary Figure 4

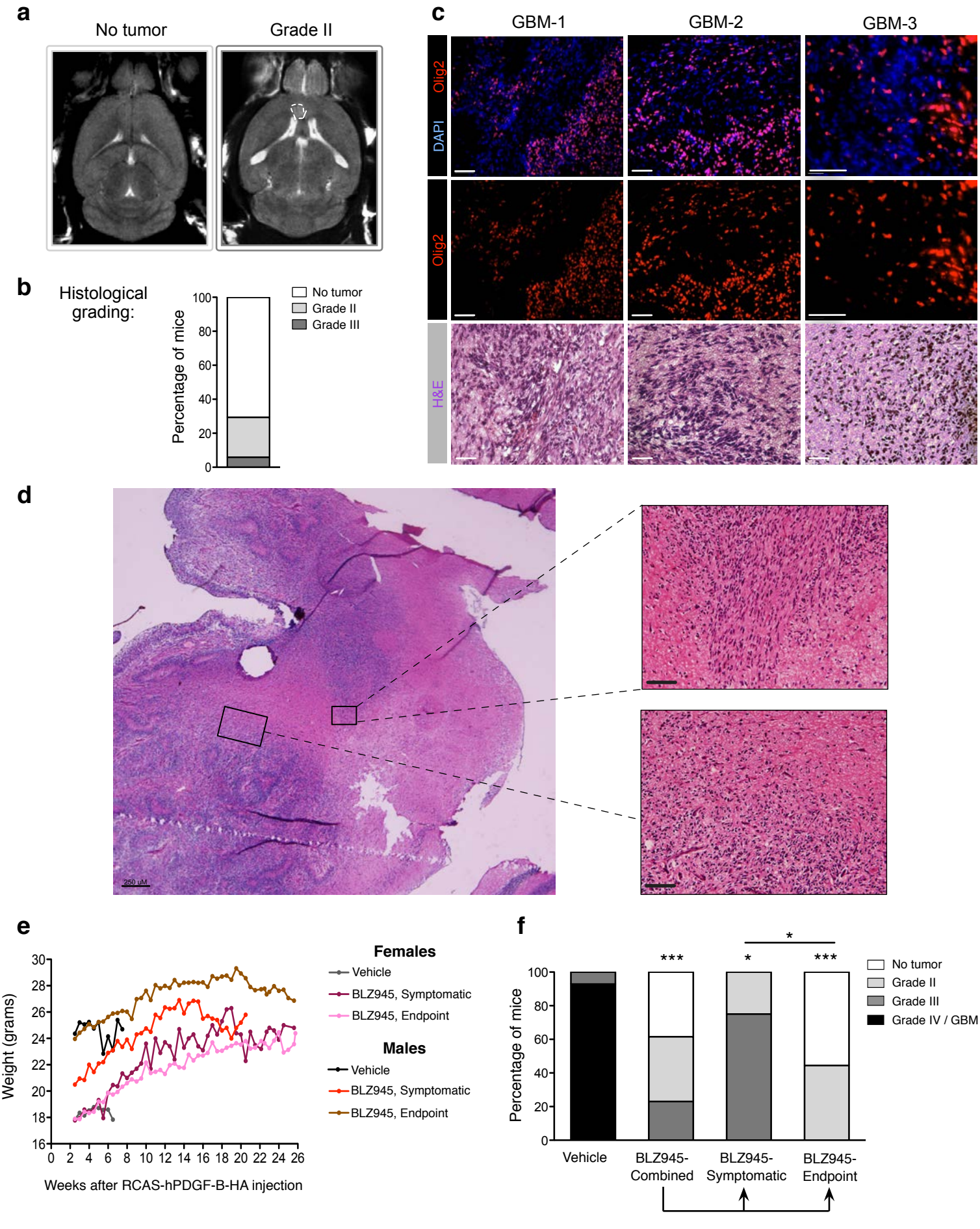

Supplementary Figure 4.
BLZ945 treatment significantly reduces tumor volume and grade, and is well-tolerated for long-term studies.
(a) Representative images of T2-weighted MRI scans from mice 2.5 weeks post-RCAS-hPDGF-B injection, corresponding to the timepoint when the trial in Fig. 1e-f was initiated. The dashed white line indicates the region where a tumor is visible in the image to the right. **(b)** Histological grading was also performed at this timepoint, and the presence or absence of a visible glioma (by hematoxylin and eosin staining) is indicated in the graph. **(c)** Representative images of GBM sections stained for Olig2 (glioma cells) and DAPI (upper panel), or H&E (lower panel) showing the infiltrative and invasive nature of PDG tumors. Representative images from three individual PDG mice (GBM 1-3) are shown. **(d)** Cross-sectional image representative of a glioma-bearing PDG mouse brain with magnified insets. Scale bars, 50 μm unless otherwise indicated. **(e)** BLZ945 is well-tolerated for up to 23.5 weeks (endpoint for long-term trial). Mean weight for female and male mice over the long-term survival trial depicted in Fig. 1f. Mice were divided by treatment group: vehicle and BLZ945. The BLZ945 treatment group was also subdivided into mice that became symptomatic and were sacrificed (symptomatic, n=3 females, n=2 males) or those mice that survived to the trial endpoint of 26 weeks (endpoint, n=3 females, n=6 males). At this timepoint these mice did not show any obvious macroscopic symptoms. **(f)** Tumor grade was examined in both cohorts of mice from the long-term survival trial shown in Fig. 1g. All vehicle-treated mice at the experimental endpoint had high-grade gliomas. By contrast, BLZ945-treated animals had significantly less-malignant tumors (vehicle and 'BLZ945 combined' groups are also shown in Fig. 1g). The BLZ945 combined group was then stratified into mice sacrificed as symptomatic during the trial (n=4), from those still asymptomatic when sacrificed at the endpoint (n=9). In each BLZ945 group, there was still a significant decrease in tumor grade compared to the vehicle cohort. Remarkably, there were no detectable lesions in 55.6% of the asymptomatic mice at end-stage. P values were obtained using Fisher's exact test; *P<0.05, ***P<0.001.

Supplementary Figure 5

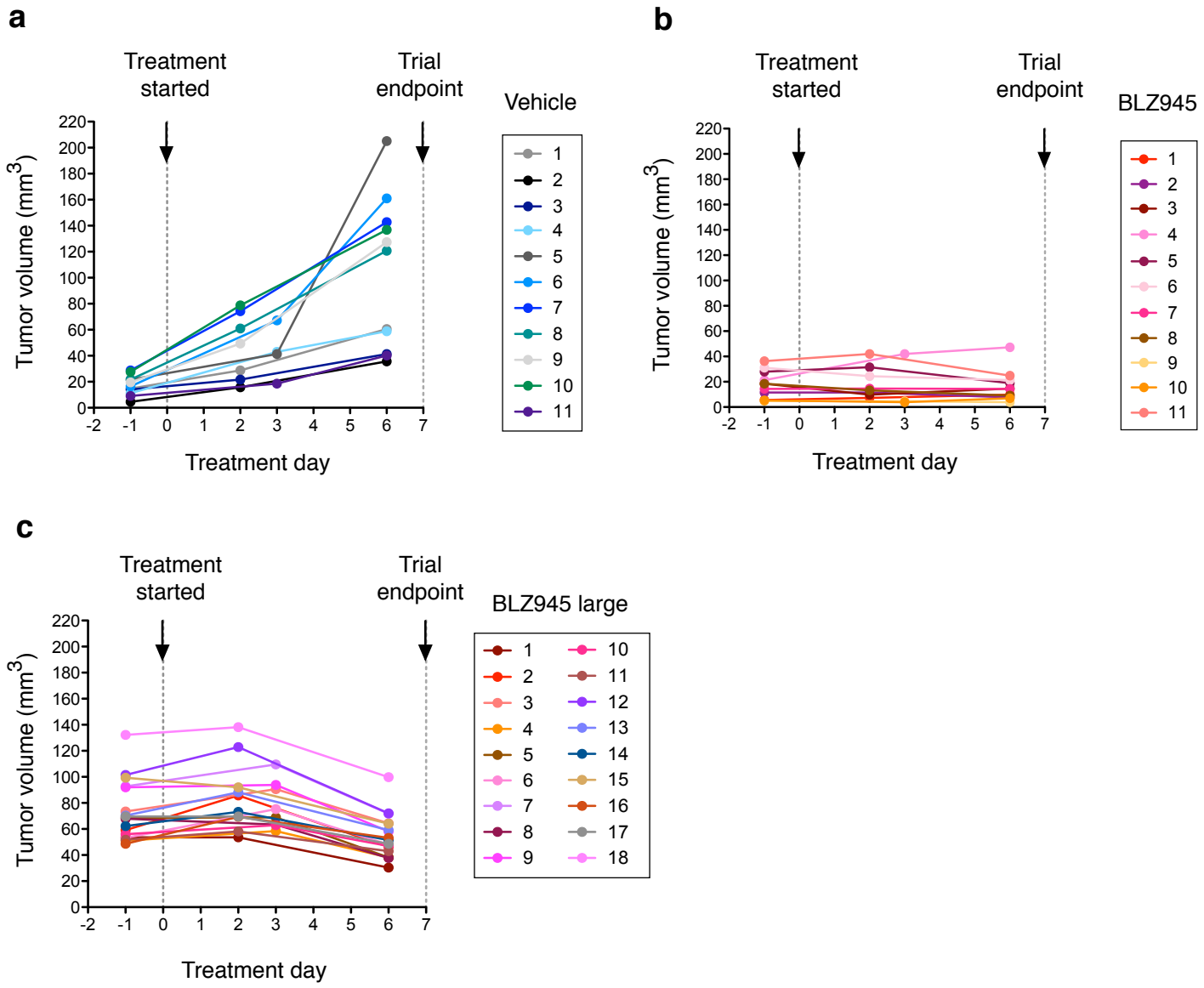

Supplementary Figure 5.
Glioma growth is inhibited in individual mice in response to BLZ945. PDG mice underwent MRI scans to assess tumor volume between 4-5 weeks post-injection and were randomly assigned to vehicle (20% captisol) or BLZ945 (200 mg/kg) treatment groups. **(a-b)** Tumor volume over the 7d time course is depicted for individual mice (from Fig. 2). Mice whose starting tumor volume was 4.5-40 mm^3 were treated with vehicle (a) or BLZ945 (b) (*n*=11 per group). **(c)** A third group of mice with tumor volume > 40 mm^3 was treated with BLZ945 ('BLZ945 large', *n*=18). Initial tumor volume in this group ranged from 48.7-132.3 mm^3. A vehicle cohort with tumor volume > 40 mm^3 was not included for comparison because the vast majority of mice would not have survived to the trial endpoint. Individual mice are represented by different colors, as shown in boxes at right of each graph.

Supplementary Figure 6

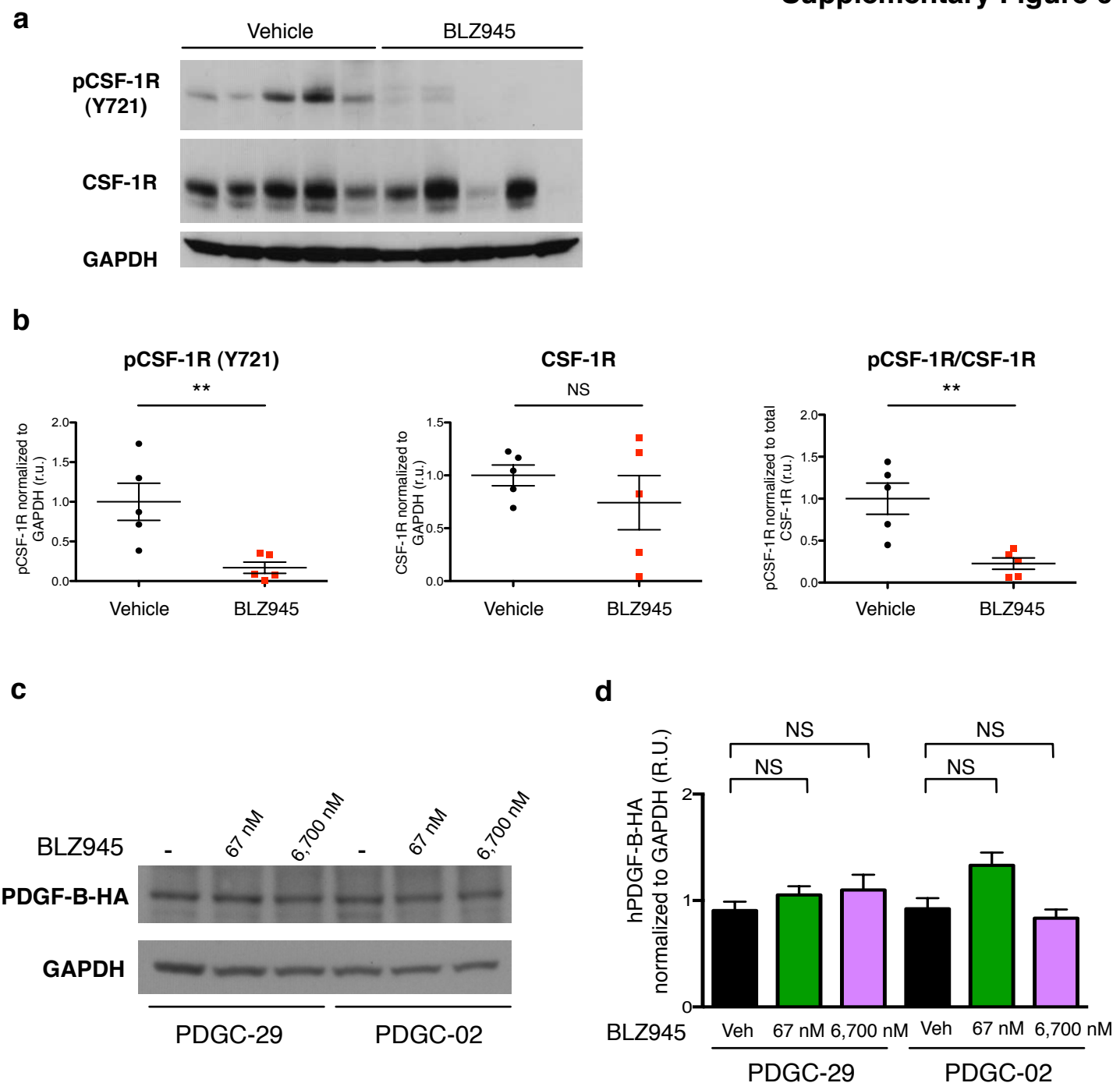

Supplementary Figure 6.
BLZ945 treatment inhibits intratumoral CSF-1R phosphorylation and does not affect tumor cell production of hPDGF-B. (a) Gliomas were harvested from PDG mice after 3d of treatment with either BLZ945 or vehicle. Samples were biochemically fractionated (see Supplementary Methods), and CSF-1R phosphorylation was assessed by western blotting. **(b)** Quantitation of the phosphorylated (pCSF-1R) and total CSF-1 receptor (CSF-1R) bands (normalized to GAPDH) using ImageJ software showed a significant reduction of pCSF-1R, but no significant change in CSF-1R levels. Each symbol represents an individual mouse. *n*=5 mice per group. **(c)** Two independent PDGC lines were treated with 67 nM, 6,700 nM BLZ945 or vehicle (veh) control. Protein was extracted 24 hours after treatment and human (h)-PDGFB levels were assessed by western blot for the HA epitope tag. (Production of RCAS-hPDGFB-HA virus is used to induce gliomas via somatic cell gene transfer in the PDG model). **(d)** Quantitation of the HA bands (normalized to GAPDH) using ImageJ software showed no significant change in hPDGF-B levels. *n*=3 replicates. These data confirm that BLZ945 does not alter hPDGF-B production by glioma cells in this model. Graphs show mean ± s.e.m. *P* values were obtained using unpaired two-tailed Student's t-test; NS= not significant, ***P*<0.01.

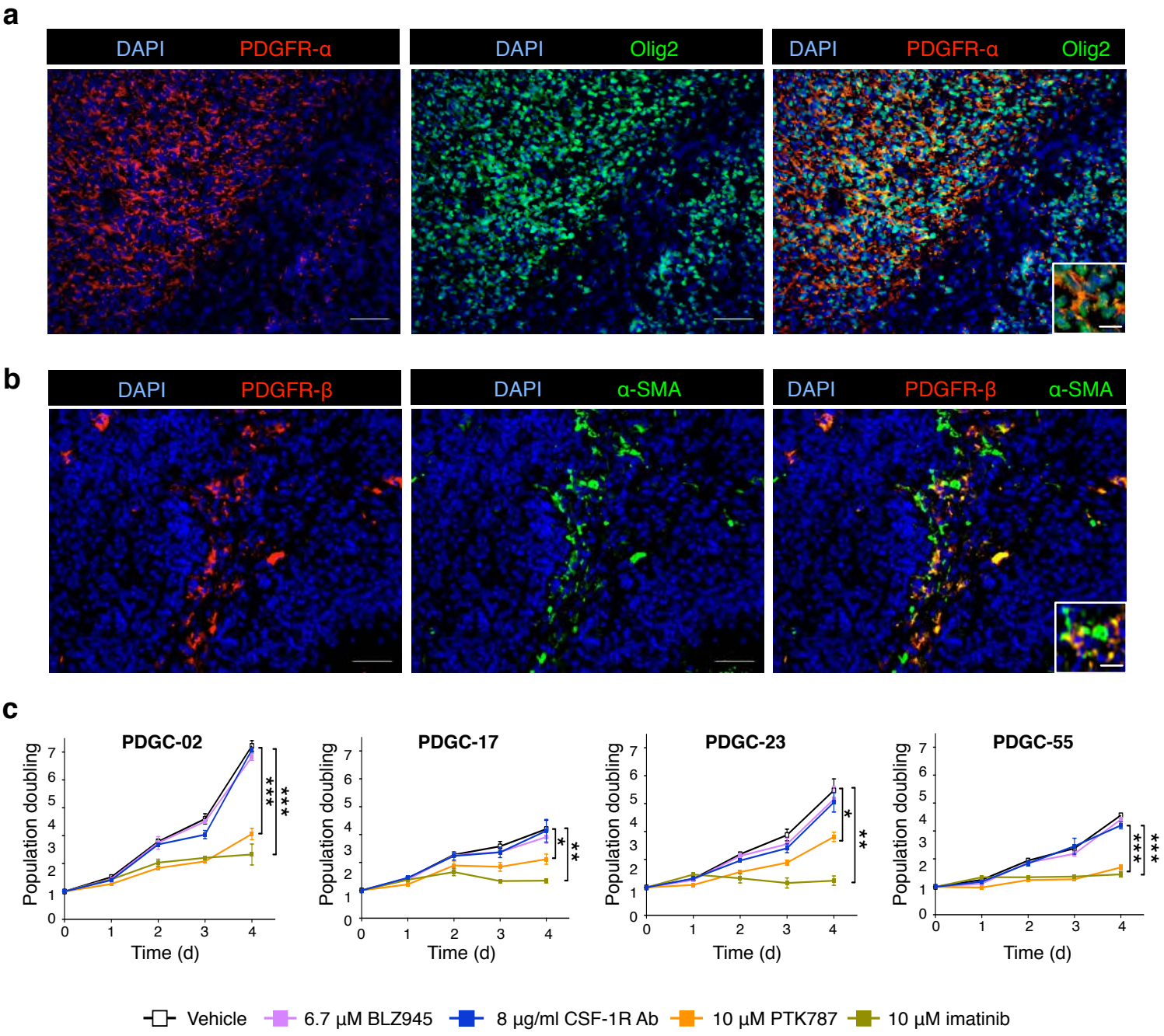

Supplementary Figure 7.
Glioma cells express PDGFR-α and are sensitive to PDGFR inhibition, but they do not respond to CSF-1R inhibition. (a-b) Representative images from PDG tumors stained for Olig2 (glioma cells), α-SMA (pericytes, vascular smooth muscle cells), PDGFR-α or PDGFR-β, and DAPI. PDGFR-α is expressed by Olig2^{+} glioma cells, and PDGFR-β is expressed by α-SMA^{+} perivascular cells. Neither receptor is detectable on macrophages by immunostaining (data not shown). Main image scale bars, 50 μm, image inset scale bars, 10 μm. **(c)** PDGC lines in culture are sensitive to the PDGFR inhibitors PTK787 and imatinib (STI-571/Gleevec) as determined by MTT assays. By contrast, glioma cell proliferation was not affected by treatment with BLZ945 at concentrations up to 6.7 μM, or treatment with a CSF-1R neutralizing antibody (AFS98) at 8 μg/ml. A rat IgG control antibody had no effect on glioma cell viability or proliferation (data not shown). *n*=3 replicates. Graphs show mean + s.e.m. *P* values were obtained using unpaired two-tailed Student's t-test compared to the vehicle (DMSO) control. **P*<0.05, ***P*<0.01, ****P*<0.001.

Supplementary Figure 8

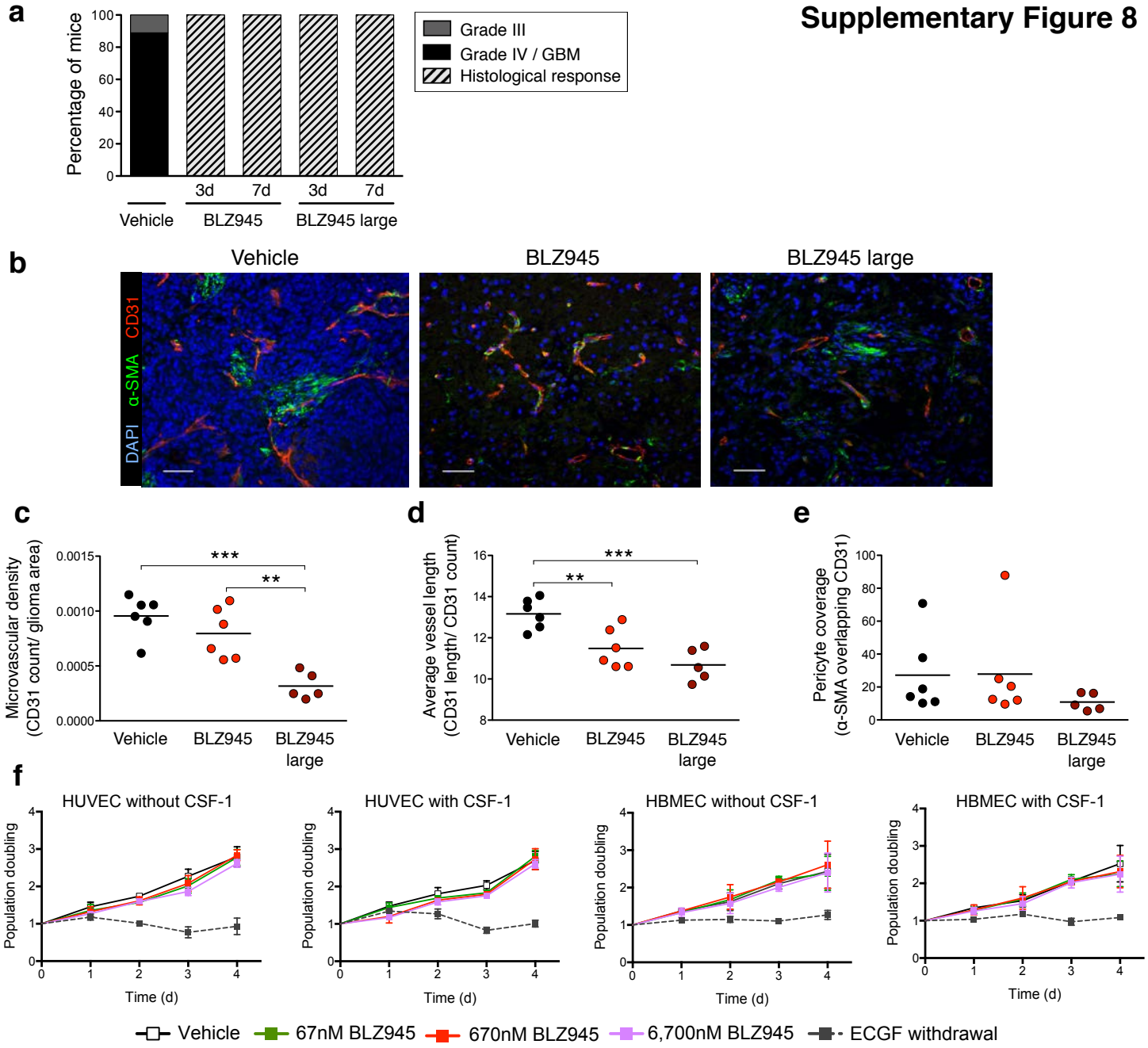

Supplementary Figure 8.
Evidence of pronounced histological response and decreased vascularity in BLZ945-treated PDG gliomas, without a direct effect on endothelial cell survival. (a) Tissues from the 7d trial in PDG mice were graded histologically (*n*=5-10 per group). While all of the vehicle-treated PDG mice had high-grade gliomas, of which 89% had grade IV GBMs, 100% of the BLZ945-treated PDG mice exhibited a histological response already evident at 3d. This response was characterized by a clear depopulation of glioma cells, with maintenance of the stroma and leukocytic infiltrate (representative image shown in Fig. 3a). **(b)** Representative images of gliomas from the endpoint of the 7d BLZ945 trial stained for CD31 (endothelial cells), smooth muscle actin (α-SMA, pericytes), and DAPI. **(c)** Graphs showing quantitation of the microvascular density (CD31 count relative to the total glioma area), **(d)** the average vessel length (CD31 length relative to the CD31 count), and **(e)** pericyte coverage (percentage of α-SMA$^+$ staining overlapping CD31$^+$ staining). There were no significant differences in pericyte coverage among the treatment groups. **(f)** Human umbilical vein endothelial cells (HUVEC, *n*=4) or human brain microvascular endothelial cells (HBMEC, *n*=4) were seeded on gelatin-coated 96 well plates (2,500 cells per well). Cells were treated for 4d with vehicle or increasing concentrations of BLZ945 (67 nM, 670 nM, and 6,700 nM) in the presence or absence of CSF-1. Cell viability was assessed by MTT assays at the indicated time points. HUVEC and HBMEC proliferation was not significantly affected by BLZ945, whereas endothelial cell growth factor (ECGF) withdrawal resulted in growth arrest of HUVEC and HBMEC cells. Circles represent individual mice (*n*=5-6 per group), and horizontal lines represent the mean. Scale bar, 50 µm. Graphs show mean (c-e) and mean ± s.e.m (f). *P* values were obtained using unpaired two-tailed Student's t-test; ***P*<0.01, ****P*<0.001.

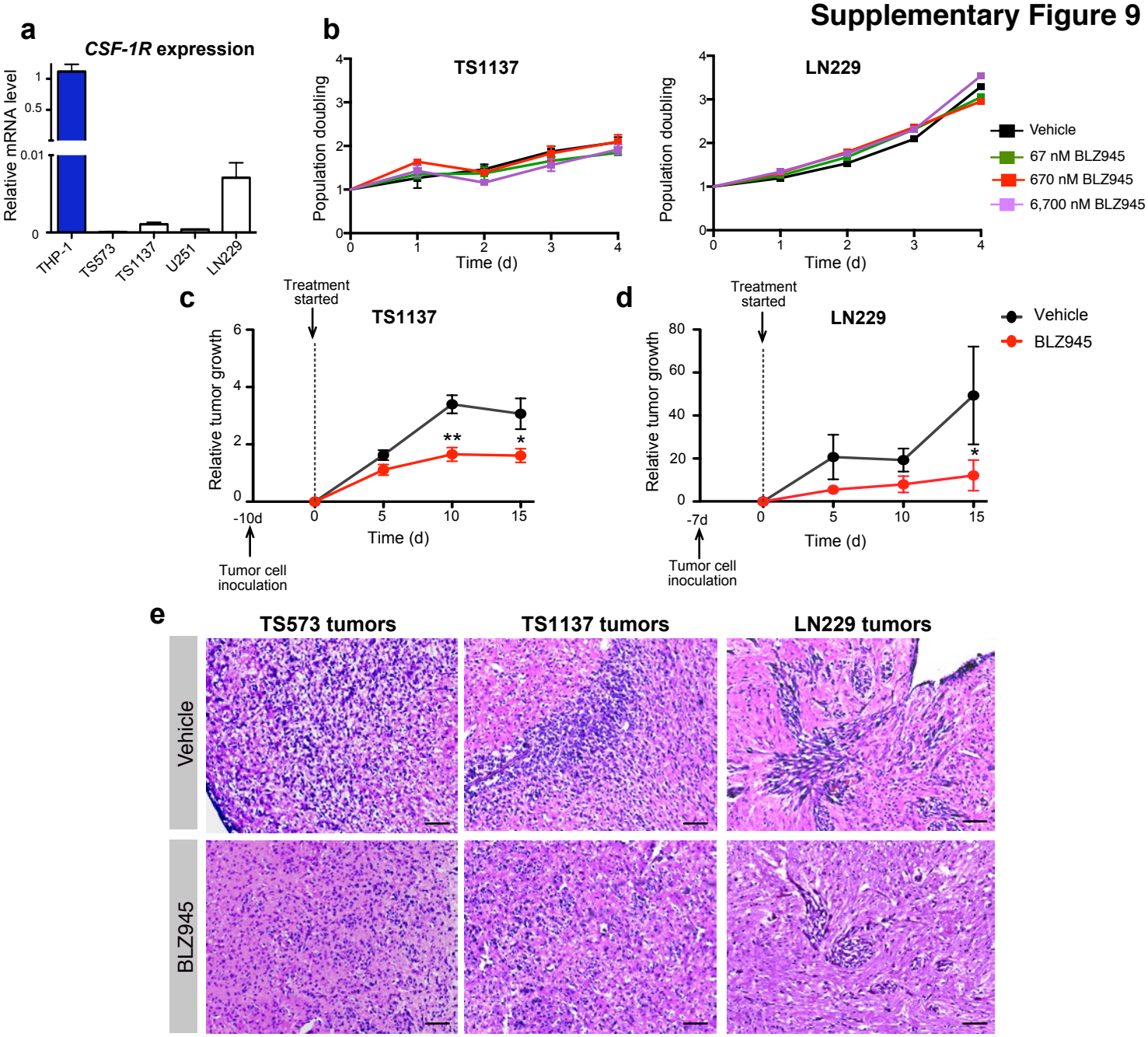

Supplementary Figure 9.

BLZ945 inhibits orthotopic growth of additional human proneural glioma tumor sphere and cell lines, and alters tumor histology of human xenografts. (a) Patient-derived proneural glioma tumor sphere cells (TS1137) and the established glioma cell line (LN229) express negligible levels of *CSF-1R* mRNA by qPCR (compared here with expression levels presented in Fig. 4a). Expression of *CSF-1R* in each cell type is graphed relative to the THP-1 macrophage cell line (used as a positive control) and fold changes are as follows: TS573, no detectable expression; TS1137, 1200-fold less; U251, 4000-fold less; LN229, 164-fold less than THP-1, *n*=3 replicates. **(b)** Concentrations up to 6,700 nM BLZ945 did not affect survival or proliferation of the human lines TS1137 and LN229 in culture as determined by MTT assay, *n*=3 independent experiments. **(c, d)** NOD/SCID mice were injected intracranially with (c) $5x10^4$ TS1137 cells or (d) $5x10^4$ LN229 cells. Treatment with BLZ945 was initiated when tumors were in a positive growth phase determined by bioluminescence imaging (BLI) output, which corresponded to 10d post-injection for TS1137, and 7d post-injection for LN229. Mice were randomly assigned to vehicle (*n*=10-18) or BLZ945 (*n*=10-16) treatment groups. Tumor growth was evaluated every 5d for 15d, at which point vehicle-treated mice became symptomatic and both cohorts were sacrificed for further analyses. **(e)** Representative H&E images of vehicle-treated (upper panels) or BLZ945-treated (lower panels) tumors from TS573, TS1137 and LN229 xenografts. Histological analyses showed a pronounced difference in BLZ945-treated tumors, which were substantially smaller in size and less invasive compared to vehicle-treated tumors. Scale bar, 50 μm. Graphs in (a-d) represent mean and s.e.m. All comparisons between treatment groups in (b) were not significant using unpaired two-tailed Student's t-test. *P* values in (c-d) were obtained using nonparametric two-tailed Mann Whitney test; **P*<0.05, ***P*<0.01.

Supplementary Figure 10

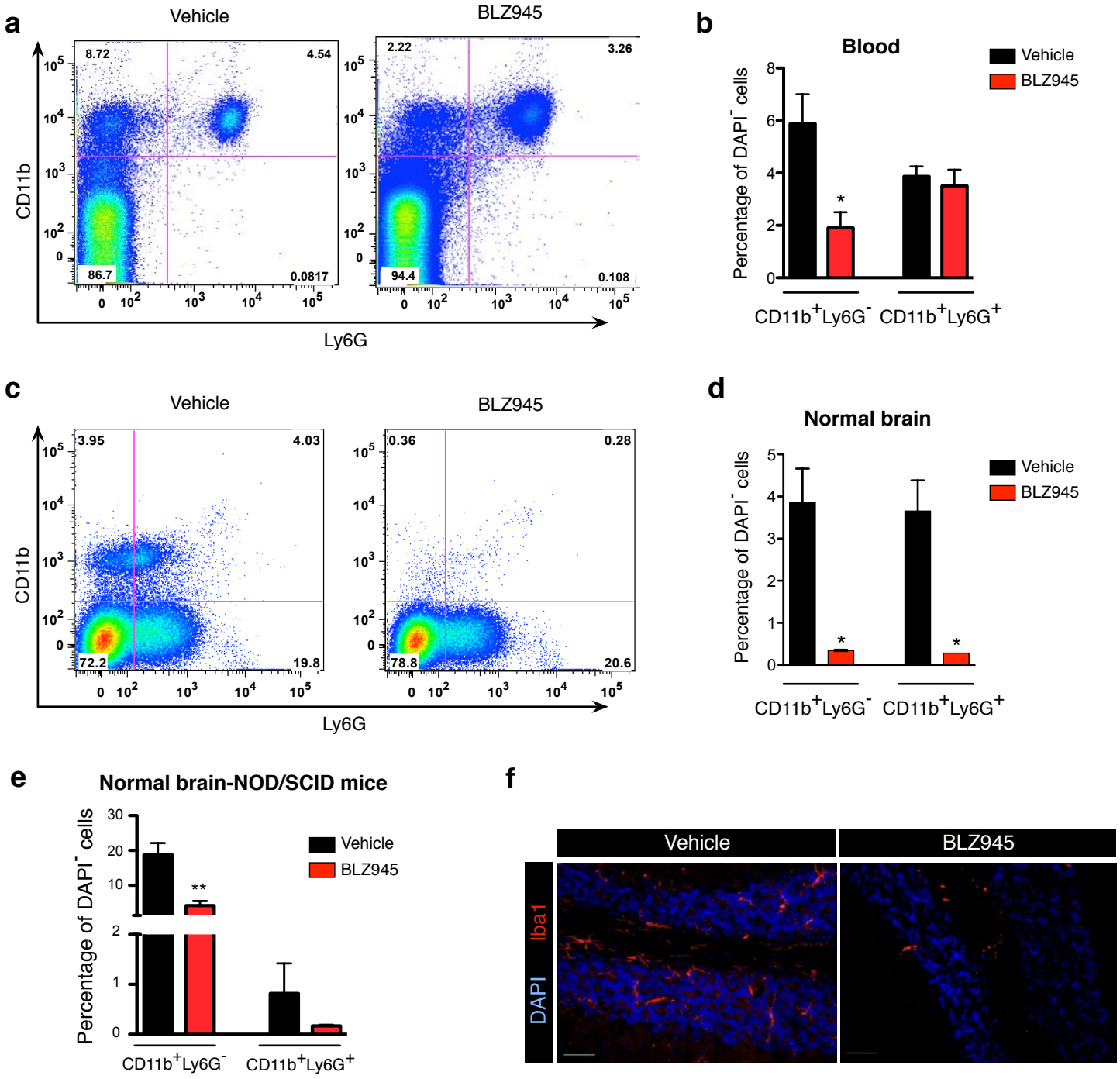

Supplementary Figure 10.
CSF-1R inhibition depletes circulating monocytes and normal microglia. (a-e) Normal non-glioma bearing WT C57BL/6 (a,b), Nestin-Tv-a;*Ink4a/Arf-/-* (c,d), or NOD/SCID (e) mice were treated with vehicle (20% captisol; *n*=3-5) or 200 mg/kg BLZ945 (*n*=2-5) once per day for 7d, and the following day the animals were sacrificed, and blood or brains prepared for flow cytometry (with collagenase III digestion for brain). Representative flow cytometry plots and quantitation of $CD11b^+Ly6G^-$ and $CD11b^+Ly6G^+$ cells are depicted for blood (a,b) and brain (c,e). Graphs show mean + s.e.m. **(f)** Representative images of the adjacent normal brain from the contralateral hemisphere opposite TS573 xenografts from vehicle- or BLZ945-treated mice stained for Iba1 and DAPI. Scale bar, 50 μm. *P* values were obtained using unpaired two-tailed Student's t-test; **P*<0.05, ***P*<0.01.

Supplementary Figure 11

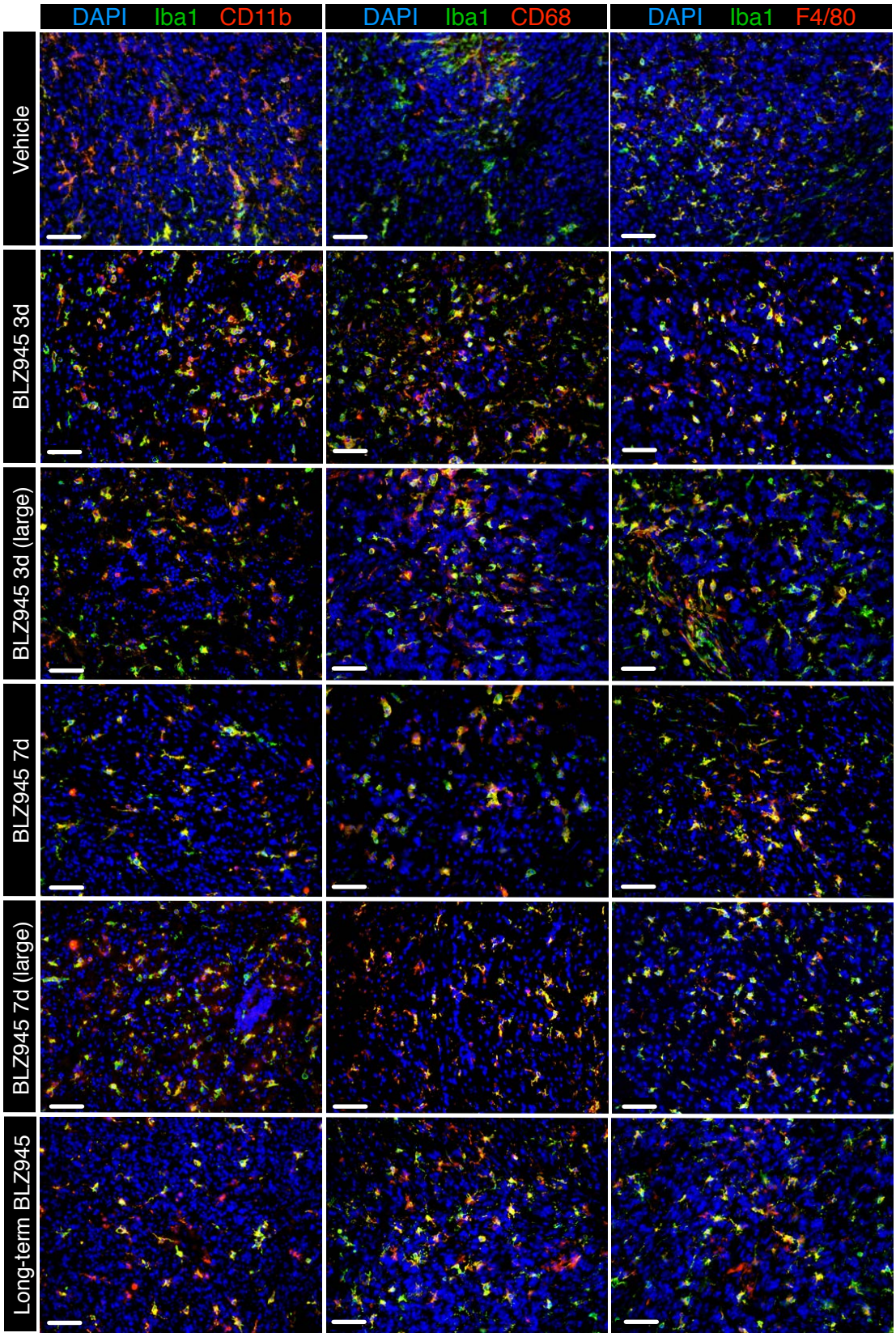

Supplementary Figure 11.
TAMs are not depleted in BLZ945-treated tumors as assessed by a series of established macrophage markers; Iba1, CD11b, CD68 and F4/80. Representative images of gliomas from 3d, 7d and 26 week short-term and long-term BLZ945 trials (see Figs.1, 2), co-stained for Iba1 with CD11b, CD68 or F4/80. Nuclei were stained with DAPI. Vehicle-treated gliomas from the 7d trial were used as a control for comparison. Using this panel of established macrophage/microglia markers, there is no evident depletion in any of the BLZ945-treated tumors compared to vehicle. Scale bar, 50 μm.

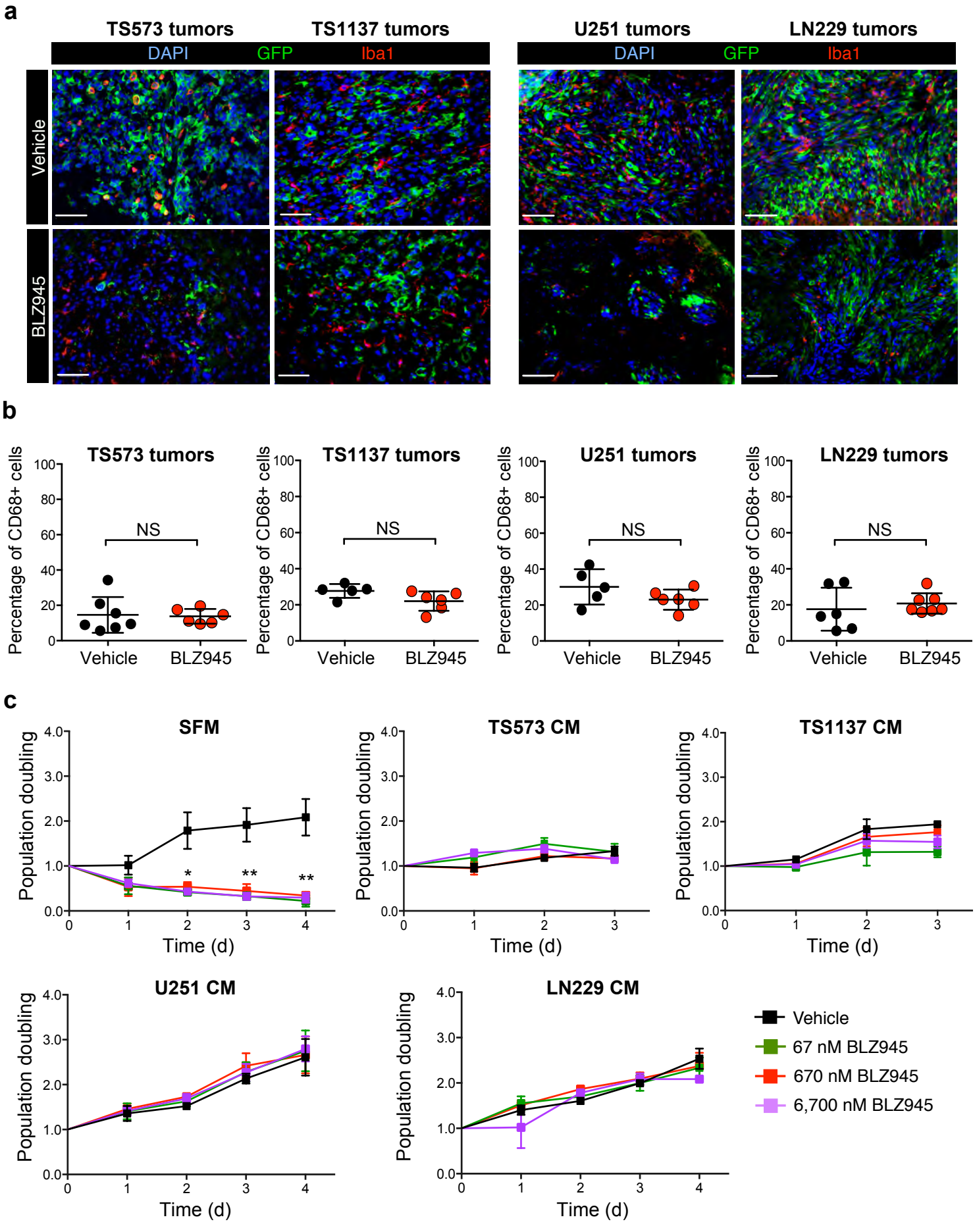
a
TS573 tumors
TS1137 tumors
U251 tumors
LN229 tumors
DAPI
GFP
Iba1
Vehicle
BLZ945
b
TS573 tumors
TS1137 tumors
U251 tumors
LN229 tumors
Percentage of CD68+ cells
NS
Vehicle
BLZ945
c
SFM
TS573 CM
TS1137 CM
U251 CM
LN229 CM
Population doubling
Time (d)
*
**
**
Vehicle
67 nM BLZ945
670 nM BLZ945
6,700 nM BLZ945

Supplementary Figure 12.

BLZ945 does not deplete TAMs in orthotopic models of human proneural glioma. (a) Representative immunofluorescence images of vehicle-treated (upper panels) or BLZ945-treated (lower panels) tumors from patient-derived tumor sphere (TS) xenografts (TS573 and TS1137) or xenografts of established human glioma cell lines (U251 and LN229) stained for GFP (tumor cells), Iba1 (macrophages/microglia) and DAPI. **(b)** Quantitation of macrophage numbers (CD68 count relative to DAPI count) in TS573, TS1137, U251 and LN229 xenograft tumors revealed no significant differences between the vehicle or BLZ945 treatment groups. **(c)** BMDMs were treated with vehicle or increasing concentrations of BLZ945 (67 nM, 670 nM, and 6,700 nM) in the presence or absence of conditioned media (CM) derived from the human GBM TS lines TS573 and TS1137, or CM from the established human glioma cell lines U251 and LN229. BMDM viability was assessed by MTT assays at the indicated time points and viability was not affected by BLZ945 when simultaneously exposed to CM from each of the different human cell lines. This is in contrast to a rapid reduction in BMDM survival when exposed to BLZ945 in the presence of serum-free media (SFM) complemented with CSF-1, as similarly observed in Fig.1c. Graphs show mean ± s.e.m. Circles represent individual mice (n=5-7 per group), and horizontal lines represent the mean. Scale bar, 50 μm. P values were obtained using unpaired two-tailed Student's t-test; NS= not significant, *P<0.05 **P<0.01.

Supplementary Figure 13

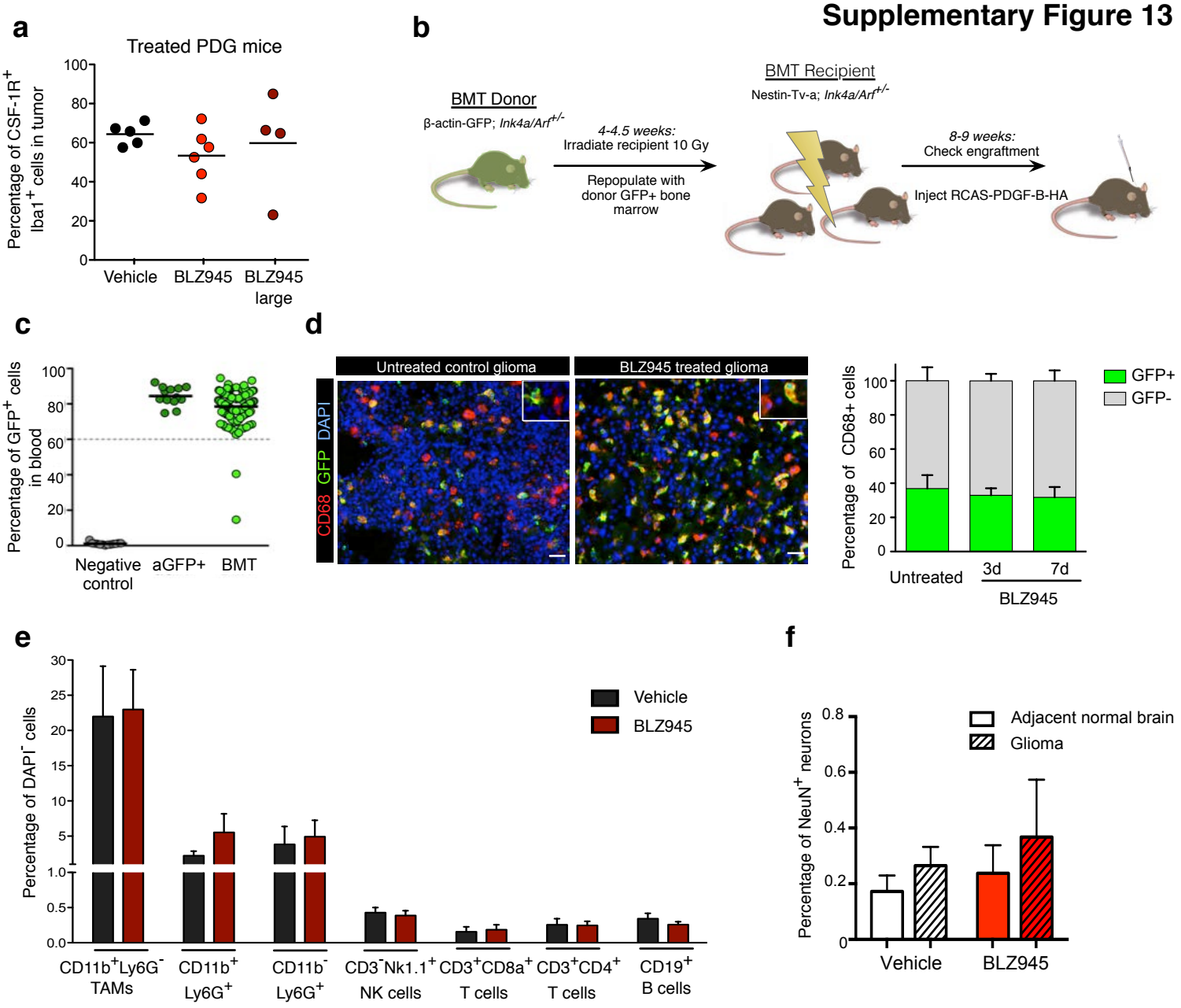

Supplementary Figure 13.

BLZ945 treatment does not affect CSF-1R expression by TAMs, recruitment of bone marrow-derived cells, or proportions of adaptive immune cells and neurons in gliomas. (a) Quantitation of the percentage of Iba1$^+$ macrophages that are CSF-1R$^+$ within treated PDG tumors at 7d. Circles represent individual mice (*n*=4-6 per group), and horizontal lines represent the mean. **(b)** Schematic of bone marrow transplantation (BMT) experiment and timing of tumor initiation in PDG mice. **(c)** The percentage of GFP$^+$ cells in the peripheral blood of GFP$^-$ control mice (*n*=13), β-actin-GFP (aGFP$^+$; *n*=13) and BMT mice (≥4 weeks after BMT; *n*=126) was analyzed by flow cytometry. **(d)** PDG tumors were initiated in a subset of the BMT cohort following confirmation of BM reconstitution, and animals were separated into two groups: untreated controls or BLZ945-treated (200 mg/kg). Representative images of untreated or 7d BLZ945-treated BMT gliomas stained for CD68 (macrophages, red), GFP$^+$ BMDMs (green), and DAPI (blue). Insets show higher magnification images of GFP$^+$ BMDMs and GFP$^-$ microglia. Scale bar, 50 μm. Quantitation of GFP$^-$ microglia and GFP$^+$ BMDMs relative to total number of CD68$^+$ macrophages by immunofluorescence from tumors of untreated (*n*=7), 3d BLZ945-treated (*n*=10) or 7d BLZ945-treated (*n*=4) BMT mice. **(e)** Gliomas from the short-term 7d BLZ945 large trial were processed to a single cell suspension with collagenase III for flow cytometric analysis of immune cell populations. Quantitation of immune cell infiltration in vehicle (*n*=5) or BLZ945 large (*n*=6) tumors showed that BLZ945 treatment does not cause a change in immune cell proportions in PDG gliomas. **(f)** Quantitation of number of NeuN$^+$ neurons relative to total DAPI$^+$ cells in adjacent normal brain or within gliomas of vehicle- or BLZ945-treated animals (*n*=4-5 per group). Data are presented as mean + s.e.m. *P* values were obtained using unpaired two-tailed Student's t-test and all comparisons between treatment groups in all panels were not statistically significant.

Supplementary Figure 14

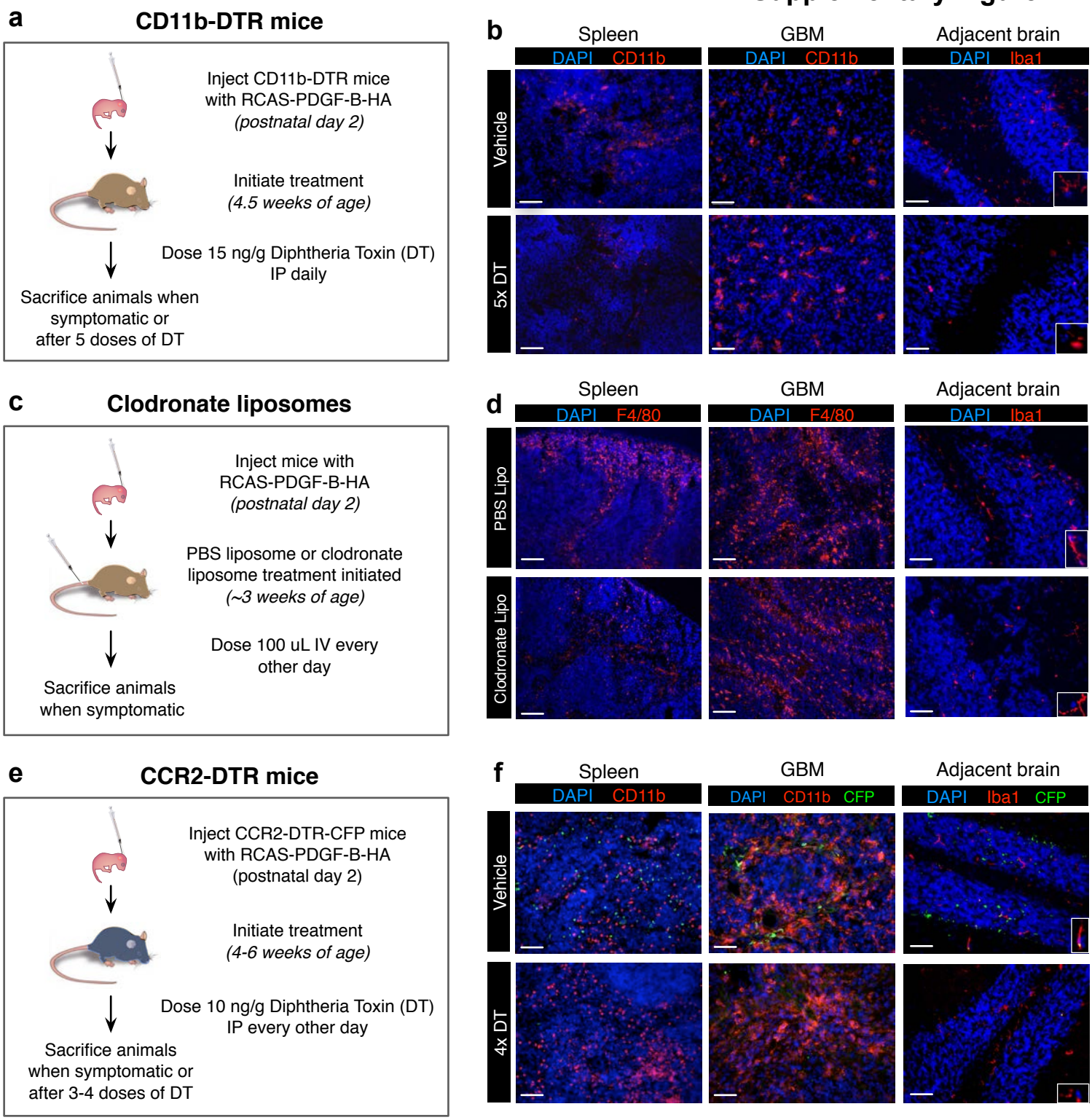

Supplementary Figure 14.

Additional strategies used with the objective of TAM depletion in the PDG model. (a) Schematic of treatment of CD11b-DTR glioma-bearing mice. We and others have previously used the transgenic CD11b-DTR model [1,2] to deplete microglia and macrophages in the brain in the context of development [3] and focal injury [4]. In an effort to deplete TAMs in gliomas, tumors were initiated in Nestin-Tv-a;Ink4a/Arf$^{+/-}$;CD11b-DTR mice by intracranial injection of RCAS-PDGF-B-HA at postnatal day 2 (P2). Starting at 4.5 weeks post-injection, when animals were beginning to show symptoms, mice were randomly assigned to vehicle or 15 ng/g diphtheria toxin (DT) treatment groups. Control and experimental mice were intraperitoneally (IP) injected every day for up to 5 days, and euthanized 24 hrs after the last injection. More extended chronic treatment was not possible because of reported DT toxicity [5]. **(b)** Representative images are shown from spleen, GBM and adjacent normal brain in mice that received 5 injections. Tissues were stained for the macrophage/ microglia markers CD11b or Iba1, showing that while macrophages were depleted in the spleen and in the normal brain by DT treatment, there was no evident depletion of GBM TAMs. **(c)** Given that BMT experiments demonstrated that macrophages originally recruited from the periphery constitute a substantial proportion of GBM TAMs (Supplementary Fig. 13d), we undertook two strategies to deplete these peripheral macrophage precursors, with the expectation that this would then result in a reduction in GBM TAM numbers. First we utilized clodronate-filled liposomes that do not cross the blood-brain barrier but selectively deplete monocytes in the circulation and peripheral tissues [6]. This clodronate liposome strategy has previously been used in multiple transplantable tumor models to deplete TAMs [7-9]. Schematic of clodronate liposome trial in PDG model: tumors were initiated in Nestin-Tv-a;Ink4a/Arf$^{-/-}$ mice by intracranial injection of RCAS- PDGF-B-HA at P2. At 21-24 days old, mice were randomly assigned to PBS liposome (vehicle) or clodronate liposome treatment groups. Liposomes were obtained from clodronateliposomes.org. Animals were intravenously (IV) injected via the tail vein with 100 µl every other day until the mice became symptomatic, at which point they were euthanized. **(d)** Representative images are shown from spleen, GBM and adjacent normal brain in mice that received 6 doses of liposomes. Tissues were stained for F4/80 or Iba1, showing that while macrophages were effectively depleted in the spleen by clodronate liposome treatment, there was no evident depletion of microglia in the adjacent normal brain or of GBM TAMs. This absence of depletion of normal microglia can be explained by the inability of clodronate liposomes to cross the blood-brain barrier, and the observation from lineage-tracing experiments that there is a minimal contribution from the bone marrow to microglia in the normal brain under resting conditions [10]. These results also indicate that despite peripheral depletion of macrophage precursors there was again no obvious reduction in glioma TAM numbers. **(e)** Schematic of treatment of CCR2-DTR glioma-bearing mice. CCR2^{+} inflammatory monocytes are commonly recruited to give rise to TAMs in other tumor microenvironments [11,12], and thus we wanted to determine if depletion of CCR2^{+} cells would lead to depletion of glioma TAMs. To generate CCR2-DTR-eCFP^{+} positive animals, Nestin-Tv-a;Inka/Arf$^{-/-}$ mice were bred to hemizygous CCR2-DTR-eCFP transgenic mice [13]. Tumors were initiated in the Nestin-Tv-a;Inka/Arf$^{+/-}$ CCR2-DTR-eCFP^{+} offspring by intracranial injection of RCAS-PDGF-B-HA at P2. Mice were then monitored for tumor development, and when the first littermate became symptomatic, mice began receiving intraperitoneal injections of 10 ng/g DT every other day; 3-4 doses of DT in total. More extended treatment was not possible because of dose-limiting toxicity of DT. **(f)** Immunofluorescence staining showed that DT treatment depleted CCR2-DTR-eCFP^{+} cells (visualized in green) from spleen, GBM and the adjacent normal brain, compared to untreated controls. However, this did not result in any evident depletion of total macrophage populations in any of these tissues. **(g)** Blood samples were collected before and after DT administration for flow cytometry, revealing no effects of DT treatment in transgene negative controls (left set of flow cytometry plots), while CCR2-DTR-eCFP^{+} cells were effectively depleted and CD11b^{+} monocytes were diminished in transgenic littermates (compare circles in pre- and post-DT plots on the right). Taken together, while each of these three approaches successfully depleted macrophages in normal tissues or the periphery of glioma-bearing animals (spleen, blood, and/ or brain), there was no evident reduction in glioma TAM numbers.

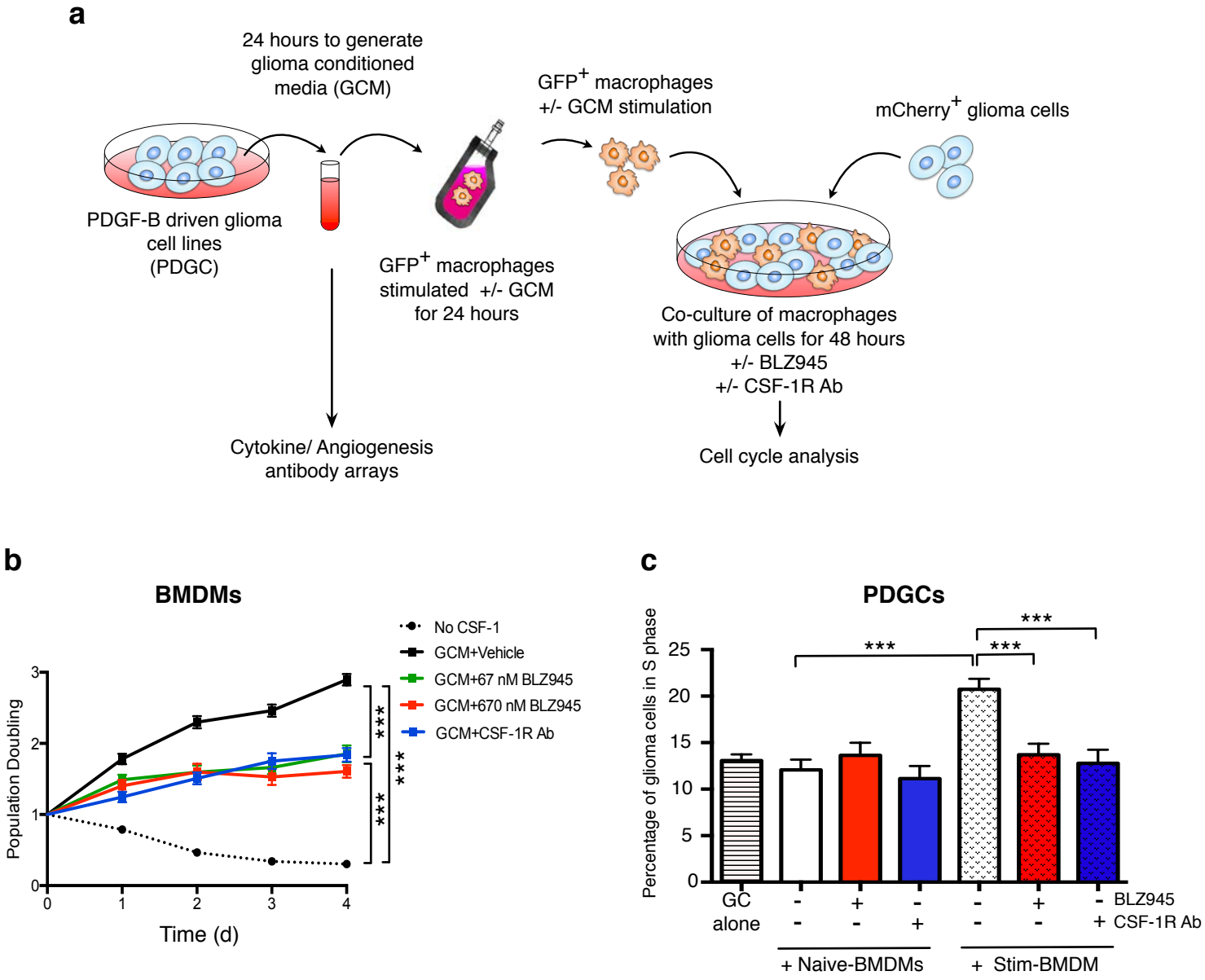

Supplementary Figure 15.
Schematic of co-culture assay used to assess stimulation of glioma cell proliferation by macrophages, and its perturbation by CSF-1R inhibition. (a) Schematic of co-culture experiments prior to glioma-conditioned media (GCM) preparation and cell cycle analysis. mCherry-labeled PDGC-23 glioma cells were plated and allowed to attach for 24h. Media was changed to serum-free DMEM for 24h in order to collect GCM. GCM was then used to stimulate GFP$^+$ macrophages (referred to as stimulated-BMDMs or Stim-BMDMs) for 24h without further addition of CSF-1 or fresh media. Stimulated-BMDMs were then collected, centrifuged and resuspended in fresh GCM. They were then mixed with mCherry$^+$ glioma cells (which had been serum-starved overnight) at a 1:1 ratio, in the presence or absence of BLZ945, or a CSF-1R antibody (AFS98, 8 μg/ml), or the relevant controls. Naïve-BMDMs that were not subjected to GCM stimulation were used for comparison. Co-culture of naïve- or stimulated-BMDMs was conducted for 48h prior to evaluation of glioma cell cycle entry by flow cytometry analysis. For the cytokine and angiogenesis arrays in Supplementary Fig. 16, GCM was collected from the different PDGC lines as described above. **(b)** Protection from cell death induced by BLZ945 or the CSF-1R neutralizing antibody is conferred when BMDMs are cultured in the presence of GCM (from the PDGC-23 line in this example). *n*=4 replicate experiments. **(c)** Glioma cells (PDGC-23) were co-cultured with naïve- or stimulated-BMDMs, as described in (a). Co-cultures were treated +/- BLZ945 or +/- CSF-1R neutralizing antibody for 48h before glioma cell (GC) cycle entry was evaluated. Results showed an increase in glioma cell proliferation when cultured with stimulated-BMDMs but not naïve-BMDMs, and this effect was reversed by BLZ945 or the CSF-1R antibody. *n*=3 replicates. BLZ945 was used at 670 nM in all cell culture assays unless otherwise specified. Graphs show mean ± s.e.m. *P* values were obtained using unpaired two-tailed Student's t-test compared to the indicated groups; ***P<0.001.

Supplementary Figure 16

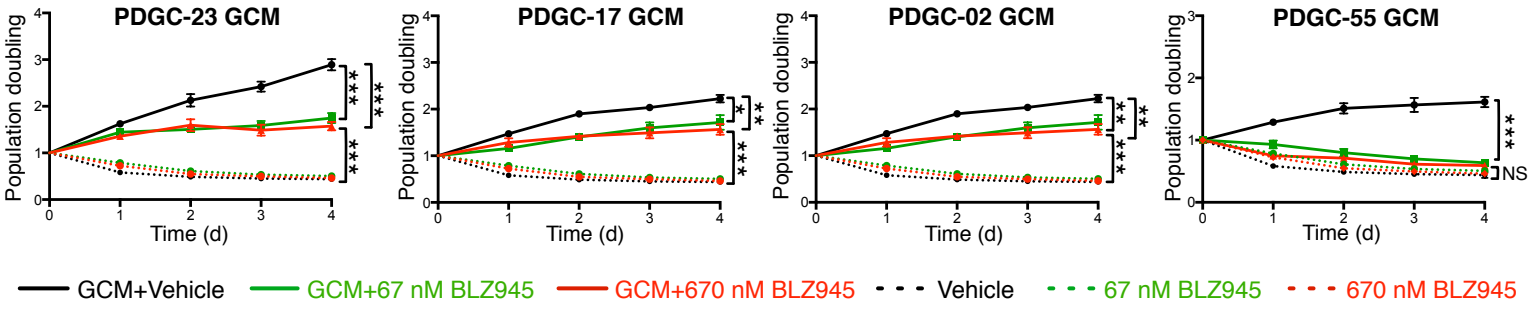

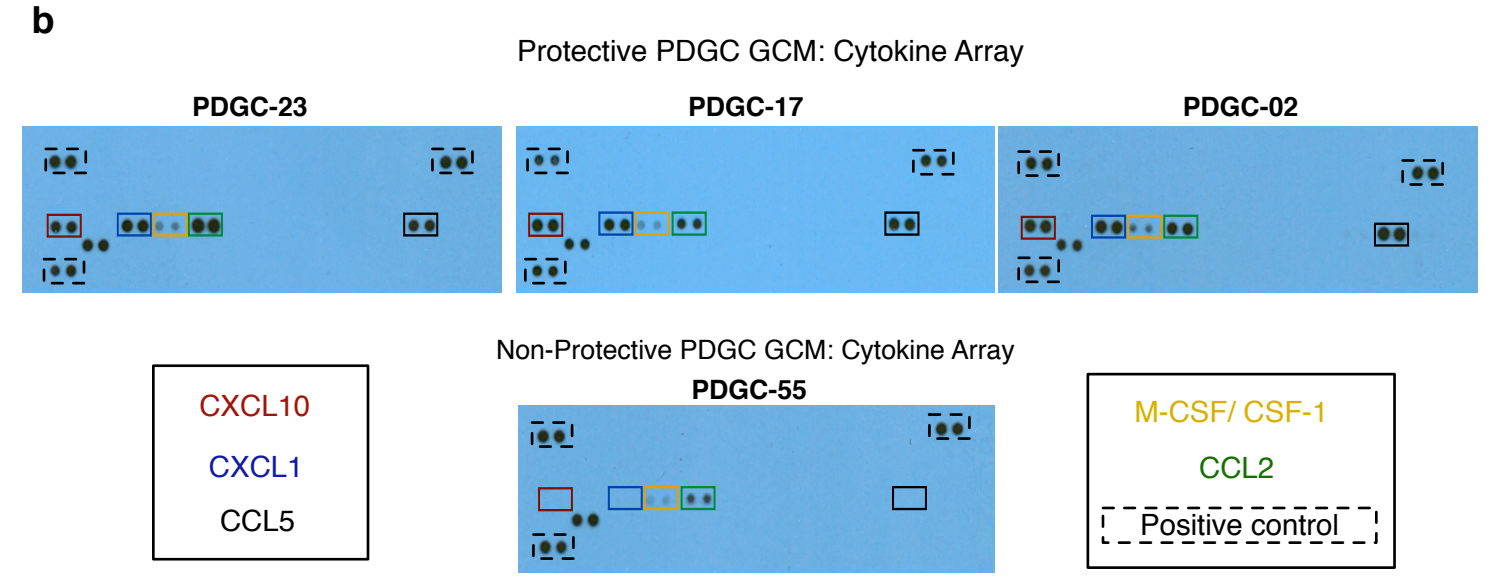

c

Cytokine Array

	CXCL10	CCL5	CXCL1	CCL2	M-CSF
PDGC-23	++	++	+	++	+
PDGC-17	++	++	+	++	+
PDGC-02	++	++	+	++	+
PDGC-55	-	-	-	+	+

Angiogenesis Array

	CXCL10	CXCL1	GM-CSF	VEGF	SDF-1	HB-EGF	Angiopietin-1	Amphiregulin	Leptin	DPPIV
PDGC-23	+++	+++	+	+	+	+	+	+	+	+
PDGC-17	+++	++++	+	+	+	+	+	+	+	+
PDGC-02	++	+++	+	+	+	+	+	+	+	+
PDGC-55	-	-	-	-	-	-	-	-	-	-

Supplementary Figure 16.
Identification of differentially secreted cytokines and angiogenic factors produced by protective and non-protective glioma cell lines. MTT assays were performed over a 4d time course on BMDMs stimulated with GCM from different PDGC lines. GCM produced by PDGC-23, PDGC-17 and PDGC-02 induced BMDM proliferation and protected BMDMs from BLZ945-induced cell death. GCM produced by the only non-protective line identified, PDGC-55, was unable to recapitulate these effects. For comparison, naïve BMDMs were cultured in non-conditioned, serum-free media supplemented with CSF-1, in the presence or absence of BLZ945 (67 nM or 670 nM, dashed lines). *n*=8-20 replicate experiments. **(b)** The secretion of cytokines and angiogenic factors by protective (PDGC-23, PDGC-17, PDGC-02) and non-protective (PDGC-55) cell lines was assessed using the 'Cytokine' and 'Angiogenesis' mouse antibody arrays (R&D Systems). The cytokine array (shown here as a representative example) and angiogenesis array (not shown) were incubated with serum-free GCM from the 4 PDGC lines as depicted in Supplementary Fig. 15a, and processed according to the manufacturer's instructions. Each array was incubated with a single GCM sample and contained three duplicate positive controls and one negative control to determine background absorbance. Each spot corresponds to a single secreted factor as indicated. Candidate proteins that were differentially secreted by protective vs. non-protective cell lines were chosen for further analyses (examples indicated by colored boxes). **(c)** Pixel density for each spot was quantified using ImageJ software, and normalized to positive control spots. Negative control spots were used to subtract background signal to yield a normalized signal ratio. Following normalization, factors were binned into either (-), (+), (++), (+++), or (++++) groups. The normalized signal bins are as follows: (-) non-detectable, (+) 0 to 0.5, (++) 0.5 to 1.5, (+++) 1.5 to 2.5, and (++++) greater than 2.5. Only factors with a detectable signal in at least one of the 4 PDGC lines are indicated in the tables. Graphs show mean ± s.e.m. *P* values were obtained using unpaired two-tailed Student's t-test; NS= not significant, **P*<0.05, ***P*<0.01, ****P*<0.001.

Supplementary Figure 17

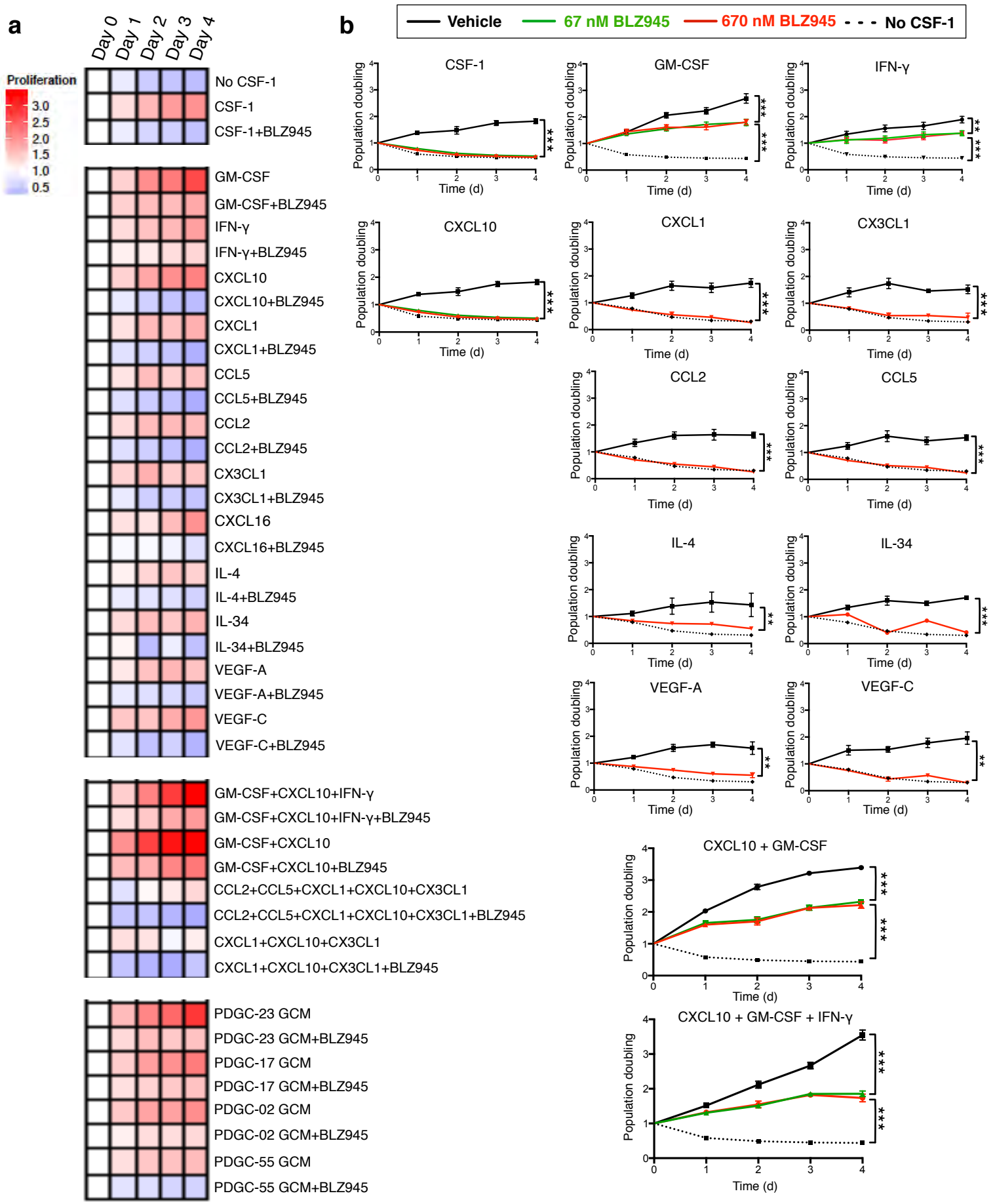

Supplementary Figure 17.

GM-CSF and IFN-γ are sufficient to prevent BLZ945-induced BMDM death while CXCL10 promotes BMDM proliferation. (a) MTT assays were performed to assess BMDM proliferation/ survival in the presence of either PDGC-derived factors and/or candidate protective factors in the presence of BLZ945 or vehicle. PDGC-induced BMDM proliferation and protection against BLZ945 (Supplementary Fig. 16a) was also plotted for comparison at the bottom of this heatmap. Each time point was normalized to day 0 within each treatment group. Continuous proliferation index values are depicted along a color scale as indicated in the legend: red (higher compared to day 0), white (no change compared to day 0), and blue (lower compared to day 0). Individual boxes represent the mean of n=3-20 independent experiments. These assays resulted in the identification of three factors from the panel of cytokines tested that were capable of conferring BMDM survival and/ or proliferation in the presence of BLZ945: GM-CSF, IFN-γ, and CXCL10. **(b)** Representative MTT assays of BMDMs treated with recombinant candidate factors (selected in (a)) over the course of 4 days. Significant effects were observed for protective factors (GM-CSF, IFN-γ), proliferative factors (CXCL10, GM-CSF), or a combination of both protective and proliferative factors (CXCL10+GM-CSF and CXCL10+GM-CSF+IFN-γ). No significant effects were observed for CXCL1, CX3CL1, CCL2, CCL5, IL-4, IL-34, VEGF-A or VEGF-C. Graphs show mean ± s.e.m. P values were obtained using unpaired two-tailed Student's t-test; $^{**}P<0.01$, $^{***}P<0.001$.

Supplementary Figure 18

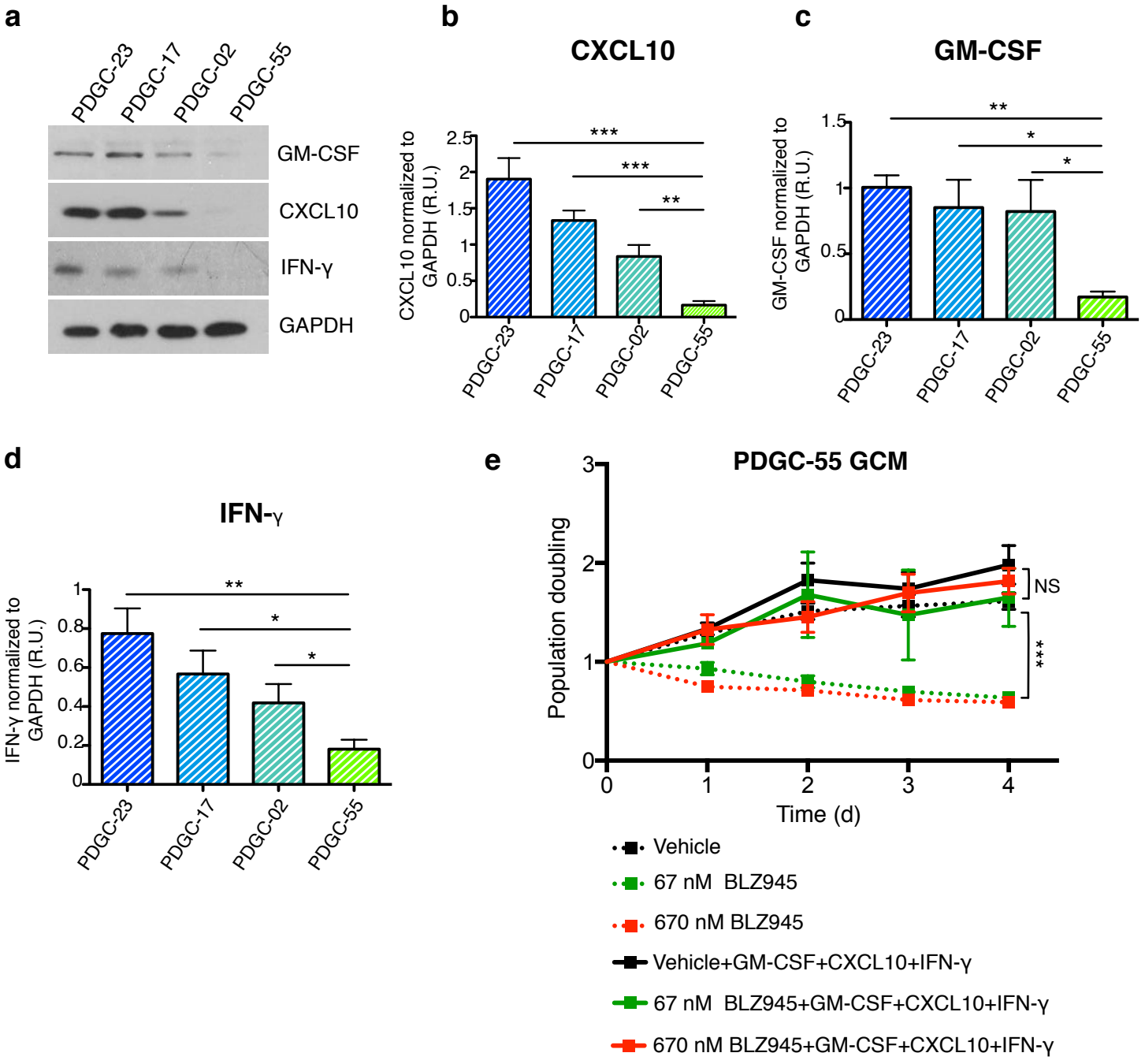

Supplementary Figure 18.
Analyses of differentially produced survival/ proliferation factors in PDGC protective and non-protective lines. **(a)** Proteins were extracted from PDGC-23, PDGC-17, PDGC-02 (protective) and PDGC-55 (non-protective) cell lines and expression of CXCL10, GM-CSF and IFN-γ was assessed by Western blot. **(b-d)** Quantitation of the CXCL10, GM-CSF and IFN-γ bands from (a) (normalized to GAPDH) using ImageJ software showed significant changes in expression levels for each protein between the protective versus non-protective lines. *n*=5 replicate experiments. **(e)** 4d MTT assay of BMDMs cultured in non-protective GCM (PDGC-55 GCM) in the presence or absence of BLZ945 (67 nM or 670 nM), or the identified protective/proliferative factors. No protective advantage was provided by PDGC-55 GCM in the presence of BLZ945; however, protection was conferred upon the addition of recombinant protective/ proliferative factors including GM-CSF, IFN-γ and CXCL10 (10ng/ml, 30ng/ml and 20ng/ml, respectively) to the PDGC-55 GCM + BLZ945. BMDM numbers were assessed after 4d of culture using MTT assays. This revealed a significant protective effect of the three factors in combination against BLZ945-induced death when added to PDGC-55 GCM. *n*=5-8 replicate experiments. Graphs show mean and s.e.m. *P* values were obtained using unpaired two-tailed Student's t-test; NS= non significant **P*<0.05, ***P*<0.01, ****P*<0.001 compared to the non-protective PDGC-55 line.

Supplementary Figure 19

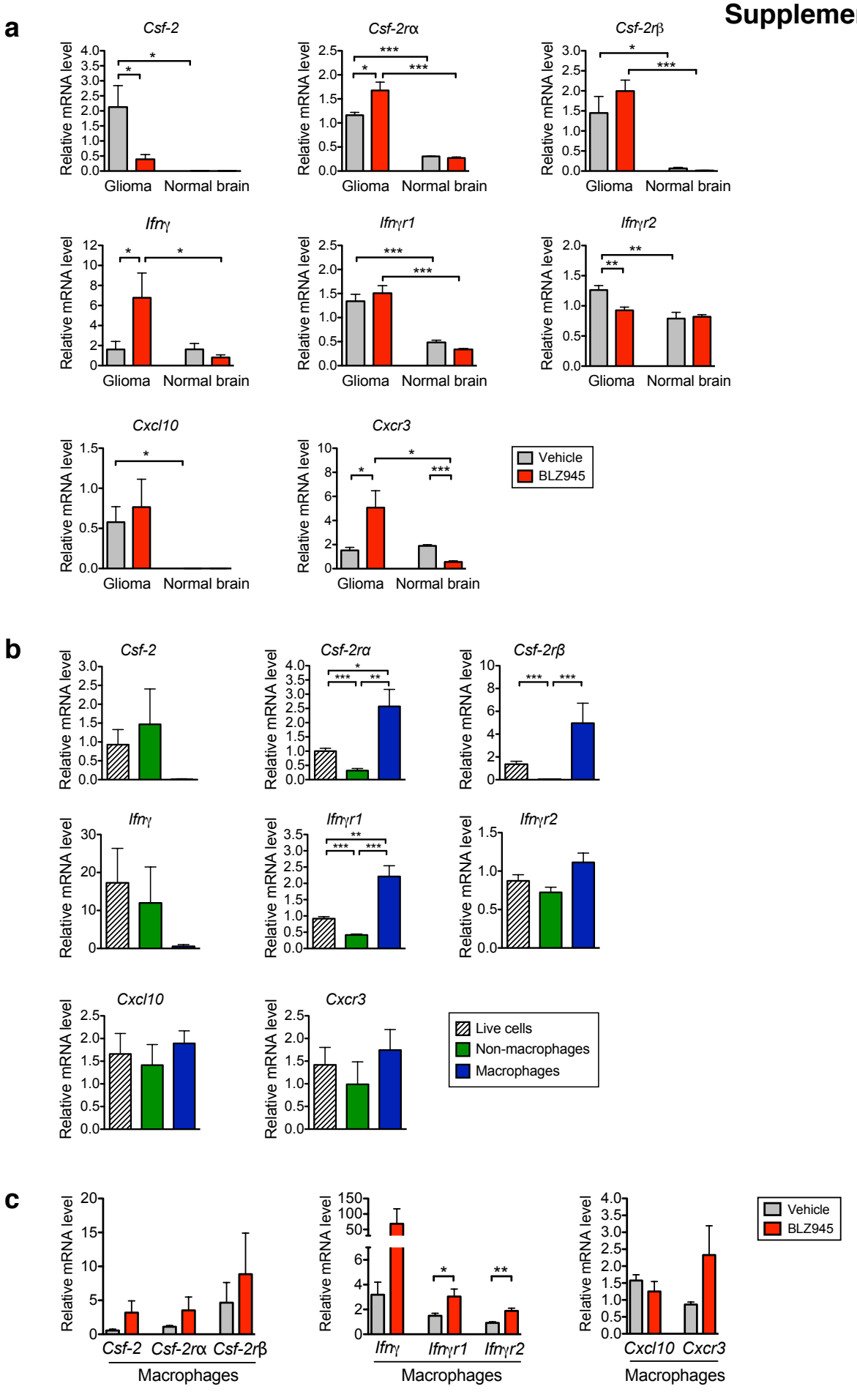

Supplementary Figure 19.

The non-macrophage population is a major source for Csf-2/ Gm-csf and Ifnγ in gliomas, and BLZ945 treatment induces expression of Csf-2 and Ifnγ in glioma-associated macrophages. (a) Cerebrum/forebrain from uninjected Nestin-Tv-a;*Ink4a/Arf-/-* mice (normal brain; *n*=5 for each group) and gliomas from PDG mice (vehicle or BLZ945 7d; *n*=6-7 per group) were used for RNA isolation and cDNA synthesis. Expression of the cytokines *Csf-2* (*Gm-csf*), *Ifn*γ and *Cxcl10* and their respective receptors (*Csf-2r*α*, Csf-2r*β*, Ifn*γ*r1, Ifn*γ*r2* and *Cxcr3*) was measured by qPCR. Expression is depicted relative to vehicle-treated gliomas. Interestingly, expression changes of the three cytokines and their receptors suggest increased responsiveness for each of the cytokines in gliomas compared to normal brain. **(b)** To determine the cell-type expression pattern of these genes we compared sorted macrophages ($CD11b^{+}Gr\text{-}1^{-}$) from vehicle-treated gliomas from PDG mice (*n*=6) to the corresponding non-macrophage cell fraction ($CD11b^{-}Gr\text{-}1^{-}$) fraction containing glioma cells, astrocytes, endothelial cells etc.), relative to the expression levels of the mixed live cell population (DAPI-). The expression of each receptor was higher in tumor-associated macrophages compared to the other cell populations (albeit to different degrees), and the ligands were either highly enriched in the non-macrophage population for *Csf-2* and *Ifn*γ, or expressed equally in both fractions for *Cxcl10*. **(c)** We further examined the macrophage-specific expression of the three cytokines and their receptors following BLZ945 treatment (*n*=6 for macrophages sorted from vehicle or BLZ945 7d-treated gliomas). It is interesting to note that the majority of genes analyzed showed an increase in expression after BLZ945, which may be indicative of a switch in production of these key factors from the glioma cells (which are severely depleted following BLZ945 treatment) to the macrophages. Expression is depicted relative to live cells isolated from vehicle-treated PDG mice for panel (b) and relative to macrophages isolated from vehicle-treated PDG mice for panel (c). All assays were run in triplicate and gene expression was normalized to *Ubc*. Graphs show mean + s.e.m. *P* values were obtained using unpaired two-tailed Student's t-test; **P*<0.05, ***P*<0.01, and ****P*<0.001.

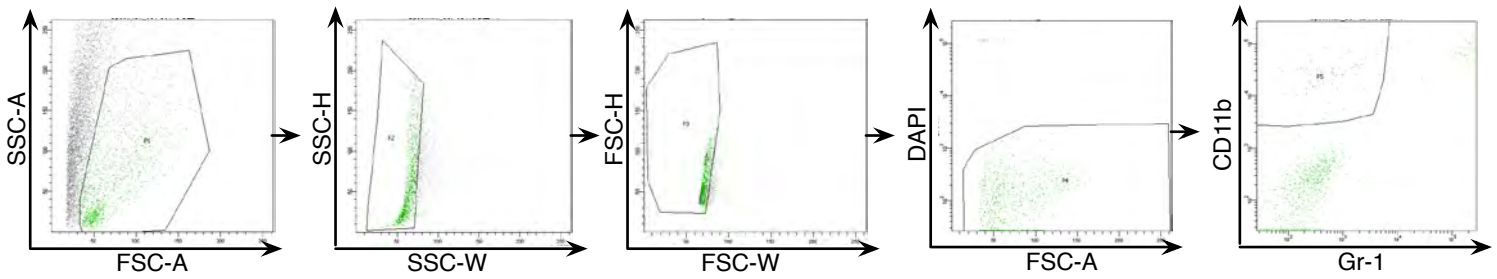
a
SSC-A
FSC-A
SSC-H
SSC-W
FSC-H
FSC-W
DAPI
FSC-A
CD11b
Gr-1

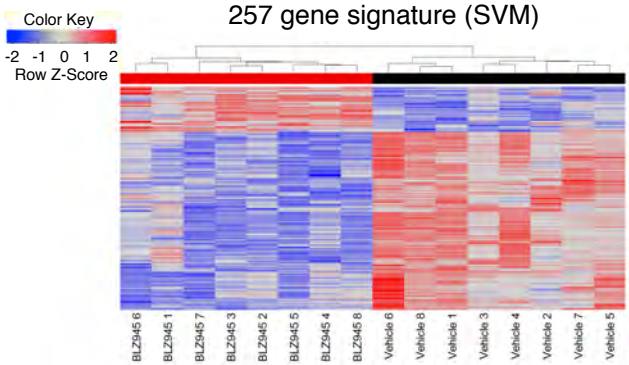
b
257 gene signature (SVM)
Color Key
-2 -1 0 1 2
Row Z-Score

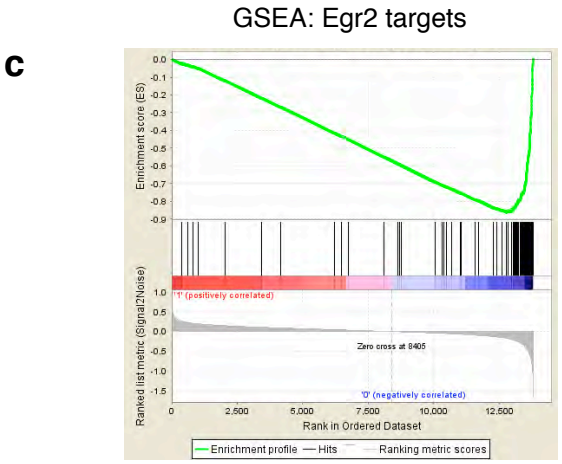
c
GSEA: Egr2 targets
Enrichment score (ES)
Ranked list metric (Signal2Noise)
Rank in Ordered Dataset
Enrichment profile
Hits
Ranking metric scores

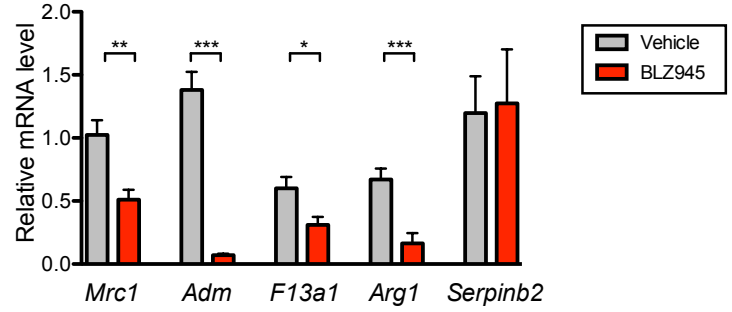
d
Relative mRNA level
Vehicle
BLZ945
Mrc1
Adm
F13a1
Arg1
Serpinb2

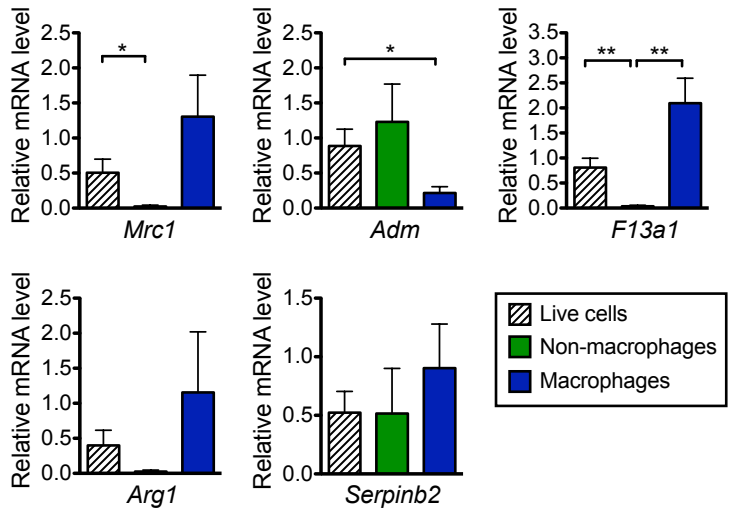
e
Relative mRNA level
Mrc1
Adm
F13a1
Arg1
Serpinb2
Live cells
Non-macrophages
Macrophages

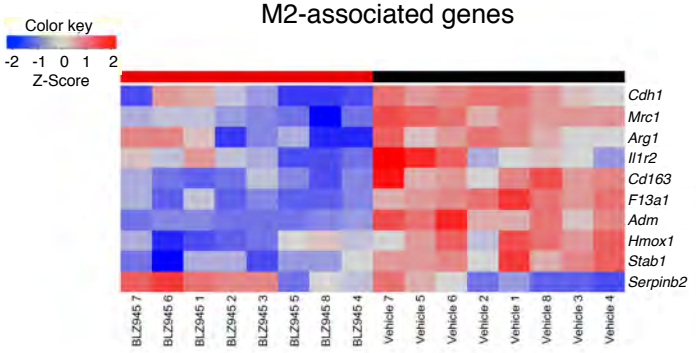
f
M2-associated genes
Color key
-2 -1 0 1 2
Z-Score
Cdh1
Mrc1
Arg1
Il1r2
Cd163
F13a1
Adm
Hmox1
Stab1
Serpinb2

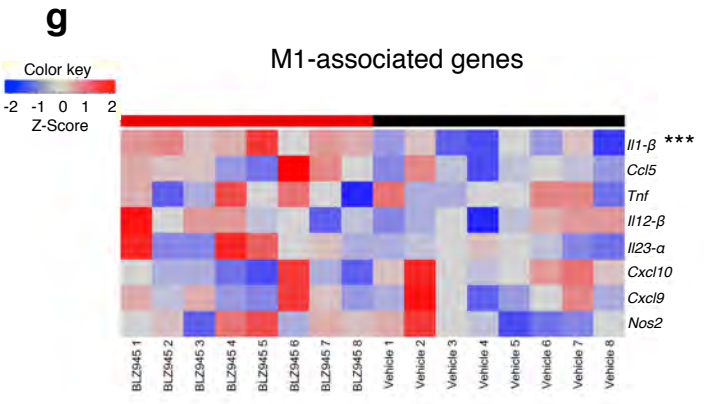
g
M1-associated genes
Color key
-2 -1 0 1 2
Z-Score
Il1-β ***
Ccl5
Tnf
Il12-β
Il23-α
Cxcl10
Cxcl9
Nos2

Supplementary Figure 20.
Gene expression profiling of BLZ945-treated TAMs reveals a downregulation of alternatively activated/ M2 polarization markers, but no overall change in classically activated/ M1 polarization markers. (a) Representative flow cytometry plots and gating strategy for sorting $CD11b^{+}Gr\text{-}1^{-}$ TAMs from PDG tumors treated with vehicle or BLZ945 for 7d. **(b)** Supervised clustering of 257 differentially expressed genes between BLZ945 and vehicle treated mice (*n*=8 per group), termed the 'total' gene signature. These genes are listed in Supplementary Table 4. BLZ945 treatment resulted in a downregulation of 205 genes and an upregulation of 52 genes in TAMs. These genes were used to train the support vector machine (SVM) in Supplementary Fig. 24 (see Supplementary Methods). **(c)** Gene set enrichment analysis (GSEA) revealed that targets of Egr2, a transcription factor downstream of CSF-1R signaling, were downregulated in BLZ945-treated TAMs. **(d, e)** qRT-PCR analysis was used to quantify expression of the 5-gene signature (Fig. 6b) in (d) whole gliomas (vehicle vs. BLZ945 7d; *n*=10 for each group) or (e) vehicle-treated gliomas sorted for live cells (DAPI-), non-macrophages ($CD11b^{-}Gr\text{-}1^{-}$) and macrophages ($CD11b^{+}Gr\text{-}1^{-}$) (*n*=4 for each group). Expression is depicted relative to vehicle-treated samples in (d), and relative to live cells in (e). Interestingly, significantly reduced expression of the 4 downregulated genes from the 5-gene signature was evident even in whole tumors. Assays were run in triplicate and expression normalized to *Ubc* for each sample. **(f)** Of the 257 differentially expressed genes, a total of ten, including those identified using lasso regression in Fig. 6b, were found to be associated with alternative/ M2 macrophage activation (see Supplementary Table 4). **(g)** Classically activated/ M1 macrophage markers represented in the 257 gene list (Supplementary Table 4) were not differentially expressed following BLZ945 treatment, with the exception of IL-1β, which was significantly upregulated. Graphs show mean + s.e.m. *P* values were obtained using unpaired two-tailed Student's t-test in (e-g); **P*<0.05, ***P*<0.01, ****P*<0.001. All *P* values in (f) are significant and can be found in Supplementary Table 4.

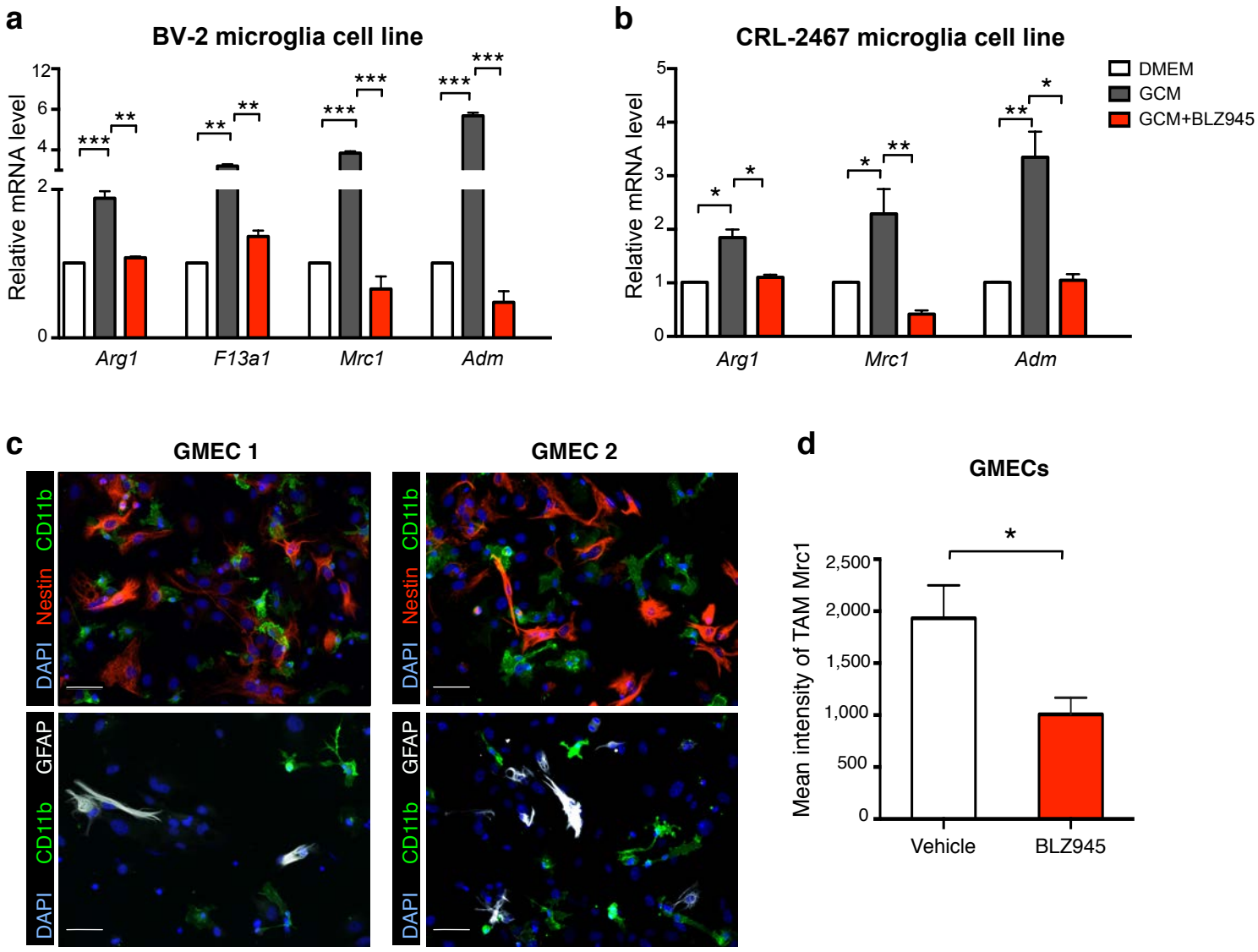

Supplementary Figure 21.
CSF-1R inhibition downregulates expression of M2-associated genes in microglia cell lines and in primary glioma microenvironment cultures. (a-b) Expression of a subset of M2-associated genes (*Arg1, F13a1, Mrc1, Adm*) identified in the total gene signature (Supplementary Fig. 20f) is upregulated in the microglia cell lines (a) BV-2 and (b) CRL-2467 following stimulation with GCM. This effect is abrogated by BLZ945 treatment. There was no detectable expression of *F13a1* in the CRL-2467 cell line. **(c)** Primary glioma microenvironment cultures (GMECs) were prepared from individual mouse PDG tumors (see Online Methods). At passage 3, the mixed cell cultures were co-stained for Nestin$^+$ glioma cells, CD11b$^+$ macrophages, and GFAP$^+$ astrocytes. DAPI was used as a nuclear counterstain. Scale bar, 50 µm. **(d)** Primary GMECs were cultured +/- BLZ945, and CD45$^+$ CD11b$^+$ TAMs analyzed for Mrc1/CD206 expression by flow cytometry (*n*=6 replicates), revealing a downregulation following treatment with BLZ945. BLZ945 was used at 670 nM in all cell culture assays. Graphs show mean + s.e.m. *P* values were obtained using unpaired two-tailed Student's t-test; **P*<0.05, ***P*<0.01, ****P*<0.001.

Supplementary Figure 22

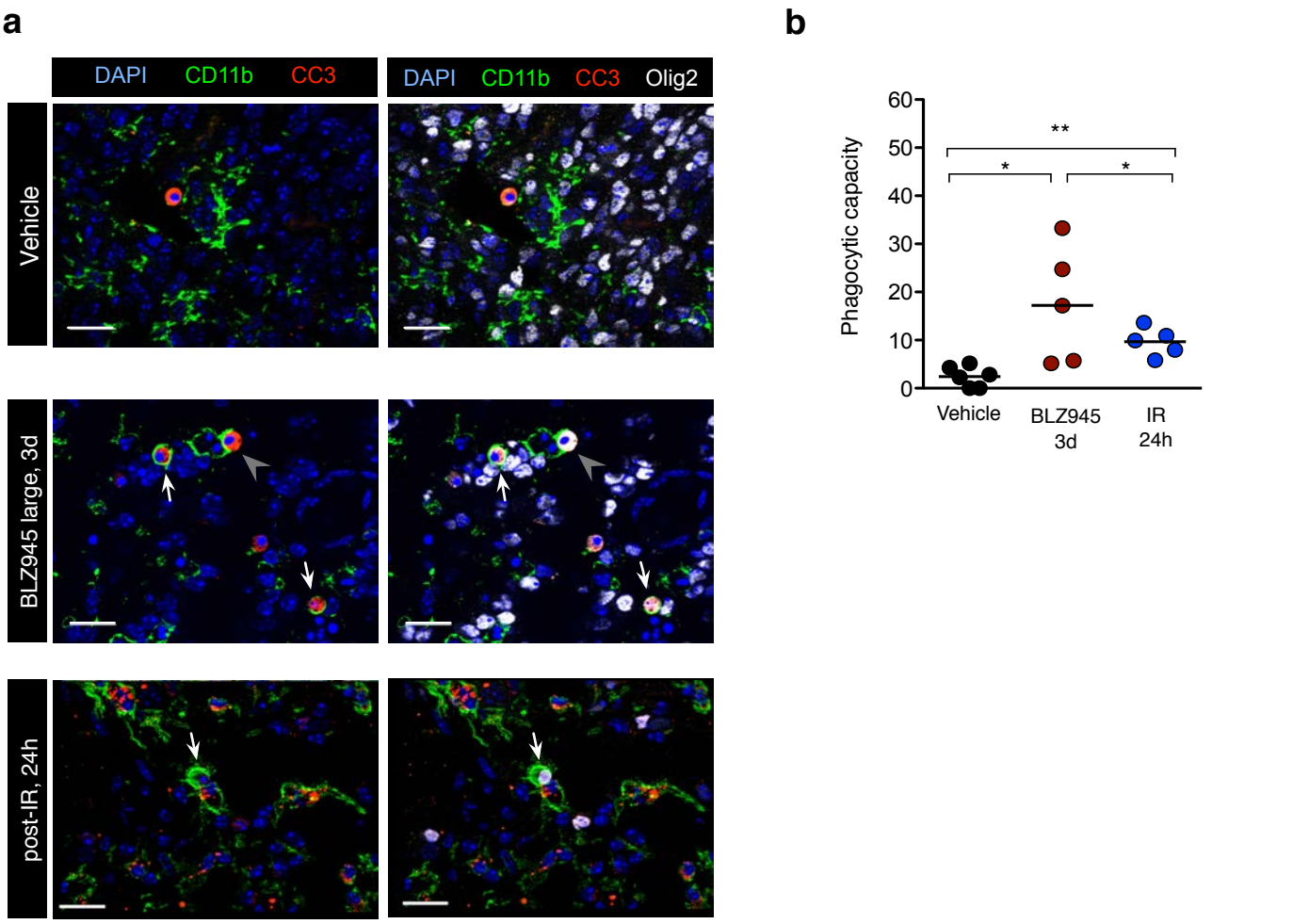

Supplementary Figure 22.
Phagocytosis is increased in BLZ945-treated gliomas. (a) Representative images of PDG tumors from the short-term BLZ945 trial (3d) or 24h after irradiation (IR, 10Gy using an X-ray irradiator) stained for CD11b (macrophages), cleaved caspase-3 (CC3), Olig2 and DAPI. White arrows indicate apoptotic glioma cells ($CC3^+Olig2^+$) that have been engulfed/phagocytosed by $CD11b^+$ macrophages. Gray arrowheads indicate apoptotic glioma cells ($CC3^+Olig2^+$) that are in close contact with, but have not been phagocytosed by, $CD11b^+$ macrophages; these types of interactions were not included for calculation of phagocytic index/capacity. **(b)** Phagocytic capacity was calculated as the mean percentage of $CD11b^+$ macrophages that had engulfed $CC3^+Olig2^+$ cells per mouse, following normalization for relative numbers of apoptotic glioma cells across treatment groups. Each circle represents an individual mouse (*n*=5-6 per group), and horizontal lines represent the mean. Scale bar, 50 μm. *P* values were obtained using unpaired two-tailed Student's t-test; **P*<0.05, ***P*<0.01. A summary of the analysis of phagocytic index and capacity in additional BLZ945-treated cohorts can be found in Supplementary Table 2.

Supplementary Figure 23

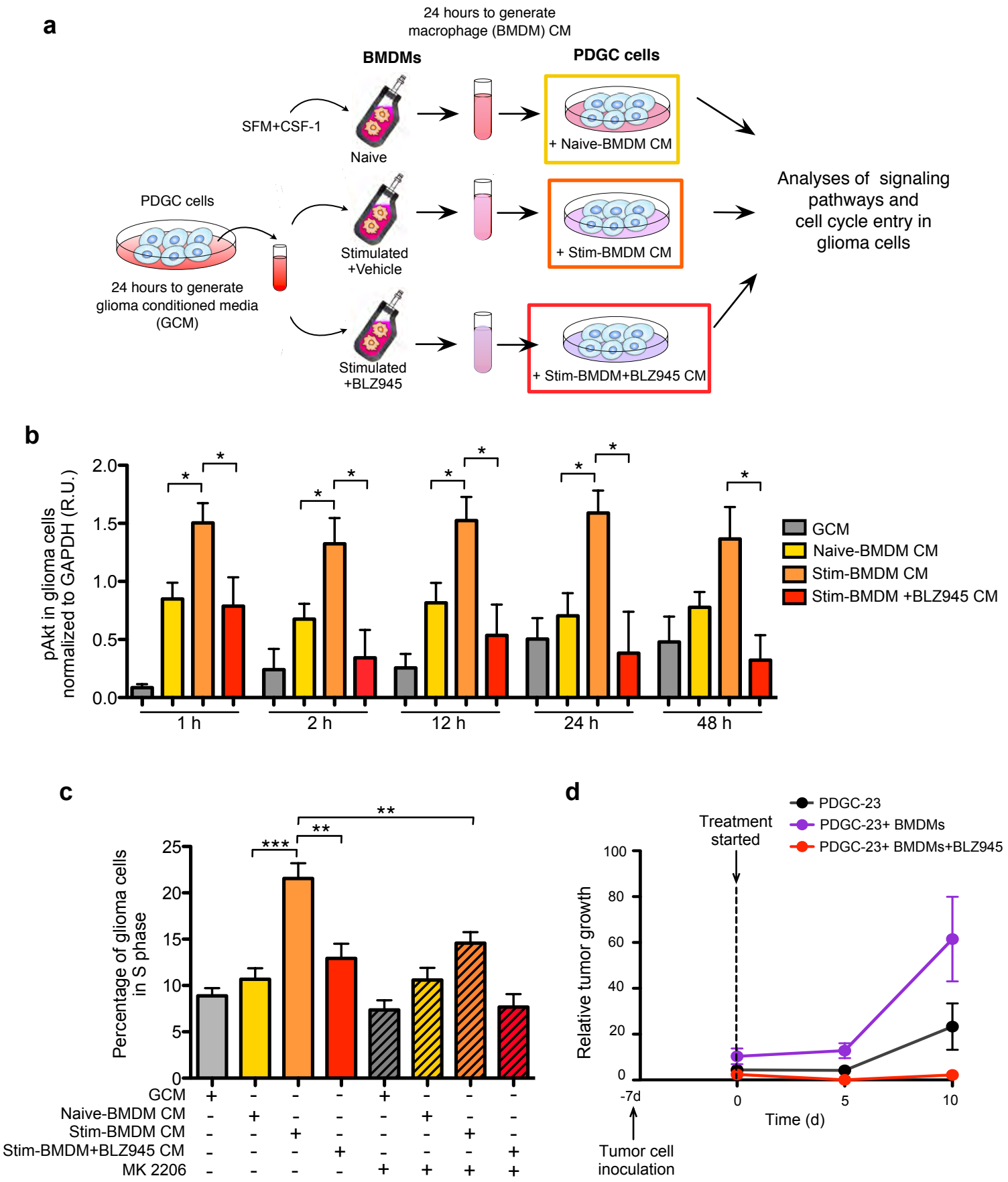

Supplementary Figure 23.

CSF-1R inhibition impairs macrophage-induced activation of Akt signaling in glioma cells, and co-injection experiments show macrophages stimulate tumor growth in a glioma allograft model. (a) Schematic of macrophage-conditioned media (CM) preparation prior to glioma cell stimulation and glioma cell cycle analysis. PDGC-23 glioma cells were plated and allowed to attach for 24h. Media was changed to serum-free DMEM for 24h in order to collect GCM. Three experimental conditions were subsequently established to produce macrophage (BMDM) conditioned media (24h): serum-free media (SFM) supplemented with CSF-1 ("naïve-BMDM CM"), GCM + vehicle ("stimulated-BMDM CM"), and GCM + BLZ945 ("stimulated-BMDM + BLZ945 CM"). Conditioned media from each of these three treatment groups was then added to serum-starved PDGC-23 glioma cells. **(b)** Quantitation of pAkt immunoblots from Fig. 6f, showing significant changes in phosphorylation between glioma cells incubated with naïve-BMDM CM, stimulated-BMDM (stim) CM, or stimulated-BMDM+BLZ945 CM at the indicated time points post-incubation (*n*=5-8 replicate experiments). Quantitation is normalized to total GAPDH. **(c)** Glioma cells were incubated with naïve-BMDM CM, stimulated-BMDM CM, or stimulated-BMDM+BLZ945 CM for 48h, in the presence or absence of the Akt inhibitor 200nM MK-2206 and subjected to cell cycle analyses. *n*=6-8 replicate experiments. BLZ945 was used at 670 nM in all cell culture assays unless otherwise specified. **(d)** Athymic/ nude mice were injected intracranially with either $5x10^4$ PDGC-23 glioma cells (labeled with a TK-GFP-Luc triple imaging vector; TGL) alone or mixed with 30% RFP+ BMDMs ($1.66x10^4$ cells), so that the number of injected TGL-labeled glioma cells was the same in each group. Treatment with BLZ945 (200 mg/kg) was initiated in mice injected with PDGC-23 cells + RFP^+ BMDMs when tumors were in a positive growth phase determined by bioluminescence imaging (BLI) output, which corresponded to 7d post-injection. Mice were either untreated (*n*=13-16) or treated with BLZ945 (*n*=5). Tumor growth was evaluated every 5d for 10d, at which point mice became symptomatic and were sacrificed for further analyses. *P* values were obtained using unpaired two-tailed Student's t-test in (b, c), and nonparametric two-tailed Mann Whitney test in (d); **P*<0.05, ***P*<0.01, ****P*<0.001.

Figure legend:

- 'BLZ945-like' class
- 'Vehicle-like' class

Supplementary Figure 24

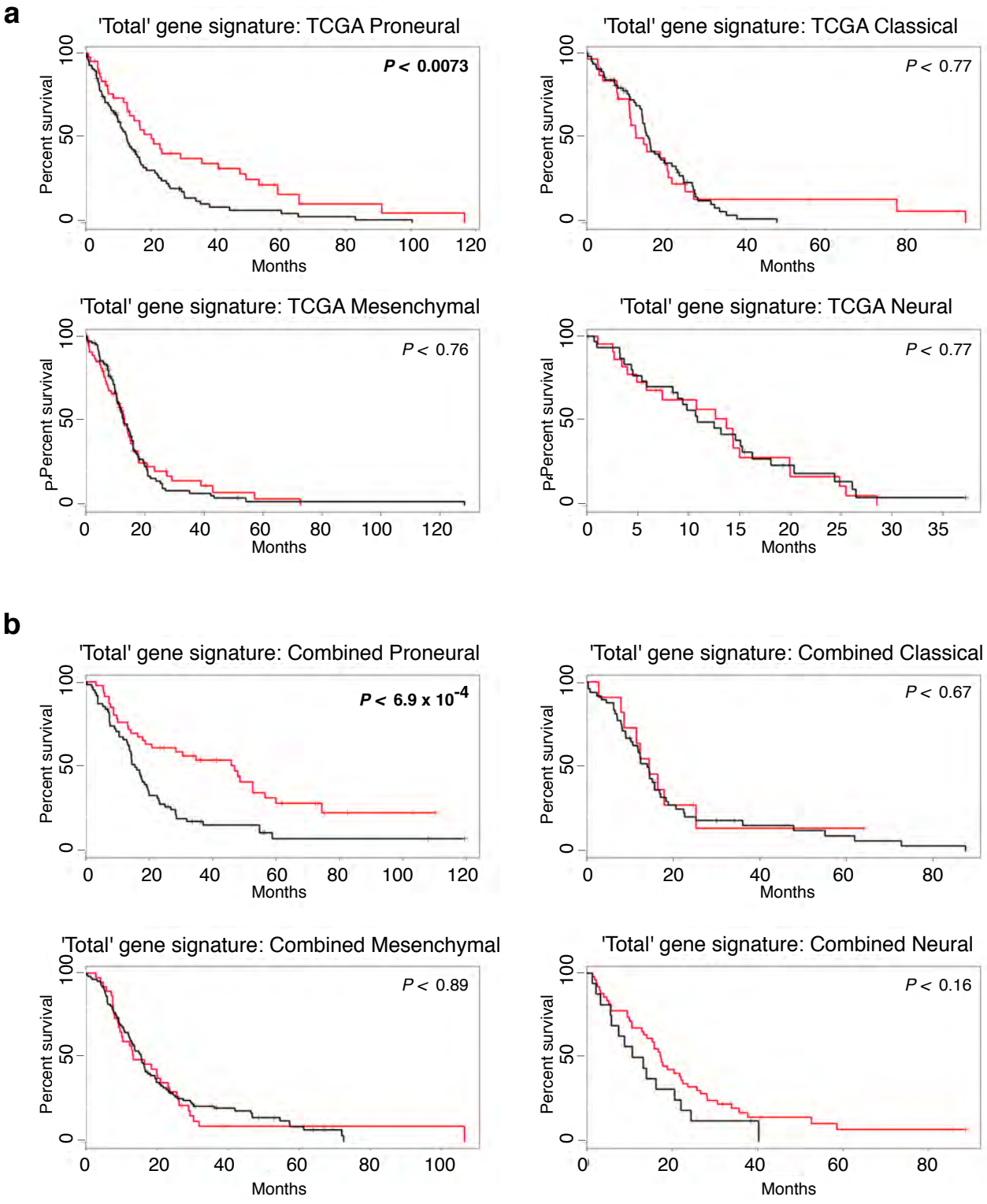

c

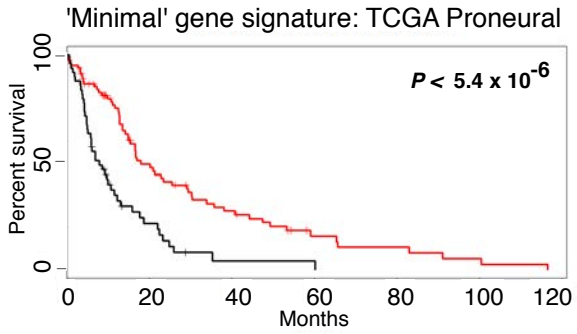
'Minimal' gene signature: TCGA Proneural
P < 5.4 x 10-6
Percent survival
Months

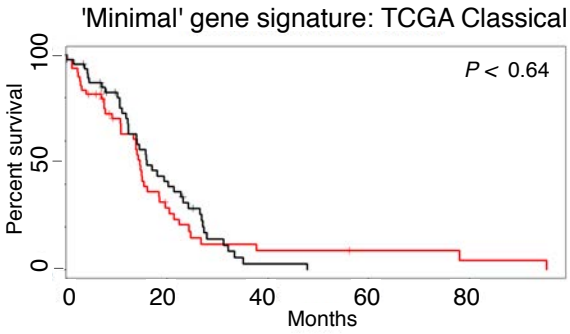
'Minimal' gene signature: TCGA Classical
P < 0.64
Percent survival
Months

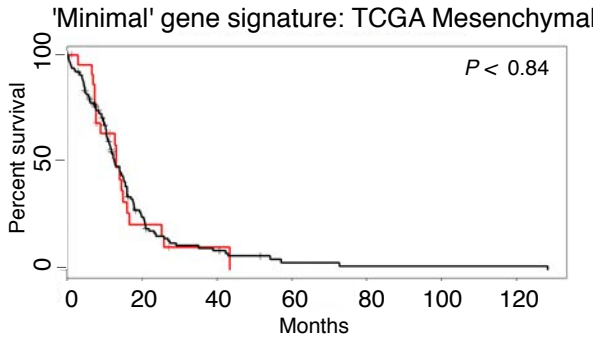
'Minimal' gene signature: TCGA Mesenchymal
P < 0.84
Percent survival
Months

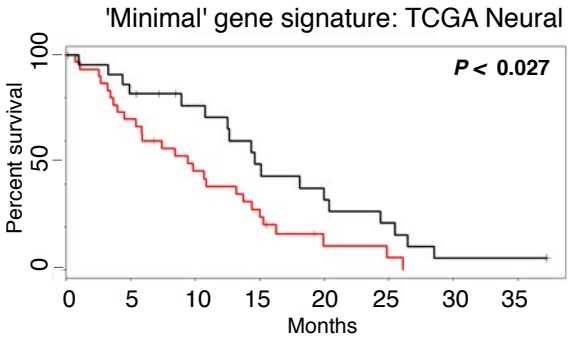
'Minimal' gene signature: TCGA Neural
P < 0.027
Percent survival
Months

d

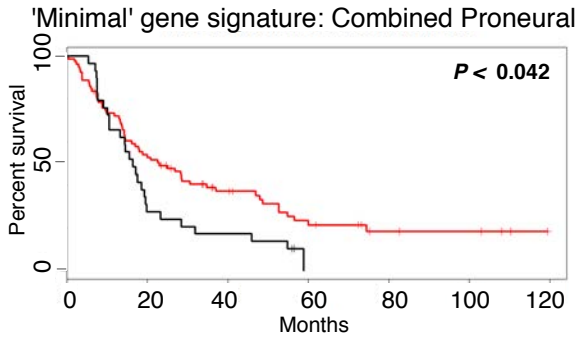
'Minimal' gene signature: Combined Proneural
P < 0.042
Percent survival
Months

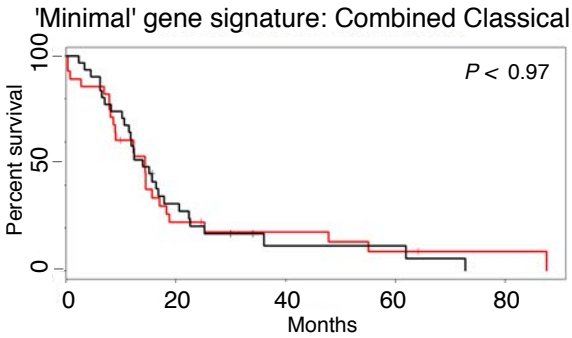
'Minimal' gene signature: Combined Classical
P < 0.97
Percent survival
Months

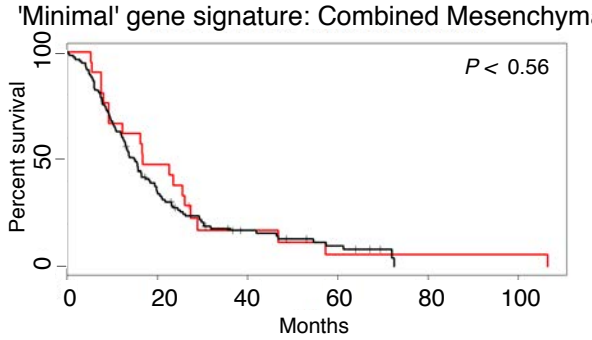
'Minimal' gene signature: Combined Mesenchymal
P < 0.56
Percent survival
Months

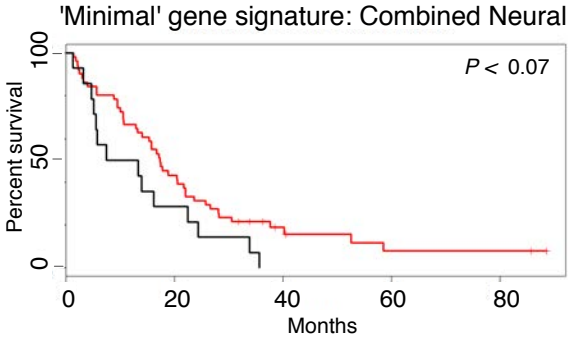
'Minimal' gene signature: Combined Neural
P < 0.07
Percent survival
Months

e

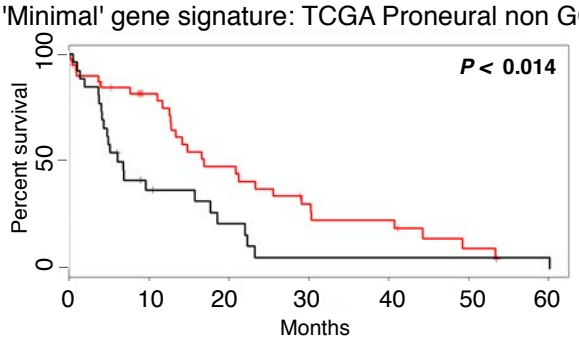
'Minimal' gene signature: TCGA Proneural non GCIMP
P < 0.014
Percent survival
Months

Supplementary Figure 24.

Minimal and total gene signatures identify 'BLZ945-like' GBM patients which demonstrate a survival advantage in a proneural-specific, G-CIMP independent manner. (a) A 'total' gene signature comprising human homologs of the mouse TAM genes identified in Fig. 6a was used to train a support vector machine (SVM) model, restricted to genes with known human homologs that were present in the TCGA total tumor expression dataset. The total gene signature was used to classify TCGA patients into 'BLZ945-like' and 'Vehicle-like' classes (see Supplementary Methods). 'BLZ945-like' classified patients showed a proneural-specific survival advantage (7.6 months). **(b)** GBM patients from the Murat, Freije, Phillips, and Rembrandt databases were subtyped as described and pooled into one 'Combined' dataset (see Supplementary Methods). As in (a), an SVM was trained and used to classify patients in the Combined datasets into 'BLZ945-like' and 'Vehicle-like' classes. Patients classified as 'BLZ945-like' also showed a proneural-specific survival advantage (31.5 months). **(c)** The 'minimal' gene signature identified in Fig. 6b was used to classify TCGA GBM patients into 'BLZ945-like' and 'Vehicle-like' classes as described in Supplemental Methods. A lasso logistic regression model was trained on the mouse TAM expression data. Expression data for *MRC1* was not present in the TCGA data, thus the lasso regression utilized *ADM, ARG1, F13A1*, and *SERPINB2* expression values to classify patients into mock 'Vehicle-like' or 'BLZ945-like' classification groups. TCGA patients that were classified as 'BLZ945-like' demonstrated an increased median survival in the proneural subtype (10 months). This increase in survival was not evident in other subtypes of GBM in the TCGA data. Although *ADM* and *F13A1* contribute the strongest weights to the signature, exclusion of any member of the 4-gene signature abrogated the described survival benefit (data not shown). **(d)** As in (c), the minimal gene signature was used to classify patients in the Combined datasets into 'BLZ945-like' and 'Vehicle-like' classes. Patients classified as 'BLZ945-like' also showed a proneural-specific survival advantage (6.5 months). While there was a significant decrease in median survival using the 'BLZ945-like' class in the neural subtype from the TCGA dataset in (c), this effect was not replicated in the Combined datasets for neural patients. **(e)** We sought to determine if the survival advantage offered by the 'BLZ945-like' signature was due to an enrichment of Glioma CpG Island Methylator Phenotype (G-CIMP) patients, which have previously been shown to be associated with improved overall survival. TCGA proneural patients with available methylation data (see Supplementary Methods) were classified into 'BLZ945-like' and 'Vehicle-like' classes using the minimal gene signature as in (c). G-CIMP-positive patients were removed from the analysis. Patients classified as 'BLZ945-like' still demonstrated a significant median survival increase among proneural non-G-CIMP patients (10.4 months). Results from these analyses are summarized in Supplementary Tables 5-9. All *P* values were obtained using a Log Rank test, with significant *P* values indicated in bold.

Supplementary Table 1: Summary of biochemical IC_{50} values for BLZ945

Enzyme	IC_{50} in μM	Enzyme	IC_{50} in μM
CSF-1R	**0.001**	Ron	> 10
c-KIT	3.2	ROS	> 10
PDGFR-β	4.8	smM LCK	> 10
Flt3	9.1	Src	> 10
Abl	> 10	Syk	> 10
Alk	> 10	TAK1	> 10
Aurora A	> 10	TRKB	> 10
Blk	> 10	TRKC	> 10
CamK11-α	> 10	TSSK1	> 10
Cdk7 cyclinH MAT1	> 10	ZAP70	> 10
Chk1	> 10	CDC2_cyclinB	> 25
Ck1-δ	> 10	COT	> 25
Ck1-γ2	> 10	FGFR1	> 25
Ck2-α1	> 10	Jak2	> 25
cRaf	> 10	KDR	> 25
Dyrk3	> 10	Mutant B-Raf_V599E	> 25
FGFR2	> 10	PAK1	> 25
Fyn	> 10	PAK2	> 25
Hck	> 10	PDK1	> 25
Hyl	> 10	PIK3C-α	> 25
IGF-1R	> 10	PIK3C-β	> 25
Insulin RK	> 10	PIK3C_VPS34	> 25
JNK2-α2	> 10	PIK4C-β	> 25
Lck	> 10	Pim1	> 25
Nek2	> 10	Pim2	> 25
PAK4	> 10	Pim3	> 25
PDGFR-α	> 10	PKA	> 25
PHKG2	> 10	PKC-ε	> 25
PKC-α	> 10	Plk1	> 25
PKC-τ	> 10	p38-α	> 25
		RAF1_4_CR	> 25

Supplementary Table 2: Summary of histological analyses performed in each BLZ945 treatment group in the PDG mouse model

Parameter	Vehicle	BLZ945, Day 3	BLZ945, Day 7	BLZ945 large, Day 3	BLZ945 large, Day 7
Tumor Volume (Day -1 vs Day 6)	+ 498%	--	+ 0.68%	--	- 24.3%
Total $DAPI^+$ Cells	--	- 72%	- 80%	- 40%	- 65%
Tumor Cells (%$Olig2^+$)	--	- 27%	- 77%	- 14%	- 73%
Proliferation (%$BrdU^+Olig2^+$)	--	- 91%	- 67%	- 98%	- 94%
Apoptosis (%$CC3^+$)	--	+ 17-fold	+ 6-fold	+ 9-fold	+ 2-fold
Vasculature (CD31 MVD)	--	--	- 17%	--	- 67%
Phagocytic Index	--	+ 2.6-fold	+ 3.0-fold	+ 2.2-fold	+ 4.1-fold
Phagocytic Capacity	--	+ 11.5-fold	+ 5.0-fold	+ 7.1-fold	+ 6.0-fold

All changes in the BLZ945 treatment groups are calculated relative to the vehicle control group.

MVD: microvessel density. Phagocytic index was calculated as the mean percentage of $CC3^+Olig2^+$ cells that had been engulfed by $CD11b^+$ macrophages per mouse. Phagocytic capacity was calculated as the mean percentage of $CD11b^+$ macrophages that had engulfed $CC3^+Olig2^+$ cells per mouse.

Supplementary Table 3: Characterization and transcriptome profiling of TS573 and TS1137 patient tissue and corresponding tumor sphere lines

Cell name	Patient info	Source of analysis	aCGH	Nanostring			Sequenom
				Transcriptome Profile BTC cohort	Transcriptome Profile TCGA	RTK and oncogene expression	IDH1/2, PI3K, EGFR, TP53 and other hotspots
TS573	62 yr old female Previously untreated	Tissue from patient	Not tested	Not tested	Not tested	Not tested	Not tested
		Tumor sphere in culture	High level amplification of PDGFRA and CDK6 loci. CSF1R is lost (-1 copy) as part of regional chr5 loss	Proneural	Proneural	PDGFRα overexpression and delta 8,9 mutation	IDH1/2 tested separately: negative
TS1137	82 yr old female Previously untreated	Tissue from patient	Not tested	Proneural	Proneural	PDGFRα overexpression and delta 8,9 mutation	Not tested
		Tumor sphere in culture	High level amplification of PDGFRA. CDKN2A homozygous deletion. CSF1R euploid	Proneural	Proneural	PDGFRα overexpression and delta 8,9 mutation	No mutations

TS, tumor sphere; aCGH, array-comparative genomic hybridization; BTC, Brain Tumor Center (MSKCC); TCGA, The Cancer Genome Atlas; RTK, receptor tyrosine kinase; PDGFRa, platelet-derived growth factor receptor-alpha; CDK6, cell division protein kinase-6; IDH, isocitrate dehydrogenase; PI3K, phosphatidylinositide 3-kinase; EGFR, epidermal growth factor receptor; TP53, tumor protein 53.

Supplementary Table 4: List of 257 differentially expressed genes from microarray analysis of BLZ945-treated TAMs from the PDG model.

Symbol	Description	Reference [1]	Fold Change BLZ945-Vehicle	Nominal *P* value
2310016C08Rik	RIKEN cDNA 2310016C08 gene		-2.14	1.12E-04
2810417H13Rik	RIKEN cDNA 2810417H13 gene		-3.96	2.33E-07
4930583H14Rik	RIKEN cDNA 4930583H14 gene		-2.37	1.25E-05
Abhd15	abhydrolase domain containing 15		-2.48	1.36E-05
Acp5	acid phosphatase 5, tartrate resistant		-2.36	2.08E-03
Ada	adenosine deaminase		-3	2.28E-07
Adm *,**	adrenomedullin	14	-10.85	2.60E-09
Akap12	A kinase (PRKA) anchor protein (gravin) 12		-2.85	1.31E-04
Aldh1a2	aldehyde dehydrogenase family 1, subfamily A2		-2.18	8.36E-04
Alox15	arachidonate 15-lipoxygenase		4.24	8.85E-03
Anln	anillin, actin binding protein		-2.99	1.38E-04
Aoah	acyloxyacyl hydrolase		-2.43	3.83E-06
Apbb2	amyloid beta (A4) precursor protein-binding, family B, member 2		2.27	2.97E-06
Apob	apolipoprotein B		-2.92	3.42E-05
Apoc1	apolipoprotein C-I		3.21	1.56E-06
Apoc4	apolipoprotein C-IV		3.14	1.91E-04
Arg1 *,,#**	arginase, liver	15-18	-8.48	5.07E-03
Arxes1	adipocyte-related X-chromosome expressed sequence 1		-2.23	1.68E-03
Arxes2	adipocyte-related X-chromosome expressed sequence 2		-2.96	3.37E-04
Asb10	ankyrin repeat and SOCS box-containing 10		2.1	1.14E-03
Asb11	ankyrin repeat and SOCS box-containing 11		2.19	3.00E-04
Aspm	asp (abnormal spindle)-like, microcephaly associated (Drosophila)		-2.22	1.02E-03
Aurka	aurora kinase A		-2.23	1.30E-03
Aurkb	aurora kinase B		-2.71	4.19E-06
Bambi	BMP and activin membrane-bound inhibitor, homolog (Xenopus laevis)		2.64	6.53E-05
Birc5	baculoviral IAP repeat-containing 5		-6.13	3.00E-06
Bub1	budding uninhibited by benzimidazoles 1 homolog (S. cerevisiae)		-2.72	4.19E-06

Calml4	calmodulin-like 4		-2.06	2.12E-05
Camkk1	calcium/calmodulin-dependent protein kinase kinase 1, alpha		-2.13	2.69E-08
Cbr2	carbonyl reductase 2		-4.15	2.93E-07
Ccna2	cyclin A2		-3.9	1.19E-05
Ccnb1	cyclin B1		-3.55	2.25E-05
Ccnb2	cyclin B2		-4.53	1.16E-05
Ccnd1	cyclin D1		-3.01	1.06E-08
Ccnd2	cyclin D2		-3.34	1.36E-05
Ccne2	cyclin E2		-5.28	3.67E-08
Ccnf	cyclin F		-2.3	1.48E-04
Ccr1	chemokine (C-C motif) receptor 1		-4.56	6.86E-05
Cd163 **	CD163 antigen	15	-2.65	3.87E-07
Cd22	CD22 antigen		2.35	1.09E-05
Cd244	CD244 natural killer cell receptor 2B4		-2.71	1.11E-07
Cd38	CD38 antigen		-3.72	4.44E-05
Cd5	CD5 antigen		3.62	2.96E-05
Cd83	CD83 antigen		2.28	2.53E-05
Cd93	CD93 antigen		-2.42	2.30E-07
Cdc20	cell division cycle 20 homolog (S. cerevisiae)		-2.75	1.16E-04
Cdc45	cell division cycle 45 homolog (S. cerevisiae)		-2.03	9.78E-08
Cdc6	cell division cycle 6 homolog (S. cerevisiae)		-3.67	8.12E-08
Cdca5	cell division cycle associated 5		-2.24	6.77E-06
Cdh1 **	cadherin 1	19, 20	-6.43	1.70E-04
Cdh2	cadherin 2		-2.23	6.25E-04
Cdk1	cyclin-dependent kinase 1		-2.18	2.75E-05
Cenpe	centromere protein E		-4.18	1.96E-05
Cenpk	centromere protein K		-2.45	1.46E-05
Cep55	centrosomal protein 55		-2.4	8.23E-05
Cfp	complement factor properdin		-2.64	2.60E-04
Chst2	carbohydrate sulfotransferase 2		2.44	5.14E-04
Ckap2	cytoskeleton associated protein 2		-2.17	1.80E-04
Cks1b	CDC28 protein kinase 1b		-2.54	1.71E-06
Clec4n	C-type lectin domain family 4, member n		-6.53	4.34E-10
Clu	clusterin		-2.34	3.55E-04
Cntn1	contactin 1		-4.93	2.80E-08
Col11a1	collagen, type XI, alpha 1		-3.49	3.09E-04
Col14a1	collagen, type XIV, alpha 1		-2.65	1.37E-06
Cpa3	carboxypeptidase A3, mast cell		2.17	6.30E-04
Cpeb1	cytoplasmic polyadenylation element binding protein 1		2.86	1.97E-05
Cpne2	copine II		-2.2	1.13E-05

Crybb1	crystallin, beta B1		-2.83	2.44E-05
Cspg5	chondroitin sulfate proteoglycan 5		-2.61	1.09E-05
Cst7	cystatin F (leukocystatin)		2.62	2.29E-07
Ctnnd2	catenin (cadherin associated protein), delta 2		-2.94	8.46E-07
Ctsf	cathepsin F		2.1	1.53E-04
Cxcr7	chemokine (C-X-C motif) receptor 7		-2.26	8.65E-03
Cyp4v3	cytochrome P450, family 4, subfamily v, polypeptide 3		2.14	1.15E-05
D17H6S56E-5	DNA segment, Chr 17, human D6S56E 5		-2.01	1.66E-03
Dck	deoxycytidine kinase		-2.07	2.50E-04
Ddhd1	DDHD domain containing 1		2.06	4.86E-03
Ddit4	DNA-damage-inducible transcript 4		-2.43	5.07E-06
Depdc1a	DEP domain containing 1a		-2.81	9.05E-05
Dhfr	dihydrofolate reductase		-2.4	5.79E-06
Dner	delta/notch-like EGF-related receptor		-2.68	2.65E-04
Dusp1	dual specificity phosphatase 1		2.33	3.55E-04
E2f8	E2F transcription factor 8		-2.71	1.20E-05
Ect2	ect2 oncogene		-3.19	1.65E-04
Eepd1	endonuclease/exonuclease/phosphatase family domain containing 1		2.7	1.62E-06
Emb	embigin		-2.59	9.66E-05
Emp1	epithelial membrane protein 1		-3.19	6.42E-04
Ephx1	epoxide hydrolase 1, microsomal		2.76	1.75E-04
Eps8	epidermal growth factor receptor pathway substrate 8		-2.51	4.00E-06
Ero1l	ERO1-like (S. cerevisiae)		-2.64	1.07E-05
Etl4	enhancer trap locus 4		2.41	1.24E-05
Ezh2	enhancer of zeste homolog 2 (Drosophila)		-2.54	1.36E-05
F13a1 *,**	coagulation factor XIII, A1 subunit	21, 22	-10.66	1.39E-09
F3	coagulation factor III		-2.11	4.58E-03
F9	coagulation factor IX		2.12	5.92E-04
Fabp3	fatty acid binding protein 3, muscle and heart		2.93	4.99E-06
Fabp7	fatty acid binding protein 7, brain		-6.77	9.66E-06
Fam20c	family with sequence similarity 20, member C		2.79	3.62E-06
Fap	fibroblast activation protein		-2.25	1.46E-03
Fbn2	fibrillin 2		-2.13	3.89E-03
Fbxo32	F-box protein 32		2.54	1.79E-05
Fhl1	four and a half LIM domains 1		-2.02	5.40E-03
Fpr2	formyl peptide receptor 2		-2.83	6.68E-05
Gadd45a	growth arrest and DNA-damage-inducible 45 alpha		2.4	2.77E-04

Gap43	growth associated protein 43		-2.56	7.42E-05
Gdf3	growth differentiation factor 3		-3.33	1.40E-07
Gem	GTP binding protein (gene overexpressed in skeletal muscle)		2.17	7.03E-04
Ggta1	glycoprotein galactosyltransferase alpha 1, 3		-2.4	2.12E-06
Gja1	gap junction protein, alpha 1		-2.78	1.97E-03
Gpm6a	glycoprotein m6a		-5.35	3.23E-06
Gpnmb	glycoprotein (transmembrane) nmb		3.22	3.98E-05
Gzma	granzyme A		3.55	4.11E-03
Hells	helicase, lymphoid specific		-3.59	9.75E-06
Hmgb3	high mobility group box 3		-2.42	2.32E-06
Hmgn5	high-mobility group nucleosome binding domain 5		-2.58	1.79E-05
Hmox1 **	heme oxygenase (decycling) 1	23-25	-2.9	7.05E-05
Hsp90aa1	heat shock protein 90, alpha (cytosolic), class A member 1		-2.23	1.01E-03
Hspa1a	heat shock protein 1A		-4.38	1.45E-05
Hspa1b	heat shock protein 1B		-8.71	1.88E-08
Ifitm1	interferon induced transmembrane protein 1		-5.18	1.21E-04
Ifitm2	interferon induced transmembrane protein 2		-2.82	1.54E-03
Ifitm3	interferon induced transmembrane protein 3		-2.06	4.73E-03
Ifitm6	interferon induced transmembrane protein 6		-4.14	6.14E-04
Igf1	insulin-like growth factor 1		2.13	8.56E-05
Igfbp2	insulin-like growth factor binding protein 2		-3.54	1.24E-06
Igfbp3	insulin-like growth factor binding protein 3		-6.53	1.05E-05
Igj	immunoglobulin joining chain		3.36	4.53E-03
Ikbke	inhibitor of kappaB kinase epsilon		2.38	1.50E-04
Il1r2 **	interleukin 1 receptor, type II	15, 26	-2.32	1.9E-02
Il18bp	interleukin 18 binding protein		3.66	4.53E-04
Il1b ***	interleukin 1 beta	15, 26, 27	2.06	4.50E-04
Il7r	interleukin 7 receptor		-2.01	4.96E-03
Itgam	integrin alpha M		-2.25	2.27E-04
Itgax	integrin alpha X		2.08	1.36E-03
Kcnk2	potassium channel, subfamily K, member 2		-2.13	8.52E-05
Khdrbs3	KH domain containing, RNA binding, signal transduction associated 3		-2.1	3.94E-04
Kif11	kinesin family member 11		-2.57	9.00E-05
Kif20a	kinesin family member 20A		-3.76	8.28E-05
Kif22	kinesin family member 22		-2.14	2.42E-04

Klrb1a	killer cell lectin-like receptor subfamily B member 1A		4.3	9.00E-05
Kpna2	karyopherin (importin) alpha 2		-2.38	1.98E-05
Lgals1	lectin, galactose binding, soluble 1		-2.11	3.24E-04
Lgals9	lectin, galactose binding, soluble 9		-2.42	6.75E-04
Lifr	leukemia inhibitory factor receptor		-2.06	1.12E-03
Lig1	ligase I, DNA, ATP-dependent		-2.66	5.22E-10
Lox	lysyl oxidase		2.42	6.19E-03
Lpl	lipoprotein lipase		3.08	2.21E-07
Lrr1	leucine rich repeat protein 1		-2.65	3.08E-06
Ltc4s	leukotriene C4 synthase		-2.52	5.69E-07
Mad2l1	MAD2 mitotic arrest deficient-like 1 (yeast)		-2.45	1.17E-05
Mcm2	minichromosome maintenance deficient 2 mitotin (S. cerevisiae)		-2.79	9.32E-08
Mcm4	minichromosome maintenance deficient 4 homolog (S. cerevisiae)		-2.93	2.05E-06
Mcm5	minichromosome maintenance deficient 5, cell division cycle 46 (S. cerevisiae)		-4.38	1.47E-08
Mcm6	minichromosome maintenance deficient 6 (MIS5 homolog, S. pombe) (S. cerevisiae)		-3.27	3.13E-07
Mcm7	minichromosome maintenance deficient 7 (S. cerevisiae)		-2.23	6.52E-07
Melk	maternal embryonic leucine zipper kinase		-3.4	5.03E-06
Mis18bp1	MIS18 binding protein 1		-2.03	1.03E-04
Mitf	microphthalmia-associated transcription factor		2.08	6.51E-07
Mki67	antigen identified by monoclonal antibody Ki 67		-7.18	2.78E-05
Mmp10	matrix metallopeptidase 10		-2.33	1.11E-02
Moxd1	monooxygenase, DBH-like 1		-2.81	3.72E-04
Mrc1 *,**	mannose receptor, C type 1 (CD206)	15, 16	-8.44	4.40E-07
Ms4a4c	membrane-spanning 4-domains, subfamily A, member 4C		-2.11	7.53E-03
Ms4a6b	membrane-spanning 4-domains, subfamily A, member 6B		-3.12	1.45E-08
Ms4a6c	membrane-spanning 4-domains, subfamily A, member 6C		-2.47	2.34E-06
Ms4a7	membrane-spanning 4-domains, subfamily A, member 7		-3.2	2.00E-07
Mt2	metallothionein 2		-2.17	1.44E-03
Mtss1	metastasis suppressor 1		-2.28	1.19E-05
Nap1l5	nucleosome assembly protein 1-like 5		-2.91	1.63E-04
Ncapd2	non-SMC condensin I complex,		-2.77	1.98E-05

	subunit D2		
Ncapg	non-SMC condensin I complex, subunit G	-3.02	3.89E-06
Ncapg2	non-SMC condensin II complex, subunit G2	-2.96	3.08E-06
Ndc80	NDC80 homolog, kinetochore complex component (S. cerevisiae)	-2.28	8.12E-05
Nkg7	natural killer cell group 7 sequence	2.04	5.16E-03
Nop58	NOP58 ribonucleoprotein homolog (yeast)	-2.14	2.49E-03
Nov	nephroblastoma overexpressed gene	3.6	1.99E-03
Nrp2	neuropilin 2	2.02	4.53E-06
Nt5dc2	5'-nucleotidase domain containing 2	-2.48	2.23E-05
Nuf2	NUF2, NDC80 kinetochore complex component, homolog (S. cerevisiae)	-5.28	5.04E-06
Olig1	oligodendrocyte transcription factor 1	-3.85	1.82E-04
Olig2	oligodendrocyte transcription factor 2	-2.35	2.75E-04
P2ry12	purinergic receptor P2Y, G-protein coupled 12	-2.55	1.86E-04
P4ha2	procollagen-proline, 2-oxoglutarate 4-dioxygenase (proline 4-hydroxylase), alpha II polypeptide	-3.54	1.25E-06
Pbk	PDZ binding kinase	-5.63	9.20E-07
Pdgfc	platelet-derived growth factor, C polypeptide	-2.25	2.98E-03
Pdgfra	platelet derived growth factor receptor, alpha polypeptide	-3.16	4.84E-06
Pdpn	podoplanin	-2.01	3.51E-04
Pf4	platelet factor 4	-2.96	1.21E-05
Pilra	paired immunoglobin-like type 2 receptor alpha	-2.35	1.51E-05
Plac8	placenta-specific 8	-2.79	6.64E-03
Plk1	polo-like kinase 1 (Drosophila)	-2.68	5.72E-05
Pmepa1	prostate transmembrane protein, androgen induced 1	-2.35	5.85E-04
Pnlip	pancreatic lipase	-2.39	1.76E-04
Pola1	polymerase (DNA directed), alpha 1	-2.37	3.52E-06
Pold2	polymerase (DNA directed), delta 2, regulatory subunit	-2.02	5.72E-06
Pole	polymerase (DNA directed), epsilon	-2.27	5.96E-05
Prc1	protein regulator of cytokinesis 1	-3.06	1.26E-04

Prickle1	prickle homolog 1 (Drosophila)		2.32	1.75E-04
Prim1	DNA primase, p49 subunit		-2.76	2.87E-07
Psmb7	proteasome (prosome, macropain) subunit, beta type 7		-2.17	4.27E-03
Ptger4	prostaglandin E receptor 4 (subtype EP4)		2.43	5.12E-05
Ptn	pleiotrophin		-3.21	4.42E-04
Ptprz1	protein tyrosine phosphatase, receptor type Z, polypeptide 1		-3.66	4.43E-05
Pttg1	pituitary tumor-transforming gene 1		-2.83	2.73E-06
Rab34	RAB34, member of RAS oncogene family		2.08	3.95E-05
Racgap1	Rac GTPase-activating protein 1		-2.56	2.92E-05
Rad51	RAD51 homolog (S. cerevisiae)		-2.9	3.33E-06
Rad51ap1	RAD51 associated protein 1		-2.61	1.26E-07
Ranbp1	RAN binding protein 1		-2.01	6.62E-07
Rbm3	RNA binding motif protein 3		-2.2	2.23E-09
Rbp1	retinol binding protein 1, cellular		-4.22	1.88E-05
Rfc4	replication factor C (activator 1) 4		-2.17	4.24E-05
Rrm1	ribonucleotide reductase M1		-2.14	1.79E-05
Rrm2	ribonucleotide reductase M2		-8.23	1.04E-07
Serpinb2 *,**	serine (or cysteine) peptidase inhibitor, clade B, member 2 (PAI2)	25, 28	6.2	1.12E-02
Serpinb6b	serine (or cysteine) peptidase inhibitor, clade B, member 6b		2.03	1.22E-03
Sh3bgr	SH3-binding domain glutamic acid-rich protein		3.33	6.84E-07
Sh3bgrl	SH3-binding domain glutamic acid-rich protein like		-2.02	4.68E-04
Shcbp1	Shc SH2-domain binding protein 1		-4.72	1.74E-06
Slamf8	SLAM family member 8		2.81	5.20E-03
Slc2a5	solute carrier family 2 (facilitated glucose transporter), member 5		-3.46	8.15E-07
Slc39a4	solute carrier family 39 (zinc transporter), member 4		2.44	7.83E-05
Slc6a1	solute carrier family 6 (neurotransmitter transporter, GABA), member 1		-2.09	5.66E-04
Slfn4	schlafen 4		-3.35	3.42E-03
Smc2	structural maintenance of chromosomes 2		-2.87	7.80E-05
Smc4	structural maintenance of chromosomes 4		-3.2	2.26E-04
Smyd2	SET and MYND domain containing 2		-2.25	6.90E-04
Snrpa1	small nuclear ribonucleoprotein polypeptide A'		-2.04	1.48E-06
Sox2	SRY-box containing gene 2		-2.5	5.13E-03

Sparcl1	SPARC-like 1		-3.23	1.06E-03
Spon1	spondin 1, (f-spondin) extracellular matrix protein		-2.5	9.32E-05
St14	suppression of tumorigenicity 14 (colon carcinoma)		2.47	4.21E-06
Stab1 **	stabilin 1	29-31	-2.64	3.92E-06
Stil	Scl/Tal1 interrupting locus		-3.15	2.15E-06
Stmn1	stathmin 1		-2.52	5.52E-05
Tcf19	transcription factor 19		-2.32	1.67E-06
Tfpi2	tissue factor pathway inhibitor 2		-2.6	3.99E-03
Tgfbi	transforming growth factor, beta induced		-3.23	1.68E-06
Tgm2	transglutaminase 2, C polypeptide		-2.94	2.86E-03
Timp1	tissue inhibitor of metalloproteinase 1		-2.07	1.64E-04
Tiparp	TCDD-inducible poly(ADP-ribose) polymerase		-2.06	1.25E-03
Tipin	timeless interacting protein		-2.5	6.24E-06
Tk1	thymidine kinase 1		-3.39	1.24E-07
Tmem119	transmembrane protein 119		-3.12	1.71E-06
Tmem163	transmembrane protein 163		2.2	5.42E-03
Tnc	tenascin C		-2.56	2.48E-03
Top2a	topoisomerase (DNA) II alpha		-2.11	2.13E-05
Topbp1	topoisomerase (DNA) II binding protein 1		-2.37	9.96E-06
Tpx2	TPX2, microtubule-associated protein homolog (Xenopus laevis)		-2.52	1.16E-05
Trim59	tripartite motif-containing 59		-2.78	3.02E-04
Trps1	trichorhinophalangeal syndrome I (human)		-2.97	1.68E-07
Ttk	Ttk protein kinase		-2.63	3.35E-05
Tubb2c	tubulin, beta 2C		-2.13	3.84E-06
Ube2c	ubiquitin-conjugating enzyme E2C		-3.98	1.12E-04
Uhrf1	ubiquitin-like, containing PHD and RING finger domains, 1		-2.96	3.73E-07
Ung	uracil DNA glycosylase		-2.5	5.81E-07
Wdhd1	WD repeat and HMG-box DNA binding protein 1		-2.01	2.52E-04
Zwilch	Zwilch, kinetochore associated, homolog (Drosophila)		-4.32	3.61E-06

Supplementary Table 4 legend: Differentially expressed genes were identified as described in the supplementary methods section; 257 genes in total, denoted as the 'total' gene signature in the main text. Downregulated genes in the BLZ945-treated group are given a negative fold change, while upregulated genes are considered positive. Nominal *P* values were obtained using Student's two tailed t-test.

[1] Citations for genes associated with M1 and M2 macrophage polarization (see Supplementary Fig. 20f, g). References are listed at the end of Supplementary Information.
* Component of 'minimal' gene signature of response to BLZ945, determine by lasso logistic regression modeling.
** M2 macrophage-associated genes.
*** M1 macrophage-associated gene.
# Arginase 1 is associated with M2 macrophage polarization in mice, but not humans (17, 18).

Supplementary Table 5: Survival data in the different GBM patient populations for the 'BLZ945-like' and 'Vehicle-like' classes using the 'minimal' and 'total' gene signatures.

Patient Population	'BLZ945-like'	'Vehicle-like'	Change in Median Survival	*P* value
Total Gene Signature				
Combined Neural	49	16	5.42	0.159
Combined Proneural	46	62	31.54	**6.86x10-4**
Combined Mesenchymal	37	102	-2.25	0.892
Combined Classical	11	48	0.40	0.667
TCGA Proneural	45	88	7.64	**0.00727**
TCGA Proneural G-CIMP	13	8	-40.60	0.201
TCGA Proneural non G-CIMP	22	44	-0.76	0.264
TCGA G-CIMP	14	8	-35.60	0.203
TCGA non G-CIMP	83	157	-1.06	0.727
TCGA Neural	23	30	2.84	0.773
TCGA Mesenchymal	53	99	0.30	0.762
TCGA Classical	31	66	-3.14	0.771
Minimal Gene Signature				
Combined Neural	51	14	7.01	0.065
Combined Proneural	79	29	6.51	**0.0415**
Combined Mesenchymal	21	118	1.88	0.555
Combined Classical	28	31	0.33	0.968
TCGA Proneural	84	49	9.98	**$5.41x10^{-6}$**
TCGA Proneural G-CIMP	20	1	NA	NA
TCGA Proneural non G-CIMP	40	26	10.84	**0.014**
TCGA G-CIMP	20	2	-16.13	0.721
TCGA non G-CIMP	100	140	0.10	0.414
TCGA Neural	31	22	-5.19	**0.0272**
TCGA Mesenchymal	23	129	0.40	0.835
TCGA Classical	49	48	-1.42	0.634

Supplementary Table 5 legend: Survival data for the minimal and total gene signatures in the different GBM patient subtypes and populations: 'Combined' and TCGA datasets are as detailed in the Supplementary Methods section. Development of gene signatures and implementation for patient classification are also detailed in the Supplementary Methods section.

An increase in median survival in the 'BLZ945-like' class compared to the 'Vehicle-like' class is depicted as a positive value, while a decrease in survival is shown as a negative value. Although TCGA neural patients classified as 'BLZ945-like' using the minimal gene signature demonstrated a decrease in survival, this was not seen in the Combined dataset, or with the total gene signature in either dataset. Only proneural patients demonstrated a consistent survival advantage in the 'BLZ945-like' class in both the TCGA and Combined datasets using either the minimal or total gene signature. *P* values for median survival were obtained using a Log Rank test, and all significant *P* values are indicated in bold.

Supplementary Table 6: Hazard ratios and associated 95% confidence intervals for the 'minimal' gene signature in different patient datasets.

Patient Population	Hazard Ratio	95% CI	*P* value
TCGA- Proneural	0.29	(0.17-0.50)	**6.32×10^{-6}**
TCGA- Classical	1.28	(0.73-2.26)	0.389
TCGA- Mesenchymal	0.93	(0.49-1.72)	0.807
TCGA- Neural	1.93	(0.83-4.46)	0.125
Combined- Proneural	0.44	(0.25-0.79)	**0.00597**
Combined- Classical	1.01	(0.47-2.17)	0.979
Combined- Mesenchymal	1.02	(0.54-1.94)	0.943
Combined- Neural	0.46	(0.22-1.01)	0.0532

Supplementary Table 6 legend: Classification using the 'minimal' gene signature in the lasso logistic regression model produced a classification probability for each sample. The probability of the 'BLZ945-like' class prediction was used as a continuous variable in a cox proportional hazards model. Of note, although TCGA neural patients classified to the 'BLZ945-like' class using the minimal gene signature showed significantly decreased median survival with the Log Rank test (Supplementary Table 5), the non-significant hazard ratio demonstrates that at any given time point, this classification does not provide a clear association with survival for neural patients. Only hazard ratios from the proneural subtypes are significant. *P* values were obtained using Wald's test, and all significant *P* values are indicated in bold.

Supplementary Table 7: Hazard ratios and associated 95% confidence intervals for the 'minimal' gene signature in different G-CIMP and non G-CIMP patient groups.

Model Term	Patient Population[1]	Model	Hazard Ratio	95% CI	*P* value
'BLZ945-like' *	Non-G-CIMP Proneural**	Univariate	0.35	(0.16-0.78)	**0.0095**
'BLZ945-like' *	All Proneural	Univariate	0.29	(0.17-0.50)	**6.32×10^{-6}**
G-CIMP	All Proneural	Univariate	0.40	(0.19-0.81)	**0.011**
G-CIMP	All Proneural	Multivariate***	0.39	(0.19-0.85)	**0.018**
'BLZ945-like' *	All Proneural	Multivariate***	0.49	(0.24-1.06)	0.070

Supplementary Table 7 legend: G-CIMP corresponds to Glioma CpG Island Methylator Phenotype. *P* values were obtained using Wald's test, and all significant *P* values are indicated in bold.

[1] Only the TCGA patients were considered due to the absence of methylation data from patients in the 'Combination' data set.

* The probability of the 'BLZ945-like' class prediction was used as a continuous variable in a cox proportional hazards model. See Supplementary Methods and Supplementary Table 6.

** Set of proneural patients with methylation data that are definitively not G-CIMP positive (67/133 total proneural TCGA patients).

*** Multivariate cox proportional hazard model using both G-CIMP and 'BLZ945-like' probability from the lasso logistic regression as additive terms.

Supplementary Table 8: Hazard ratios and associated 95% confidence intervals for select macrophage markers in the TCGA and Combined datasets

Model Term	Patient Population	Hazard Ratio	95% CI	*P* Value
Univariate Cox Model: TCGA Dataset				
ITGAM	Proneural	1.31	0.93-1.82	0.12
AIF1	Proneural	1.05	0.92-1.21	0.48
CD68	Proneural	1.02	0.74-1.41	0.91
ITGAM	Mesenchymal	0.95	0.59-1.61	0.87
AIF1	Mesenchymal	0.83	0.64-1.08	0.17
CD68	Mesenchymal	0.90	0.66-1.20	0.48
ITGAM	Classical	1.08	0.63-1.89	0.77
AIF1	Classical	1.02	0.83-1.27	0.84
CD68	Classical	1.38	0.81-2.33	0.24
ITGAM	Neural	1.30	0.63-2.69	0.48
AIF1	Neural	1.07	0.81-1.42	0.64
CD68	Neural	1.24	0.74-2.06	0.42
Univariate Cox Model: Combined Dataset				
ITGAM	Proneural	0.54	0.28-1.01	0.057
AIF1	Proneural	0.71	0.51-0.98	**0.035**
ITGAM	Mesenchymal	0.85	0.51-1.41	0.53
AIF1	Mesenchymal	0.78	0.57-1.07	0.13
ITGAM	Classical	0.84	0.27-2.65	0.77
AIF1	Classical	1.02	0.56-1.85	0.95
ITGAM	Neural	0.36	0.13-0.96	**0.043**
AIF1	Neural	0.61	0.37-0.98	**0.045**

Supplemental Table 8 legend: Hazard ratios and associated 95% confidence intervals (CI) are shown for scaled gene expression of select macrophage markers: *CD68*, *AIF1* (*Iba1* in mouse) and *ITGAM* (*CD11b* in mouse). *P* values were obtained using Wald's test and all significant *P* values are indicated in bold. *AIF1* expression was found to positively correlate with improved survival in proneural GBM in the combined dataset. Both *ITGAM* and *AIF1* were found to positively correlate with improved survival in neural GBM in the combined dataset.

Note: *CD68* expression data was not available in the Phillips et al dataset and was thus excluded from the survival analysis in the Combined dataset.

Supplementary Table 9: Interaction based cox proportional hazard model: assessing the contribution of macrophage abundance to the prognostic value of the 'minimal' gene signature.

Model Term	Model	Patient Population	Hazard Ratio	95% CI	*P* Value
Multivariate Cox Model TCGA Dataset					
Minimal term	Minimal * *ITGAM*	Proneural	0.26	0.13-0.49	**3.45×10^{-5}**
ITGAM term	Minimal * *ITGAM*	Proneural	1.29	0.49-3.35	0.598
Interaction	Minimal * *ITGAM*	Proneural	0.73	0.22-2.33	0.599
Minimal term	Minimal * *CD68*	Proneural	0.23	0.12-0.44	**8.72×10^{-6}**
CD68 term	Minimal * *CD68*	Proneural	0.71	0.29-1.74	0.465
Interaction	Minimal * *CD68*	Proneural	1.10	0.33-3.61	0.869
Minimal term	Minimal * *AIF1*	Proneural	0.25	0.13-0.46	**9.63×10^{-6}**
AIF1 term	Minimal * *AIF1*	Proneural	1.05	0.66-1.66	0.832
Interaction	Minimal * *AIF1*	Proneural	0.89	0.52-1.53	0.689
Minimal term	Minimal * *ITGAM*	Mesenchymal	0.83	0.38-1.82	0.647
ITGAM term	Minimal * *ITGAM*	Mesenchymal	0.85	0.40-1.81	0.678
Interaction	Minimal * *ITGAM*	Mesenchymal	1.30	0.22-7.65	0.770
Minimal term	Minimal * *CD68*	Mesenchymal	0.99	0.48-2.01	0.979
CD68 term	Minimal * *CD68*	Mesenchymal	0.96	0.66-1.39	0.837
Interaction	Minimal * *CD68*	Mesenchymal	0.79	0.33-1.88	0.603
Minimal term	Minimal * *AIF1*	Mesenchymal	0.71	0.32-1.59	0.417
AIF1 term	Minimal * *AIF1*	Mesenchymal	0.77	0.55-1.08	0.132
Interaction	Minimal * *AIF1*	Mesenchymal	1.27	0.50-3.21	0.606
Minimal term	Minimal * *ITGAM*	Classical	1.29	0.65-2.58	0.458
ITGAM term	Minimal * *ITGAM*	Classical	1.54	0.51-4.61	0.438
Interaction	Minimal * *ITGAM*	Classical	0.67	0.16-2.85	0.597
Minimal term	Minimal * *CD68*	Classical	2.27	0.91-5.63	0.075
CD68 term	Minimal * *CD68*	Classical	1.31	0.58-2.92	0.505
Interaction	Minimal * *CD68*	Classical	2.16	0.43-10.8	0.343
Minimal term	Minimal * *AIF1*	Classical	1.24	0.60-2.55	0.555
AIF1 term	Minimal * *AIF1*	Classical	1.16	0.69-1.95	0.563
Interaction	Minimal * *AIF1*	Classical	0.87	0.47-1.59	0.663
Minimal term	Minimal * *ITGAM*	Neural	2.43	0.94-6.26	0.064
ITGAM term	Minimal * *ITGAM*	Neural	0.87	0.23-3.32	0.848
Interaction	Minimal * *ITGAM*	Neural	3.76	0.33-42.0	0.281
Minimal term	Minimal * *CD68*	Neural	2.36	0.95-6.18	0.080
CD68 term	Minimal * *CD68*	Neural	0.48	0.14-1.58	0.230
Interaction	Minimal * *CD68*	Neural	14.8	1.69-130.2	**0.014**
Minimal term	Minimal * *AIF1*	Neural	1.58	0.58-4.30	0.364
AIF1 term	Minimal * *AIF1*	Neural	0.87	0.53-1.45	0.617
Interaction	Minimal * *AIF1*	Neural	1.60	0.68-3.78	0.279

Multivariate Cox Model Combined Dataset					
Minimal term	Minimal * *ITGAM*	Proneural	0.41	0.22-0.79	**7.08x10 $^{-3}$**
ITGAM term	Minimal * *ITGAM*	Proneural	0.98	0.34-2.85	0.983
Interaction	Minimal * *ITGAM*	Proneural	0.34	0.066-1.75	0.198
Minimal term	Minimal * *AIF1*	Proneural	0.41	0.22 -0.78	**6.33x10 $^{-3}$**
AIF1 term	Minimal * *AIF1*	Proneural	0.88	0.55-1.43	0.632
Interaction	Minimal * *AIF1*	Proneural	0.61	0.26-1.39	0.244
Minimal term	Minimal * *ITGAM*	Mesenchymal	1.87	0.68-5.09	0.220
ITGAM term	Minimal * *ITGAM*	Mesenchymal	1.10	0.61-1.99	0.742
Interaction	Minimal * *ITGAM*	Mesenchymal	0.19	0.028-1.41	0.106
Minimal term	Minimal * *AIF1*	Mesenchymal	1.64	0.65-4.11	0.288
AIF1 term	Minimal * *AIF1*	Mesenchymal	0.91	0.64-1.29	0.611
Interaction	Minimal * *AIF1*	Mesenchymal	0.25	0.055-1.16	0.078
Minimal term	Minimal * *ITGAM*	Classical	0.90	0.23-3.45	0.882
ITGAM term	Minimal * *ITGAM*	Classical	1.20	0.23-6.29	0.821
Interaction	Minimal * *ITGAM*	Classical	0.38	0.011-13.2	0.598
Minimal term	Minimal * *AIF1*	Classical	1.60	0.51-4.98	0.416
AIF1 term	Minimal * *AIF1*	Classical	0.88	0.37-2.05	0.771
Interaction	Minimal * *AIF1*	Classical	1.66	0.322-8.61	0.542
Minimal term	Minimal * *ITGAM*	Neural	0.58	0.253-1.35	0.212
ITGAM term	Minimal * *ITGAM*	Neural	0.24	0.022-2.64	0.247
Interaction	Minimal * *ITGAM*	Neural	1.35	0.050-36.3	0.857
Minimal term	Minimal * *AIF1*	Neural	0.50	0.21-1.19	0.118
AIF1 term	Minimal * *AIF1*	Neural	0.37	0.14-1.00	0.051
Interaction	Minimal * *AIF1*	Neural	1.86	0.45-7.70	0.391

Supplemental Table 9 legend: To determine if the 'minimal' gene signature showed any interaction with macrophage marker expression with regard to survival, we utilized a multivariate cox proportional hazard model. In proneural GBM, where the minimal gene signature showed the greatest prognostic value, there was no indication that the interaction term between the minimal term and any macrophage marker was significantly associated with survival.

Hazard ratios and associated 95% confidence intervals (CI) are shown for interactions between the minimal gene signature and select macrophage markers. *P* values were obtained using Wald's test and all significant *P* values are indicated in bold. The terms used in the cox proportional hazards model are indicated, where (*) refers to an interaction based model between the probability of the 'BLZ945-like' class in the minimal gene signature and the scaled expression values of the gene of interest.

Note: *CD68* expression data was not available in the Phillips et al dataset and was thus excluded from the survival analysis in the Combined dataset.

Supplementary Table 10: List of antibodies used for immunostaining.

Antibody	Species	Clone	Vendor	Dilution
BrdU	Rat anti-BrdU	BU1/75(ICR1)	Serotec	1:200
Cleaved caspase 3 (CC3)	Rabbit anti-human / mouse	--	Cell Signaling Technology	1:500
CD11b	Rat anti-mouse	M1/70	BD Pharmingen	1:200
CD31	Goat anti-mouse	--	R&D Systems	1:100
CD68	Rat anti-mouse	FA-11	Serotec	1:1,000
CSF-1R	Rabbit anti-human	C-20	Santa Cruz	1:200
GFAP	Chicken anti-cow	--	Abcam	1:1,000
Green fluorescent protein (GFP)	Chicken anti-jellyfish	--	Abcam	1:1000
Iba1	Rabbit anti-human	--	Wako	1:1,000
Nestin	Mouse anti-rat	--	BD Pharmingen	1:500
NeuN	Mouse IgG1	A60	Millipore/Chemicon	1:500
Olig2	Rabbit anti-mouse	--	Millipore/Chemicon	1:200
PDGF receptor alpha	Rabbit anti-human / mouse	D1E1E	Cell Signaling Technology	1:500
PDGF receptor beta	Rabbit anti-human / mouse	28E1	Cell Signaling Technology	1:500
α-Smooth muscle actin (α-SMA)	Mouse anti-human	1A4	DakoCytomation	1:100

Supplementary Table 11: List of antibodies used for flow cytometry analysis.

Antibody	Species	Clone	Vendor	Fluorophore(s)	Dilution
CD3e	Hamster anti-mouse	145-2C11	BD Pharmingen	PE-Cy7	1:250
CD4	Rat anti-mouse	GK1.5	BD Pharmingen	PE	1:1,000
CD8a	Rat anti-mouse	53-6.7	Biolegend	A488	1:1,000
CD11b	Rat anti-mouse	M1/70	eBioscience	A488, APC, PE	1:200
CD19	Rat anti-mouse	6D5	Biolegend	PE	1:2,000
CD45	Rat anti-mouse	30-F11	BD Pharmingen	FITC, APC, PE-Cy7	1:100 -1:200
CD206	Rat anti-mouse	MR5D3	Biolegend	A488	1:50
F4/80	Rat anti-mouse	CI:A3-1	Serotec	PE	1:50
Gr-1	Rat anti-mouse	RB6-8C5	BD Pharmingen	FITC	1:200
Ly6G	Rat anti-mouse	1A8	BD Pharmingen	PE-Cy7	1:2,000
NK1.1	Rat anti-mouse	PK136	Biolegend	APC	1:1,000

Supplementary Methods

Synthetic routes to BLZ945

Starting Materials:
6-ethoxy2-mercaptobenzothiazole and (1R,2R)-(-)-2-Benzyloxycyclohexylamine (98% ee) were purchased from Alfa Aezar. mCPBA, $AlCl_3$, $CsCO_3$ and picolinic acid were purchased from Sigma Aldrich. All other solvents/reagents are readily available from multiple suppliers.

Abbreviations

br	Broad
d	Doublet
DCM	Dichloromethane
dd	Doublet of doublets
DIEA	N,N-Diisopropylethylamine
DME	Dimethoxyethane
DMF	*N,N*-Dimethylformamide
DMSO	Dimethyl sulfoxide
eq.	Equivalents
ESI-MS	Electrospray Ionization Mass Spectrometry
EtOAc	Ethylacetate
EtOH	Ethanol
HCl	Hydrochloric acid
HOAc	Acetic acid
HPLC	High Performance Liquid Chromatography
HRMS	High Resolution Mass Spectroscopy
LCMS	Liquid Chromatography Mass Spectroscopy
m	Multiplet
mCPBA	*meta*-Chloroperoxybenzoic acid
MeOH	Methanol
MS	Mass Spectrometry
NMR	Nuclear Magnetic Resonance
q	Quartet
RT	Retention time
s	Singlet
Sat.	Saturated
t	Triplet
UPLC	Ultra Performance Liquid Chromatography

General Procedures:

NMR spectra were recorded on one of the following instruments:

- Bruker AVANCE-500 spectrometer operating at a frequency of 500.13 MHz for ^{1}H and 125.77 MHz for ^{13}C equipped with a 5 mm BBO probe with Z-gradient. Chemical shifts for ^{1}H and ^{13}C spectra were referenced to internal tetramethylsilane (TMS) at 0 ppm. All spectra were recorded at a temperature of 300°K.

- Bruker ASCEND-500 NMR spectrometer operating at a frequency of 500.08 MHz for ^{1}H and 100.56 MHz for ^{13}C equipped with a 5 mm BBO Cryo-probe with a Z-gradient. Deuteriated DMSO was used as the NMR solvent for all the experiments. Chemical shifts for ^{1}H and ^{13}C spectra were referenced to the DMSO solvent peak at 2.5ppm and 39.5ppm respectively. The spectra were recorded at a temperature of 298°K.
- Varian 400MR spectrometer operating at a frequency of 399.88 MHz for ^{1}H and 100.56 MHz for ^{13}C equipped with a 5 mm PFG AutoX H/F with Z-gradient. Chemical shifts for ^{1}H and ^{13}C spectra were referenced to the DMSO solvent peak at 2.5ppm and 39.5ppm respectively. The spectra were recorded at a temperature of 298°K.

LCMS was performed on a Waters Alliance HT HPLC with a Micromass ZQ mass spectrometer (molecular weight range 200-1,500, cone voltage 20V). Column was an Eclipse XDB-C18 (2.1 x50 mm, column temperature 40^{o}C) run with a gradient 5-95% acetonitrile in water with 0.05% TFA with a flow rate of 0.8 ml/min over a 4-minute period.

ESI-MS data were recorded using a Synapt G2 HDMS (TOF mass spectrometer, Waters) with electrospray ionization source. The resolution of the MS system was approximately 15,000. Leucine Enkephalin was used as lock mass (internal standards) infused from lockspary probe. The compound was infused into the mass spectrometer by UPLC (Acquity, Waters) from sample probe. The separation was performed on Acquity UPLC BEH C18 1x50 mm column at 0.2 ml/min flow rate with the gradient from 5% to 95% in 3 min. Solvent A was Water with 0.1% Formic Acid and solvent B was Acetonitrile with 0.1% Formic Acid. The mass accuracy of the system has been found to be <5 ppm with lock mass.

Supplementary Scheme 1 – Synthetic Route to 4-chloro-N-methylpicolinamide

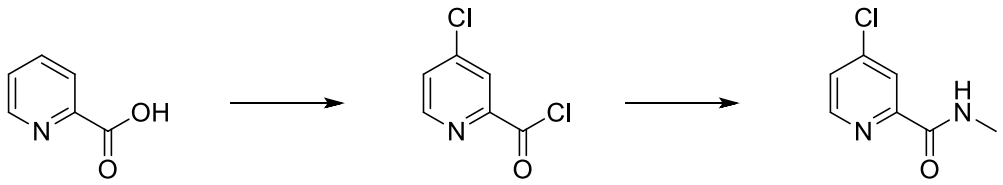

A B C

4-chloro-N-methylpicolinamide was prepared for picolinic acid following the methods described by Bankston, Donald; Dumas, Jaques; Natero, Reina, Riedl, Bernd; Monahan, Mary-Katherine; Sibley, Robert. *Organic Process Research & Development* **2002**, *6*, 777-781.

1H NMR (400 MHz, DMSO-d_6) d ppm 2.82 (d, J=4.70 Hz, 3 H) 7.69 - 7.76 (m, 1 H) 8.00 (s, 1 H) 8.60 (d, J=5.09 Hz, 1 H) 8.83 (br. s., 1 H); ESI-MS calc. [M+H]+ 171.0325, found [M+H]+ = 171.0320, RT = 1.15 min;

Supplementary Scheme 2 – Synthetic Route to (1*R*,2*R*)-2-aminocyclohexanol hydrochloride

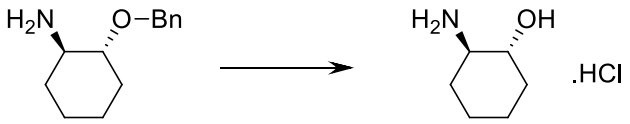

D E

To an ice bath cooled solution of (1*R*,2*R*)-(-)-2-Benzyloxycyclohexylamine (20 g, 97.4 mmol) in dry MeOH (390 ml) was added 4.0 M HCl solution in dioxane (49 ml, 195 mmol) slowly via syringe. The ice bath was removed and resulting solution was sparged with N_2 for 10 minutes. 10 % Pd/C (3 g, 28 mmol) was added to the solution and the reaction was purged with hydrogen and maintained under a hydrogen atmosphere. After 4 hours, an additional 10 ml of 4.0 M HCl solution in dioxane was added and the reaction was maintained under a H_2 atmosphere overnight (~16-18 hours).

Starting material was consumed as indicated by LCMS. The reaction was filtered through a thin, tightly packed pad of Celite and the collected solids were washed successively with MeOH and EtOAc. The combined organic filtrates were evaporated *in vacuo* to give (1*R*,2*R*)-2-aminocyclohexanol hydrochloride as a pale-colored solid, (13.8 g, 91 mmol, 93%). No further purification was required. MS [M+H]+ 116.0

Supplementary Scheme 3 – Synthetic Route to 2-(methylthio)benzothiazol-6-ol

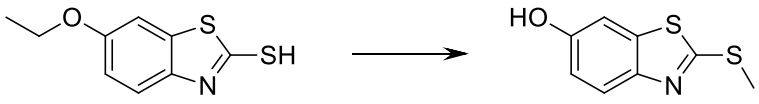

F G

Following the method outlined in patent US4873346, a suspension of 6-ethoxybenzothiazole-2-thiol (59 g, 279 mmol) in toluene (1L) in a 2L reaction vessel was cooled to 0°C. $AlCl_3$ (155 g) was added in portions over ~15 minutes. The reaction vessel was fitted with a reflux condenser and with stirring the reaction was then heated to 115°C for ~3.5 hours. The reaction was then cooled to 0°C to provide a light greenish-yellow solid (Solid A). The Solid_A was removed by filtration and the toluene eluent was saved for later processing. The Solid A was added slowly in portions to a large beaker (2L) containing ice (~1/5 of container volume). Upon final addition of the solid the pH of the water was then less than 1. At this time the remaining solid (Solid_B) was then collected by filtration.

The above toluene eluent was cooled to 0°C and then quenched by slow addition of ice to provide additional solid (Solid_C).

Solid_B and Solid_C were combined and taken up in 1N NaOH (~750 ml, keeping solution basic, pH 9-10). Remaining solids at this point were removed by filtration and discarded. The pH of the solution was then adjusted to ~7 by slow addition of HOAc to provide a white solid which was collected by filtration, rinsed with water and then rinsed with 30% EtOH in water. The solid was dried *in vacuo* to provide the intermediate 2-Mercaptobenzothiaz-6-ol as a white solid (45.26 g, MS [M+H]+ 184.0)

The 2-mercapto-benzothiazol-6-ol (45.26 g, 246 mmol, 1.0 eq) was taken up in triethyl amine (85.7 ml, 615 mmol, 2.5 eq), cooled to 0°C and treated with dropwise addition of methyliodide (38.42g, 270 mmol, 1.1 eq) over ~30 minutes while maintaining reaction temperature at 0°C. The reaction was then allowed to warm to room temperature and stir for ~4 hours. Solvent was evaporated *in vacuo* to provide a solid. The solid was portioned between EtOAc (500 ml) and water (~400 ml). With stirring, pH was adjusted to ~7 with dropwise addition of 6N HCl and then the mixture was transferred to a separatory funnel. The organic layer was removed and the aqueous layer was extracted with EtOAc (4x200 ml) until no further UV detectable in organic extract. The combined organics were dried over MgSO4, filtered and concentrated to provide a solid. The solid was triturated with DCM (~200 mL), the solid collected, rinsed with DCM (2x100 ml), rinsed with EtOAc (1x75 ml). The solid was dried *in vacuo* to provide 2-(methylthio)benzothiazol-6-ol (43 g, 218 mmol, 88%) as an off white solid. No further purification was required. 1H NMR (400 MHz, Chloroform-d_1) d ppm 2.78 (s, 3 H) 6.92 (dd, *J*=8.80, 2.54 Hz, 1 H) 7.21 (d, *J*=2.35 Hz, 1 H) 7.73 (d, *J*=8.61Hz, 1 H); ESI-MS calc. [M+H]+ 198.0047, found [M+H]+ = 198.0052, RT = 1.51 min.

Supplementary Scheme 4 – Synthetic Route to N-methyl-4-((2-(methylthio)benzothiazol-6-yl)oxy)picolinamide

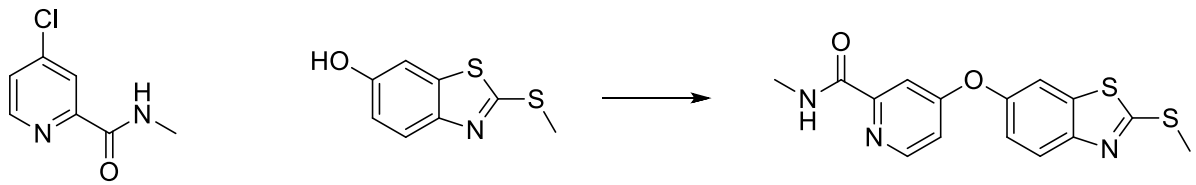

C G H

To a 350 ml glass pressure tube was added a solution of 2-(methylthio)benzothiazol-6-ol (20 g, 101 mmol, 1.0eq) in NMP (150 ml), $CsCO_3$ (85 g, 261.5 mmol, 2.6 eq), and 4-Chloro-pyridine-2-carboxylic acid methylamide (21.08 g, 124 mmol, 1.23eq). The reaction mixture was heated at 70°C with stirring for 24 hours. As starting material was still present by LCMS, the reaction mixture was heated at 80°C with stirring for an additional 18 hours. The reaction mixture was cooled to room temperature, transferred to separatory funnel, diluted with EtOAc (500 ml) and washed twice with 25% brine (2x250 ml). The aqueous washings were extracted with DCM (2x250 ml) after which all solids had dissolved during the last extraction. The EtOAc and DCM extracts were combined, dried over Na_2SO_4, filtered and evaporated *in vacuo* to give an off white solid. The solid was triturated with diethylether (~75 ml) followed by hexane (25 ml). The solid was collected by filtration and dried *in vacuo* to provide N-methyl-4-((2-(methylthio)benzothiazol-6-

yl)oxy)picolinamide as a white solid (22 g, 66.4 mmol). 1H NMR (400 MHz, DMSO-d_6) d ppm 2.78-2.82 (m, 6 H) 7.16 (dd, *J*=5.67, 2.54 Hz, 1 H) 7.31 (dd, *J*=8.80, 2.54 Hz, 1 H) 7.42 (d, *J*=2.74 Hz, 1 H) 7.90 - 7.95 (m, 2 H) 8.50 (d, *J*=5.48 Hz, 1 H) 8.76 (d, *J*=4.70 Hz, 1 H); 13C NMR (Bruker ASCEND-500, 500 MHz, DMSO-d_6) d ppm 14.3, 25.6, 109.1, 119.7, 122.1, 114.2, 114.2, 136.2, 149.8, 150.5, 150.6, 152.6, 163.9, 168.6, 165.9; ESI-MS calc. [M+H]+ 332.0546, found [M+H]+ = 332.0540, RT = 1.91 min.

Supplementary Scheme 5 – Synthetic Route to 4-((2-(((1*R*,2*R*)-2-hydroxycyclohexyl)amino) benzothiazol-6-yl)oxy)-N-methylpicolinamide (BLZ945)

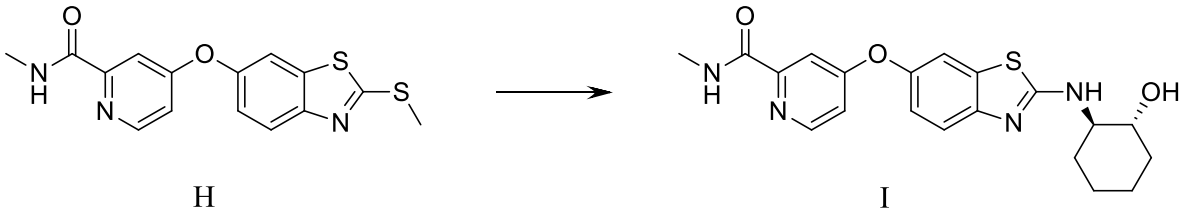

H I

To a solution of *N*-methyl-4-(2-(methylthio)benzothiazol-6-yloxy)picolinamide (15.9 g, 48.0 mmol) in 700 ml of DCM was added mCPBA (77%, 11.3 g, 50.4 mmol) portion-wise at 0°C. After being stirred at room temperature for 2 hours, the mixture was diluted with 700 ml of DCM. The resulting mixture was washed with 300 ml of *aq*. 2M $NaHSO_3$, 300 ml of *aq*. *sat*. $NaHCO_3$, 300 ml of brine, dried over $MgSO_4$, filtered and solvent was evaporated *in vacuo* to give crude *N*-methyl-4-(2-(methylsulfinyl)benzothiazol-6-yloxy)picolinamide2-(3-chloroquinoxalin-2-ylamino)-4-methylpentan-1-ol (16.2 g, ~46.7 mmol) which was dissolved in 170 ml of DMA. To this solution was added at room temperature DIEA (36.5 ml, 210 mmol) followed by (1*R*,2*R*)-2-aminocyclohexanol hydrochloride (21.2 g, 140 mmol). With stirring the reaction mixture was heated to 110°C and held at this temperature for ~60 hours. The reaction mixture was cooled to room temperature and transferred to a separatory funnel with EtOAc (1L). The organic layer was washed successively with 200 ml of *aq*. *sat*. $NaHCO_3$, 200 ml of brine. The combined aqueous layers were extracted with additional EtOAc (1L) and this organic extract was separated and washed with 200 ml of brine. The combined EtOAc extracts were dried over $MgSO_4$, filtered and evaporated *in vacuo* to leave a solid residue.

The product was purified by column chromatography (~200 g EMD Silica Gel 60; elute with 3:47:50 MeOH:EtOAc:hexane). Enriched fractions containing product, identified by TLC and confirmed by LCMS, were combined and solvents were concentrated *in vacuo* until ~350 ml of solvents remained. This mixture was then stored at –4°C overnight. Solids were collected by filtration (11.8 g, >98% pure) and then dissolved in 300 ml of MeOH and 200 ml of DCM at 50°C. Solvents were concentrated *in vacuo* to ~200 mL remained. This mixture was stored at –4°C overnight. Solids were collected by filtration and dried *in vacuo* to give 4-((2-(((1*R*,2*R*)-2-hydroxycyclohexyl)amino)benzothiazol-6-yl)oxy)-N-methylpicolinamide (10.86 g, 27.2 mmol). 1H NMR (400 MHz, DMSO-*d6*) d ppm 1.11 - 1.41 (m, 4 H) 1.64 (br. s., 2 H) 1.90 (d, *J*=10.56 Hz, 1 H) 1.99 - 2.18 (m, 1 H) 2.78 (d, *J*=4.70 Hz, 3H) 3.28 - 3.42 (m, 1 H) 3.57 (br. s., 1 H) 4.76 (d, *J*=5.48 Hz, 1 H) 7.04 (dd, *J*=8.61, 2.35 Hz, 1 H) 7.12 (dd, *J*=5.48, 2.74 Hz, 1 H) 7.37 (d, *J*=2.35 Hz, 1H) 7.43 (d, *J*=8.61

Hz, 1H) 7.59 (d, *J*=2.35 Hz, 1 H) 8.01 (d, *J*=7.43 Hz, 1 H) 8.48 (d, *J*=5.87 Hz, 1 H) 8.75 (q, *J*=4.30 Hz, 1 H); 13C NMR (Bruker Advance-500, 500 MHz, DMSO-d_6) d ppm 23.5, 23.9, 25.9, 30.5, 33.9, 59.6, 71.2, 108.6, 113.7, 113.8, 118.3, 118.6, 131.6, 146.7, 150.2, 150.7, 152.3, 163.7, 166.3, 166.6; ESI-MS calc. [M+H]+ 399.1491, found [M+H]+ = 399.1489, RT = 1.21 min.

Comparison of the above material to racemic material, prepared in the same manner above, showed the compound to be ca. 98% pure by chiral HPLC. Chiral HPLC chromatography experiments were carried out on a CHIRALPAK OD-H, 4.6 mm ID x150 mm long column. The solvent system was 20% EtOH/80% Heptane at the flow rate of 1 ml/min with a total run time of 30 minutes. RT = 8.78 min.

Intracranial injections of DF-1:RCAS-hPDGF-B-HA cells in Nestin-Tv-a;Ink4a/Arf$^{-/-}$ mice (PDGF-driven glioma/ PDG model)

The initiation of tumors with RCAS-hPDGF-B-HA in adult mice has been previously described [32,33]. Briefly, mice were fully anesthetized with 10 mg ml^{-1} ketamine/1 mg ml^{-1} xylazine and were subcutaneously injected with 50 μl of the local anesthetic 0.25% bupivacaine at the surgical site. Mice were intracranially injected with 1 μl containing 2 x 10^5 DF-1:RCAS-hPDGF-B-HA cells between 5-6 weeks of age using a fixed stereotactic apparatus (Stoelting). Injections were made to the right frontal cortex, approximately 1.5 mm lateral and 1 mm caudal from bregma, and at a depth of 2 mm.

For a subset of experiments (Figure 1a, Supplementary Fig. 14), Nestin-Tv-a; *Ink4a/Arf*$^{-/-}$ pups were injected with 1 μl containing 2 x 10^5 DF-1:RCAS-hPDGF-B-HA or DF-1:RCAS-hPDGF-B-HA-SV40-eGFP cells on post-natal day 2 into the left cortex between the eye and ear [34].

Characterization of human primary glioma tumor spheres

Nanostring-based analyses: The nCounter Analysis System (Nanostring Technologies, Seattle, WA) allows for multiplexed digital mRNA profiling without amplification or generation of cDNA. Briefly, a pair of approximately 50 bp probes complementary to each target mRNA are hybridized to a sample of interest in solution phase followed by solid phase immobilization of ternary complexes. Fluorescent barcodes on each reporter probe are then counted by an nCounter Digital Analyzer. In the present study, samples were tested on a custom Nanostring codeset composed of 147 probes. Gene expression space centroids corresponding to TCGA molecular subclasses (i.e. proneural, neural, classical, and mesenchymal) were defined by running 192 TCGA samples of known subclass. Test samples were then run and classified by nearest centroid methodology. In all cases, 150–300 ng of total RNA was tested.

aCGH analyses: Genomic DNA was extracted from primary tumors or tumor spheres using standard techniques. DNA was then digested, labeled and hybridized to 1M CGH arrays according to manufacturer guidelines (Genomic DNA labeling kit PLUS, Agilent), and aCGH profiles were processed as previously described [35]. Normal male genomic DNA (Promega, Madison, WI) was used as a reference.

Sequenom analyses: Mutational analyses were conducted using iPLEX mass spectrometry–based genotyping (Sequenom), as previously described [36]. Briefly, a multiplexed PCR reaction using amplification primers bracketing a specific mutation is followed by a one-base extension at the nucleotide of interest, and the difference in mass between extended products allows the distinction between wild-type and mutant alleles.

BLZ945 short–term trial and tumor volume calculation

To determine tumor volume, regions of interest (ROI) were circumscribed on T2 weighted images and their corresponding area in mm^2 was multiplied by the slice height of 0.7 mm. The total tumor volume is the sum of the ROI volume in each slice, and the volume for the first and last slice in which the tumor appear is halved to approximate the volume of a trapezoid. When tumor volume was in the range of 4.5–40 mm^3, animals were randomly assigned to treatment groups. A third cohort of mice with tumors larger than 40 mm^3 was also treated with BLZ945 (denoted as BLZ945 large). A size-matched vehicle treated cohort was not included for this larger starting tumor burden because these mice would not have been able to survive to the trial endpoint.

Diphtheria toxin (DT)/DTR-mediated macrophage depletion

To generate animals for diphtheria toxin experiments, Nestin-Tv-a;*Ink4a/Arf*$^{-/-}$ mice were bred to homozygous CD11b-DTR mice. Tumors were initiated in the Nestin-Tv-a;*Ink4a/Arf*$^{+/-}$;CD11b-DTR offspring at postnatal day two by intracranial injection of DF-1: RCAS-hPDGF-B-HA cells. When mice began to display mild symptoms of gliomas (4.5 weeks of age), mice were randomly assigned to diphtheria toxin (DT 15 ng g^{-1}; List Biologicals) or vehicle (deionized water) treatment groups. Mice were dosed by intraperitoneal injection daily for up to 5 d, and were euthanized 24 h after the last injection and tissues collected for frozen histology. More extended treatment was not possible because of dose-limiting toxicity of DT [5].

Similarly, Nestin-Tv-a;*Ink4a/Arf*$^{-/-}$ mice were bred to hemizygous CCR2-DTR mice, to generate Nestin-Tv-a;*Ink4a/Arf*$^{+/-}$ animals of which approximately half had the CCR2-DTR-CFP transgene. Tumors were initiated in all offspring at postnatal day two by intracranial injection of DF-1: RCAS-hPDGF-B-HA cells. At weaning, CCR2-DTR+ animals were identified based on the presence of CFP+ cells in the blood by flow cytometry. When the first littermate began to display mild symptoms (4–6 weeks of age), mice were randomly assigned to DT (10 ng g^{-1}) or vehicle treatment groups. Mice were dosed by intraperitoneal injection every other day, receiving a maximum of 4 doses in total. Mice were euthanized 24 h after the last injection and blood and tissues collected for flow cytometry and frozen histology, respectively.

Clodronate liposome treatment

Tumors were initiated in Nestin-Tv-a;*Ink4a/Arf*$^{-/-}$ mice at postnatal day two by intracranial injection of DF-1: RCAS-hPDGF-B-HA cells. At 21–24 d, mice were randomly assigned to PBS liposome (vehicle) or clodronate liposome treatment groups (suspensions from clodronateliposomes.org) [6]. Mice were intravenously injected via the tail vein with 100 μl of liposome suspension every other day until the mice became symptomatic, at which point they were euthanized.

Blood collection

Blood was collected from the retroorbital sinus of anesthetized mice into K2 EDTA coated vacutainer tubes (BD) on ice. Samples were then subjected to red blood cell lysis by two washes with 1x BD PharmLyse or alternative buffer (10 mM $KHCO_3$, 150 mM NH_4Cl, 0.1 mM EDTA), prior to a PBS wash and resuspension in FACS buffer (1% IgG Free bovine serum albumin (BSA) in PBS (Jackson Immunoresearch)).

Flow cytometry

After counting, single cell suspensions in FACS buffer (1% IgG Free BSA in PBS (Jackson Immunoresearch)) were incubated with 1 μl of Fc Block (BD) for every

million cells for at least 15 min at 4 °C. Cells were then stained with the antibodies for 10 min at 4 °C, washed with FACS buffer, and resuspended in FACS buffer containing DAPI (5 mg ml^{-1} diluted 1:5,000) for live/dead cell exclusion, unless otherwise noted. Antibodies used for flow cytometry are listed in Supplementary Table 11. For analysis of Mrc1/ CD206 expression, cells were first stained for CD45 and CD11b, followed by fixation and permeabilization using the BD Cytofix/Cytoperm™ kit (BD Biosciences) according to the manufacturer's instructions, and then stained with anti-CD206 antibody (Mrc1; Supplementary Table 11).

For analysis, samples were run on a BD LSR II (Becton Dickinson), and all subsequent compensation and gating performed with FlowJo analysis software (TreeStar). For sorting, PDG mice or PDG-GFP mice were used. A mixed population of $DAPI^-$ cells (live cells), $CD11b^-Gr\text{-}1^-$ (non-macrophages) and $CD11b^+Gr\text{-}1^-$ (macrophages) were isolated from gliomas from PDG mice. The mixed population of non-macrophages contains multiple cell types including glioma cells, astrocytes, pericytes, endothelial cells and any $CD11b^-$ immune cells. Usage of PDG-GFP mice allowed purification of GFP^+ tumor cells. Samples were run on a BD FACSAria (Becton Dickinson) cell sorter and cells were collected into FACS buffer. Cells were then centrifuged and resuspended in 500 μl Trizol (Invitrogen) before snap freezing in liquid nitrogen and storage at –80 °C.

Proliferation assays

Cell growth rate was determined using the MTT cell proliferation kit (Roche). Briefly, cells were plated in triplicate in 96-well plates: 1 x 10^3 cells per well for glioma cell lines, 5 x 10^3 cells per well for BMDM and CRL-2467, and 2.5 x 10^3 cells per well for HUVEC and HBMEC cell lines. For all experiments, media was changed every 48 h. Cells were grown in the presence or absence of 6.7–6,700 nM of BLZ945, or 8 μg ml^{-1} of CSF-1R neutralizing antibody. To test the sensitivity to PDGFR inhibition, PDGC lines were cultured in the presence of 10,000 nM imatinib or 10,000 nM PTK787 (diluted from 10 mM stock solutions in DMSO; LC laboratories).

BMDM and CRL-2467 cells were supplemented with 10 ng ml^{-1} and 30 ng ml^{-1} recombinant mouse CSF-1, respectively, unless otherwise indicated. Where indicated, BMDM were supplemented with the following concentrations of recombinant proteins (R&D Systems) diluted in 0.1% IgG Free BSA in PBS: IFN-γ at 30 ng ml^{-1}; CXCL1, CX3CL1, IL-34, CCL2, CCL5, CXCL10 at 20 ng ml^{-1}; VEGF-A, VEGF-C, IL-4, CXCL16, GM-CSF at 10 ng ml^{-1}. For BMDM stimulated with GCM derived from protective or non-protective PDGC lines, CSF-1 was not included in the culture conditions. HUVEC and HBMEC cells were supplemented with ECGF supplied by the manufacturer unless otherwise indicated.

Reduction of the MTT substrate was detected by colorimetric analysis using a plate reader as per the manufacturer's protocol. 10 μl of MTT labeling reagent was added to each well and then incubated for 4 h at 37 °C, followed by the addition of 100 μl MTT solubilization reagent overnight. The mixture was gently resuspended and absorbance was measured at 595 nm and 750 nm on a spectraMax 340pc plate reader (Molecular Devices).

Histology, immunohistochemistry, and analysis

For analysis of tumor histology and grading of tumor malignancy, hematoxylin and eosin (H&E) staining was performed, and the tissues blindly scored by a neuropathologist (Dr. Jason Huse, MSKCC). For all other imaging analyses reported

herein, tissues were also analyzed blindly, and samples unblinded only at the end of the study.

For immunofluorescence, 10 μm frozen sections were thawed and dried at room temperature and washed in PBS. For the standard staining protocol, tissue sections were blocked in 0.5% PNB in PBS for at least 1 h at room temperature or up to overnight at 4 °C, followed by incubation in primary antibody in 0.25% PNB for 2 h at room temperature or overnight at 4 °C. Primary antibody information and dilutions are listed in Supplementary Table 10. Sections were then washed in PBS and incubated with the appropriate fluorophore-conjugated secondary antibody (Molecular Probes) at a dilution 1:500 in 0.25% PNB for 1 h at room temperature. After washing in PBS, tissue sections were counterstained with DAPI (5 mg ml^{-1} stock diluted 1:5,000 in PBS) for 5 min prior to mounting with ProLong Gold Antifade mounting media (Invitrogen).

For angiogenesis and proliferation analyses, tissue sections were first subjected to citrate buffer based antigen retrieval by submerging in antigen unmasking solution (0.94% v/v in distilled water; Vector Laboratories) and microwaving for 10 min on half power, followed by cooling to room temperature for at least 30 min. For angiogenesis analysis, tissues were then washed in PBS and blocked with mouse Ig blocking reagent (Vector Laboratories) according to the manufacturer's instructions for 1 h at room temperature. For proliferation analysis, after antigen retrieval, tissue sections were incubated with 2 M HCl for 15 min at room temperature to denature DNA and then in neutralizing 0.1 M sodium borate buffer (pH 8.5) for 5 min. After PBS washes, the rest of the staining was performed according to the standard protocol.

For staining for phagocytosis analysis, 10 μm thick frozen sections were thawed and dried at room temperature and then washed in PBS. Tissue sections were blocked in 0.5% PNB in PBS for at least 1 h at room temperature, followed by incubation in rabbit anti-cleaved caspase-3 primary antibody diluted 1:500 in 0.5% PNB overnight at 4 °C. The next day, slides were washed 6 times for 5 min in PBS prior to incubation with goat-anti-rabbit Alexa 568 secondary antibody (1:500 in 0.5% PNB) for 1 h at room temperature. Tissue sections were then washed 6 times for 5 min in PBS and blocked overnight at 4 °C in a new buffer of 5% donkey serum, 3% BSA, and 0.5% PNB in PBS. The following day, slides were incubated for 2 h at room temperature with the next set of primary antibodies: rabbit anti-Olig2 (1:200) and rat anti-CD11b (1:200) diluted in 5% donkey serum, 3% BSA, and 0.5% PNB in PBS. Slides were washed 6 times for 5 min in PBS prior to incubation with donkey-anti-rabbit Alexa647 (1:500) and donkey-anti-rat Alexa488 (1:500) secondary antibodies in 0.5% PNB for 1 h at room temperature. Tissue sections were then washed 4 times for 5 min in PBS prior to staining with DAPI (5 mg ml^{-1} stock diluted 1:5,000 in PBS) for 5 min, washed twice more in PBS for 5 min, and mounted with ProLong Gold Antifade mounting media (Invitrogen). Co-staining for CSF-1R (first primary antibody) and Iba1 (second primary antibody) was also performed in series in the same manner, with the addition of citrate buffer based antigen retrieval at the outset.

Tissue sections were visualized under a Carl Zeiss Axioimager Z1 microscope equipped with an ApoTome.2. The analysis of immunofluorescence staining, cell number, proliferation, apoptosis, and colocalization studies were performed using TissueQuest analysis software (TissueGnostics) as previously described [37]. Overviews of tissue sections from gliomas stained for angiogenesis analysis were generated by TissueGnostics acquisition software by stitching together individual 200x images. All parameters of angiogenesis were quantitated using MetaMorph (Molecular Devices), as previously described [38]. For analysis of phagocytosis, fifteen

randomly selected fields of view from within the tumor were acquired using the 63x oil immersion objective (total magnification 630x) and the Apotome to ensure cells were in the same optical section. Positive cells were counted manually using Volocity (PerkinElmer) and were discriminated by the presence of a $DAPI^+$ nucleus. Apoptotic cells were counted as those that had cytoplasmic cleaved caspase-3 $(CC3)^+$ staining and condensed nuclei. A cell was considered to have been engulfed by a macrophage when it was surrounded by a contiguous $CD11b^+$ ring that encircled at least two-thirds of the cell border. The numbers of mice analyzed are specified in the figure legends.

Protein isolation and western blotting

Whole tissues: Mice treated with BLZ945 or vehicle were sacrificed 1 h following the final dose and tumors harvested, snap frozen in liquid nitrogen, and stored at –80 °C. Samples were biochemically fractionated as described previously [39]. Synaptosomal membrane fractions were lysed in NP-40 lysis buffer (0.5% NP-40, 50 mM Tris-HCl [pH 7.5], 50 mM NaCl, 1x complete Mini protease inhibitor cocktail (Roche), 1x PhosSTOP phosphatase inhibitor cocktail (Roche)), and protein quantified by BCA assay (Pierce). Protein lysates were (90 μg per lane) separated by SDS-PAGE and transferred to PVDF membranes for immunoblotting. Membranes were probed with antibodies against pCSF-1R Y721 (1:1,000; Cell Signaling Technology), CSF-1R (1:1,000; Santa Cruz Biotechnology), or GAPDH (1:1,000; Cell Signaling Technology) and detected using HRP-conjugated anti-rabbit (Jackson Immunoresearch) antibodies using chemiluminescence detection (Millipore). Bands from western blots were quantified in the dynamic range using the Gel analysis module in ImageJ software.

Cell culture: BMDMs from WT mice were cultured in the absence of CSF-1 for 12 h prior to 10 ng ml^{-1} CSF-1 stimulation for the indicated time points (Supplementary Fig. 2b, d) ± 67 nM, 670 nM BLZ945 or 8 μg ml^{-1} of the CSF-1R neutralizing antibody (clone AFS98 [40], eBioscience and MSKCC Monoclonal Antibody Core Facility). Whole protein lysates were isolated with NP40 lysis buffer and detected by western blot as described above.

For analysis of phosphorylated Akt (pAkt) in macrophages, BMDMs were cultured without CSF-1 for 12 h and then stimulated for 5 min with non-conditioned media (DMEM) containing CSF-1 (10 ng ml^{-1}), protective GCM (PDGC-23, PDGC-17, PDGC-02 GCM), non-protective GCM (PDGC-55 GCM), or non-protective GCM (PDGC-55 GCM) supplemented with GM-CSF (10 ng ml^{-1}), IFN-γ (30 ng ml^{-1}) and CXCL10 (20 ng ml^{-1}). Akt activation was compared between vehicle and BLZ945-treated BMDMs (670 nM), using an antibody specific to the Ser473 phosphorylation site of Akt (1:1,000; Cell Signaling Technology).

For analysis of pAkt and pErk activation in glioma cells, PDGC-23 cells were starved by culture in serum-free media overnight prior to exposure to BMDM CM from the three experimental groups described above (Naïve CM, Stim-CM, and Stim + BLZ945 CM) for the indicated timecourse. Erk activation was analyzed using an antibody specific for the Thr202/Tyr204 phosphorylation site (1:1,000; Cell Signaling Technology).

PDGC lines were cultured with vehicle or BLZ945 (67, 670 or 6,700 nM) for 24 h. Whole protein lysates were isolated with NP-40 lysis buffer containing 1x complete Mini protease inhibitor cocktail (Roche) and 1x PhosSTOP phosphatase inhibitors cocktail (Roche). Lysates were run on SDS-PAGE gels as described above. HA-tagged hPDGF-B was detected using a monoclonal antibody against the HA epitope

(1:500; Roche). Cytokines were also detected by the following antibodies: goat polyclonal anti-GM-CSF (1:500; R&D Systems), rat monoclonal anti-CXCL10 (1:1,000; R&D Systems), and goat polyclonal anti-IFN-γ (1:500; R&D Systems).

RNA isolation, cDNA synthesis and quantitative real-time PCR

RNA was isolated with Trizol, DNase treated, and 0.5 µg of RNA was used for cDNA synthesis. Taqman probes (Applied Biosystems) for *Adm* (Mm00437438_g1), *Arg1* (Mm00475988_m1), *Cd11b* (Mm00434455_m1), *Cd163* (Mm00474091_m1), *Cd68* (Mm03047343_m1), *Cdh1* (Mm00486906_m1), *Csf-1* (Mm00432688_m1), *Csf-1r* (Mm00432689_m1), *Csf-2* (Mm01290062_m1), *Csf-2rα* (Mm00438331_g1), *Csf-2rβ* (Mm00655745_m1), *Cxcl10* (Mm00445235_m1), *Cxcr3* (Mm00438259_m1), *F13a1* (Mm00472334_m1), *Hmox1* (Mm00516005_m1), *Ifnγ* (Mm00801778_m1), *Ifnγr1* (Mm00599890_m1), *Ifnγr2* (Mm00492626_m1), *Il34* (Mm00712774_m1), *Mrc1* (Mm00485148_m1), *Serpinb2* (Mm00440908_g1), *Stab1* (Mm00460390_m1) and *Tv-a* (custom), were used for qPCR. Assays were run in triplicate and expression was normalized to ubiquitin C (*Ubc,* Mm01201237_m1) for each sample.

Human glioma datasets

TCGA expression data was downloaded from the TCGA data portal and all clinical data was downloaded from the data portal (http://tcga-data.nci.nih.gov/tcga/tcgaHome2.jsp) [41]. Clinical and expression data for the Rembrandt data set was downloaded from (https://caintegrator.nci.nih.gov/rembrandt/). The Freije (GSE4412), Murat (GSE7696), and Phillips (GSE4271) datasets were downloaded from the NCBI (http://www.ncbi.nlm.nih.gov/geo/) [42-44]. For the Freije dataset, we only considered samples that were run on the HGU133A platform as samples on the HGU133B platform contained minimal overlap with the remaining datasets. Datasets were individually processed and normalized as described above. Within each dataset, genes were mean centered across subjects.

Subtyping of non-TCGA individuals

To investigate subtype specific survival differences in all publically available datasets, we utilized a subtype classification described previously [45] to train a support vector machine (SVM). The 840 genes used by Verhaak and colleagues for the ClacNc analysis were used to subset the dataset [45]. The remaining 776 genes that were common across all subject data sets were used to train a multiclass SVM (one-against-one) on the Core samples from the TCGA dataset. The SVM was trained using the Gaussian radial basis kernel function using the 'kernlab' package[46]. This model was then used to predict the subtype of the remainder of the TCGA patients and public datasets. The same SVM approach was used for subtyping of the LN229 and U251 glioma cell lines. Gene expression data for these cell lines was attained through the CCLE (http://www.broadinstitute.org/ccle/home) [47].

Human glioma classification

We trained an SVM on mouse expression data to classify patients into "Vehicle-like" or "BLZ945-like" classes. Human expression data was subsetted for common genes across all data sets and genes that have known mouse homologues. Similarly, mouse expression data was subsetted for genes with human homologues that were common across all human samples. Subsequently, mouse data was subsetted for differentially expressed genes identified using the 'limma' package. Human data was subsetted for the human homologues of these differentially expressed genes. This led to a reduction from 257 differentially expressed genes to 206 differentially

expressed genes with known human homologues across all human glioma datasets. The 'kernlab' package was then used to train a SVM on the mouse expression data using a linear kernel. This SVM was then used to predict patients into either "Vehicle-like" class or "BLZ945-like" class.

A similar approach was used to classify patients with a lasso logistic regression model. The restriction to genes with human-mouse homologs in the patient and mouse data was identical to that described above. Instead of using the 'kernlab' package, we trained a lasso logistic regression model using the 'glmnet' package. This model was then used to predict patient classification into either "Vehicle-like" class or "BLZ945-like" class. G-CIMP patient status was determined by hierarchical clustering of patient methylation data [48] as described below.

Stratification of patients by G-CIMP status

We determined if the survival advantage offered by the "BLZ945-like" treatment signature was potentially due to an enrichment of Glioma CpG Island Methylator Phenotype (G-CIMP) patients, which have previously been shown to be associated with improved overall survival [48]. Of the 435 GBMs analyzed from the TCGA dataset, 263 also had genomic methylation data and were classified into the methylation clusters as described previously [48]. Of the 21 G-CIMP patients, 20 (95%) were classified into the "BLZ945-like" class, showing a strong enrichment of BLZ945 samples in the G-CIMP patients. Despite this enrichment, survival analysis of proneural patients known to be G-CIMP negative (67/133 total proneural patients) revealed that the "BLZ945-like" class still showed an increase in survival of ~10.8 months (P= 0.014). Moreover, cox proportional hazard models demonstrated that the increase in survival demonstrated by "BLZ945-like" class was not dependent upon G-CIMP patients. The hazard ratio associated with the BLZ945 signature was significant with and without G-CIMP patients (Supplementary Table 7). Also, the hazard ratio for G-CIMP strata was not significant when the BLZ945 signature was also considered in a mixed model (Supplementary Table 7). Thus, although the G-CIMP patients are clearly enriched for mock "BLZ945-like" classification samples, the survival benefit offered by this classification is not dependent upon G-CIMP status.

The prognostic value of the "BLZ945-like" signature is independent of macrophage marker gene expression

We used an interaction based cox proportional hazard model to assess the prognostic value of the "BLZ945-like" signature when macrophage number was considered in the model. Gene expression of *AIF1* (*Iba1* in mouse), *CD68,* and *ITGAM* (*Cd11b* in mouse) were used as surrogates for macrophage number. *CD68* expression level was not available in the Phillips *et al*. dataset; therefore the hazard ratios reported in Supplementary Tables 8-9 for *CD68* are only in the TCGA dataset, not the Combined dataset.

As shown in Fig. 6g, h and Supplementary Fig. 24, only the proneural subtype of patients showed a significant association with survival using the "BLZ945-like" signature. *AIF1* expression was positively correlated with survival in Combined dataset proneural patients with a hazard ratio of 0.71 (CI: 0.51-0.98), i.e. higher *AIF1* expression actually correlated with increased survival. This was not found in the TCGA dataset. Both *ITGAM* and *AIF1* were also found to positively correlate with improved survival in the neural GBM subtype in the combined dataset. Additionally, none of the macrophage markers added any prognostic value when considered in either an additive model or interaction based model with the "BLZ945-like" signature.

In all cases the “BLZ945-like” signature was significantly associated with survival in a proneural specific manner. These findings were observed both in the TCGA dataset and the Combined dataset.

Code and data deposition

All code used to generate the figures and execute the analyses is publicly available and can be found at: (https://sourceforge.net/projects/joycelab-csf1r-inhibition-gbm/). All microarray data was deposited to the GEO: http://www.ncbi.nlm.nih.gov/geo/query/acc.cgi?token=npsxbyqqwequeda&acc=GSE37475

References for Supplementary Information

1. Cailhier, J.F., *et al.* Conditional macrophage ablation demonstrates that resident macrophages initiate acute peritoneal inflammation. *J Immunol* 174, 2336-2342 (2005).
2. Duffield, J.S., *et al.* Selective depletion of macrophages reveals distinct, opposing roles during liver injury and repair. *J Clin Invest* 115, 56-65 (2005).
3. Ueno, M., *et al.* Layer V cortical neurons require microglial support for survival during postnatal development. *Nat Neurosci* 16, 543-551 (2013).
4. Amankulor, N.M., *et al.* Sonic hedgehog pathway activation is induced by acute brain injury and regulated by injury-related inflammation. *J Neurosci* 29, 10299-10308 (2009).
5. Stoneman, V., *et al.* Monocyte/macrophage suppression in CD11b diphtheria toxin receptor transgenic mice differentially affects atherogenesis and established plaques. *Circ Res* 100, 884-893 (2007).
6. van Rooijen, N. & Hendrikx, E. Liposomes for specific depletion of macrophages from organs and tissues. *Methods Mol Biol* 605, 189-203 (2010).
7. Zeisberger, S.M., *et al.* Clodronate-liposome-mediated depletion of tumour-associated macrophages: a new and highly effective antiangiogenic therapy approach. *Br J Cancer* 95, 272-281 (2006).
8. Qian, B., *et al.* A distinct macrophage population mediates metastatic breast cancer cell extravasation, establishment and growth. *PLoS One* 4, e6562 (2009).
9. Meng, Y., *et al.* Blockade of tumor necrosis factor alpha signaling in tumor-associated macrophages as a radiosensitizing strategy. *Cancer Res* 70, 1534-1543 (2010).
10. Ginhoux, F., *et al.* Fate mapping analysis reveals that adult microglia derive from primitive macrophages. *Science* 330, 841-845 (2010).
11. Qian, B.Z., *et al.* CCL2 recruits inflammatory monocytes to facilitate breast-tumour metastasis. *Nature* 475, 222-225 (2011).
12. Ryder, M., *et al.* Genetic and pharmacological targeting of CSF-1/CSF-1R inhibits tumor-associated macrophages and impairs BRAF-induced thyroid cancer progression. *PLoS One* 8, e54302 (2013).
13. Hohl, T.M., *et al.* Inflammatory monocytes facilitate adaptive CD4 T cell responses during respiratory fungal infection. *Cell Host Microbe* 6, 470-481 (2009).
14. Chen, P., *et al.* Tumor-associated macrophages promote angiogenesis and melanoma growth via adrenomedullin in a paracrine and autocrine manner. *Clin Cancer Res* 17, 7230-7239 (2011).
15. Biswas, S.K. & Mantovani, A. Macrophage plasticity and interaction with lymphocyte subsets: cancer as a paradigm. *Nat Immunol* 11, 889-896 (2010).
16. Lawrence, T. & Natoli, G. Transcriptional regulation of macrophage polarization: enabling diversity with identity. *Nat Rev Immunol* 11, 750-761 (2011).
17. Scotton, C.J., *et al.* Transcriptional profiling reveals complex regulation of the monocyte IL-1 beta system by IL-13. *J Immunol* 174, 834-845 (2005).

18. Raes, G.*, et al.* Arginase-1 and Ym1 are markers for murine, but not human, alternatively activated myeloid cells. *J Immunol* 174, 6561; author reply 6561-6562 (2005).
19. Van den Bossche, J.*, et al.* Alternatively activated macrophages engage in homotypic and heterotypic interactions through IL-4 and polyamine-induced E-cadherin/catenin complexes. *Blood* 114, 4664-4674 (2009).
20. Moreno, J.L., Mikhailenko, I., Tondravi, M.M. & Keegan, A.D. IL-4 promotes the formation of multinucleated giant cells from macrophage precursors by a STAT6-dependent, homotypic mechanism: contribution of E-cadherin. *J Leuk Biol* 82, 1542-1553 (2007).
21. Torocsik, D., Bardos, H., Nagy, L. & Adany, R. Identification of factor XIII-A as a marker of alternative macrophage activation. *Cell Mol Life Sci* 62, 2132-2139 (2005).
22. Torocsik, D.*, et al.* Factor XIII-A is involved in the regulation of gene expression in alternatively activated human macrophages. *Thromb Haemost* 104, 709-717 (2010).
23. Weis, N., Weigert, A., von Knethen, A. & Brune, B. Heme oxygenase-1 contributes to an alternative macrophage activation profile induced by apoptotic cell supernatants. *Mol Biol Cell* 20, 1280-1288 (2009).
24. Choi, K.M.*, et al.* CD206-positive M2 macrophages that express heme oxygenase-1 protect against diabetic gastroparesis in mice. *Gastroenterology* 138, 2399-2409, 2409 e2391 (2010).
25. Sierra-Filardi, E.*, et al.* Activin A skews macrophage polarization by promoting a proinflammatory phenotype and inhibiting the acquisition of anti-inflammatory macrophage markers. *Blood* 117, 5092-5101 (2011).
26. Mantovani, A.*, et al.* The chemokine system in diverse forms of macrophage activation and polarization. *Trends Immunol* 25, 677-686 (2004).
27. Pelegrin, P. & Surprenant, A. Dynamics of macrophage polarization reveal new mechanism to inhibit IL-1beta release through pyrophosphates. *EMBO J* 28, 2114-2127 (2009).
28. Hamilton, J.A.*, et al.* Interleukin-4 suppresses plasminogen activator inhibitor-2 formation in stimulated human monocytes. *Blood* 80, 121-125 (1992).
29. Kzhyshkowska, J.*, et al.* Novel function of alternatively activated macrophages: stabilin-1-mediated clearance of SPARC. *J Immunol* 176, 5825-5832 (2006).
30. Park, S.Y.*, et al.* Stabilin-1 mediates phosphatidylserine-dependent clearance of cell corpses in alternatively activated macrophages. *J Cell Sci* 122, 3365-3373 (2009).
31. Brocheriou, I.*, et al.* Antagonistic regulation of macrophage phenotype by M-CSF and GM-CSF: implication in atherosclerosis. *Atherosclerosis* 214, 316-324 (2011).
32. Shih, A.H.*, et al.* Dose-dependent effects of platelet-derived growth factor-B on glial tumorigenesis. *Cancer Res* 64, 4783-4789 (2004).
33. Hambardzumyan, D., Amankulor, N.M., Helmy, K.Y., Becher, O.J. & Holland, E.C. Modeling adult gliomas using RCAS/t-va technology. *Transl Oncol* 2, 89-95 (2009).
34. Fomchenko, E.I.*, et al.* Recruited cells can become transformed and overtake PDGF-induced murine gliomas in vivo during tumor progression. *PLoS One* 6, e20605 (2011).
35. Brennan, C.*, et al.* Glioblastoma subclasses can be defined by activity among signal transduction pathways and associated genomic alterations. *PLoS One* 4, e7752 (2009).
36. Gorovets, D.*, et al.* IDH mutation and neuroglial developmental features define clinically distinct subclasses of lower grade diffuse astrocytic glioma. *Clin Cancer Res* 18, 2490-2501 (2012).
37. Steiner, G.E., Ecker, R.C., Kramer, G., Stockenhuber, F. & Marberger, M.J. Automated data acquisition by confocal laser scanning microscopy and image analysis of triple stained immunofluorescent leukocytes in tissue. *J Immunol Methods* 237, 39-50 (2000).
38. Gocheva, V., Chen, X., Peters, C., Reinheckel, T. & Joyce, J.A. Deletion of cathepsin H perturbs angiogenic switching, vascularization and growth of tumors in a mouse model of pancreatic islet cell cancer. *Biol Chem* 391, 937-945 (2010).

39. Hallett, P.J., Collins, T.L., Standaert, D.G. & Dunah, A.W. Biochemical fractionation of brain tissue for studies of receptor distribution and trafficking. *Curr Prot Neurosci* Chapter 1, Unit 1 16 (2008).
40. Sudo, T.*, et al.* Functional hierarchy of c-kit and c-fms in intramarrow production of CFU-M. *Oncogene* 11, 2469-2476 (1995).
41. McLendon, R. et al., Comprehensive genomic characterization defines human glioblastoma genes and core pathways. *Nature* 455, 1061-1068 (2008).
42. Freije, W.A.*, et al.* Gene expression profiling of gliomas strongly predicts survival. *Cancer Res* 64, 6503-6510 (2004).
43. Murat, A.*, et al.* Stem cell-related "self-renewal" signature and high epidermal growth factor receptor expression associated with resistance to concomitant chemoradiotherapy in glioblastoma. *J Clin Oncol* 26, 3015-3024 (2008).
44. Phillips, H.S.*, et al.* Molecular subclasses of high-grade glioma predict prognosis, delineate a pattern of disease progression, and resemble stages in neurogenesis. *Cancer Cell* 9, 157-173 (2006).
45. Verhaak, R.G.*, et al.* Integrated genomic analysis identifies clinically relevant subtypes of glioblastoma characterized by abnormalities in PDGFRA, IDH1, EGFR, and NF1. *Cancer Cell* 17, 98-110 (2010).
46. Karatzoglou, A., Smola, A., Hornik, K. & Zeileis, A. kernlab - An S4 Package for Kernel *Methods in R* 11(2004).
47. Barretina, J.*, et al.* The Cancer Cell Line Encyclopedia enables predictive modelling of anticancer drug sensitivity. *Nature* 483, 603-607 (2012).
48. Noushmehr, H.*, et al.* Identification of a CpG island methylator phenotype that defines a distinct subgroup of glioma. *Cancer Cell* 17, 510-522 (2010).